# VII-A

## SONIC BOOM & NOISE

COMMERCIAL SUPERSONIC TRANSPORT PROGRAM

PHASE II-A COMPREHENSIVE REPORT

NOVEMBER 1, 1964 CONTRACT NO. FA-SS-64-4

THE BOEING COMPANY AIRPLANE DIVISION

RENTON, WASHINGTON, U.S.A. D6--8686-7



Issue 7 2

CONTENTS

## 1.0 SUMMARY

The Boeing Company has submitted for Phase II-A evaluation an airplane design, which, in its intercontinental and domestic versions, will provide economical supersonic transports meeting the diverse requirements of various operators and also meeting the design objectives of the FAA. The two models of the airplane are identical in all respects except for operational empty weight and maximum gross weight.

Both the domestic and intercontinental versions meet or are lower than all noise objectives established by the FAA. Notable progress has been made during Phase II-A toward developing a supersonic transport that has both interior and exterior noise levels lower than present subsonic airplanes. Significant configuration changes from the Phase I proposal that have contributed to improvement are:

- Development of engine inlet and nozzle noise suppression techniques with no performance penalty
- Relocation of engines aft on the wing to reduce engine noise heard in the cabin

These changes, coupled with test-proven structural design concepts, will ensure a 50,000-hour fatigue life for the airplane with minimum weight penalty.

This document presents the substantiating data for sonic boom, engine noise, interior noise, and sonic fatigue effect on structures.

### 1.1 SONIC BOOM

For domestic operation, where sonic boom will be of significant importance, the Model 733-291 is designed to provide a range of 2900 statute miles (2600 nautical miles) with a payload of 43,000 pounds without exceeding the sonic boom objectives of 2 psf maximum in climb and 1.5 psf in cruise and descent.

The Model 733-290 is designed for intercontinental operation, where transition and cruise will occur over water or uninhabited land areas on routes requiring maximum range-payload performance. This airplane achieves a range of 4010 statute miles (3485 nautical miles) with a payload of 43,000 pounds when limited to sonic boom overpressure of 2.3 psf in climb and 1.7 psf in cruise and descent.

Both models possess considerable operational flexibility with respect to the sonic boom created in flight as summarized in Table 1-A.

The sonic boom characteristics have been calculated in the manner prescribed by the FAA and NASA. All of the airplane components and incremental lift forces have been considered, including the wing camber lift, angle of attack lift, tail lift, and nacelle induced lift. The configuration has been optimized to obtain the best sonic boom character-

**TABLE 1-A EFFECT OF SONIC BOOM ON AIRPLANE PERFORMANCE**

| | 733-290 INTERCONTINENTAL | | | 733-291 DOMESTIC | | |
|---|---|---|---|---|---|---|
| RAMP G. WT. | 500,000 LB | | | 425,000 LB | | |
| PAYLOAD | 43,000 LB | | | 43,000 LB | | |
| CLIMB $\Delta P_{MAX}$ | 2.0 | 2.3 | 2.5 | 1.8 | 2.0 | 2.3 |
| CRUISE $\Delta P_{MAX}$ | 1.62 | 1.67 | 1.68 | 1.46 | 1.49 | 1.50 |
| RANGE | | | | | | |
| N. MI. | 3240 | 3485 | 3525 | 2445 | 2600 | 2665 |
| ST.MI. | 3730 | 4010 | 4060 | 2810 | 2990 | 3065 |

istics at all Mach numbers, commensurate with minimum drag and structural weight considerations. As detailed in Section 2.0, the sonic boom parameter for this airplane in cruise is only 19 percent greater than the theoretical lower bound.

1.2 ENGINE NOISE

The Model 733-290 provides a marked reduction in community noise for all phases of operation, as compared to present long range jets. Fig. 1-1 illustrates a takeoff at maximum gross weight with maximum dry thrust. The airport noise is 116 PNdb at 1500 feet to the side of the runway. The community noise is 105.5 Pndb at the 3-mile point, with thrust set for 500 feet per minute rate of climb. The corresponding community noise for the domestic 733-291 is 96.8 PNdb. Trades between airport and community noise are possible by using varying takeoff thrust settings. For example, with maximum augmented thrust, the airport noise if 117.7 PNdb with community levels of 103.8 PNdb and 95 PNdb, respectively for the 733-290 and 733-291.

The greatest improvements have been achieved in landing approach noise. At maximum design landing weight, a conventional approach on a 3 degree glideslope results in 112 PNdb for the 733-290 at 1 mile from the runway. A noise abatement approach procedure using automatic throttle control has been studied. This procedure offers a potential reduction to 105 PNdb at the 1-mile point.

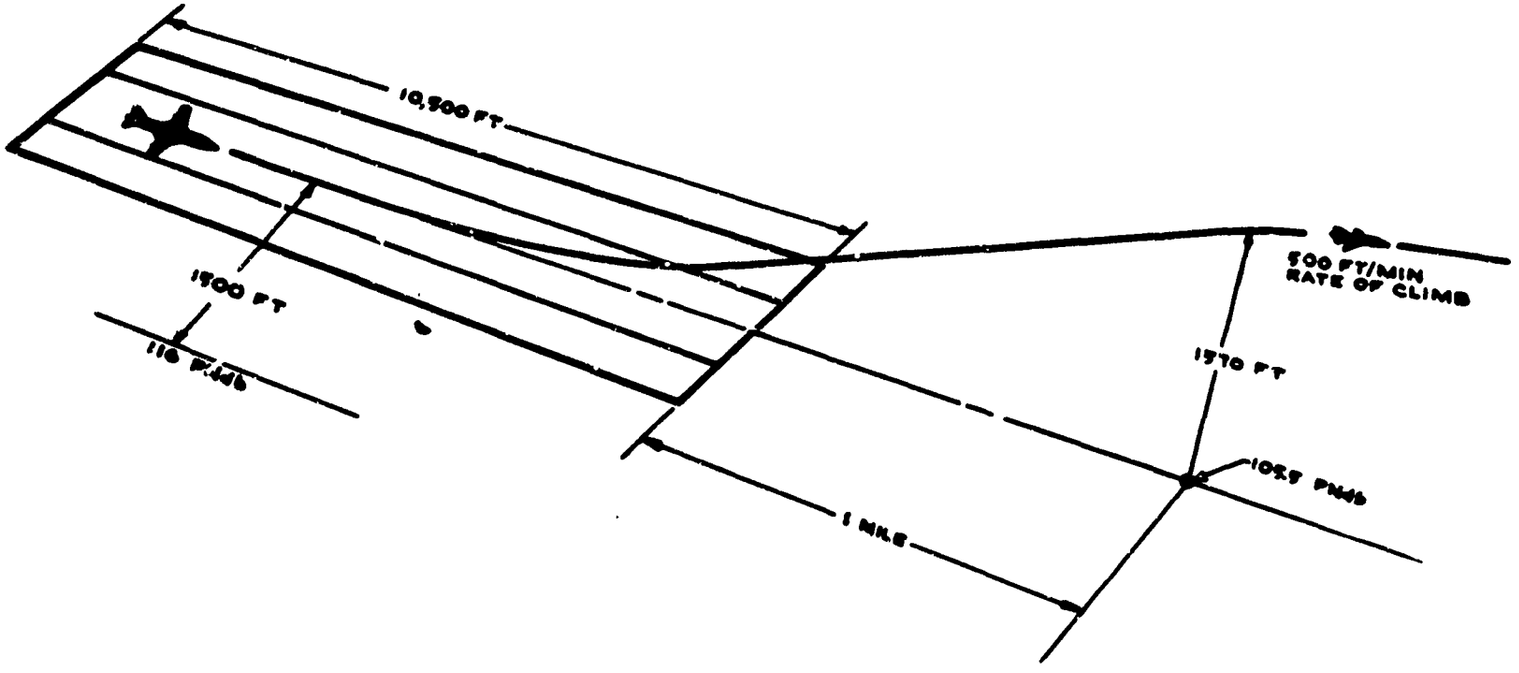


FIG. 1-1 AIRPORT AND COMMUNITY NOISE LEVELS DURING TAKEOFF, MODEL 733-290

Sound suppression has been achieved through the use of a choked inlet to suppress compressor noise and a "star shaped" primary throat to suppress jet noise. Tests that provided verification for the noise analyses are described in Section 3.0.

## 1.3 INTERNAL NOISE

Internal sound levels in the Boeing supersonic transport are less than those in current subsonic airplanes. A thorough review of available boundary layer noise data has been made during Phase II-A. The most reliable boundary layer data have been used in conjunction with a detailed analysis of the transmission characteristics of the body structure and insulation to develop the noise estimates shown in Table 1-B. As the data indicate, both the overall sound levels and the speech interference levels are less than in the 707 airplane. The proposed supplementary standard, NCA-65, is shown in the table for comparison.

***TABLE 1-B WINDOW SEAT SOUND LEVEL COMPARISONS***

| | TAKEOFF | | | | CRUISE | | | |
|---|---|---|---|---|---|---|---|---|
| | FWD CABIN | | AFT CABIN | | FWD CABIN | | AFT CABIN | |
| | OA* | SIL** | OA | SIL | OA | SIL | OA | SIL |
| 733-290 | 96 | 60 | 108 | 74 | 85 | 63.5 | 85 | 63 |
| 707 | 96 | 63 | 113 | 84 | 87 | 68 | 93.5 | 65.5 |
| NCA-65 | | | | | 95.5 | 65 | 95.5 | 65 |
| NCA-65 + 10 | 105.5 | 75 | 105.5 | 75 | | | | |

* Overall sound pressure level ** Speech interference level

## 1.4 SONIC FATIGUE PARAMETERS

The sonic environment on the Boeing supersonic transport has been verified by test. The change in engine location and the noise reduction due to the jet nozzle design have reduced the sound pressure level on the structure to 163 db with augmented thrust. Furthermore, a significant reduction in the area of structure subjected to noise levels greater than 150 db has been achieved.

Test results have shown that chem-milled skins on primary structure and titanium-faced fiberglass honeycomb on secondary structure possess outstanding sonic fatigue characteristics. This improved structure, together with the reduced sonic environment, requires only 100 pounds of reinforcement be added to the strength-designed structure in order to achieve a 50,000-hour life.

## 2.0 SONIC BOOM

The calculation of the sonic boom characteristics for the models 733-290 and 733-291 is presented in this section. The external geometry of these two models is identical; therefore, the sonic boom characteristics are the same for each. The sonic boom overpressures produced on the ground under the flight track have been computed and are shown in Figs. 2-1 and 2-2. Sonic boom data related to the performance of both airplanes are shown in Volume V-A.

The theoretical method used in estimating the sonic boom characteristics of these airplanes is consistent with that outlined in the FAA Procedures, Ref. 2-1. Specifically, the airplane area distributions were obtained by the use of supersonic area-rule cutting planes and include all of the components. The lift "equivalent area distributions" include the contribution of wing camber, angle of attack, nacelle induced lift, and tail lift for trim.

In addition to the basic sonic boom data, discussion of the effect of nonstandard atmosphere, the effect of elastic deformations, and an evaluation of slight variations in calculation procedures are presented. Basic data for use in the NASA computer programs are tabulated in Par. 2.5.

## 2.1 SONIC BOOM CHARACTERISTICS

The sonic boom characteristics of the 733-290 airplane, as computed by the method described in subsequent paragraphs, are shown in Fig. 2-3.

The data in Fig. 2-3 have been referred to the lift coefficient of the wing. The sonic boom characteristics of the configuration may be found by entering the chart with the wing lift coefficient ($C_{L_{wing}} = C_L - C_{L_{tail}}$). The lift coefficient of the tail ($C_{L_{tail}}$) may be obtained from the data presented in Section 4.0 Volume V-A, Book One, Aerodynamics. The sonic boom characteristics tabulated as requested by NASA appear in Par. 2.5.

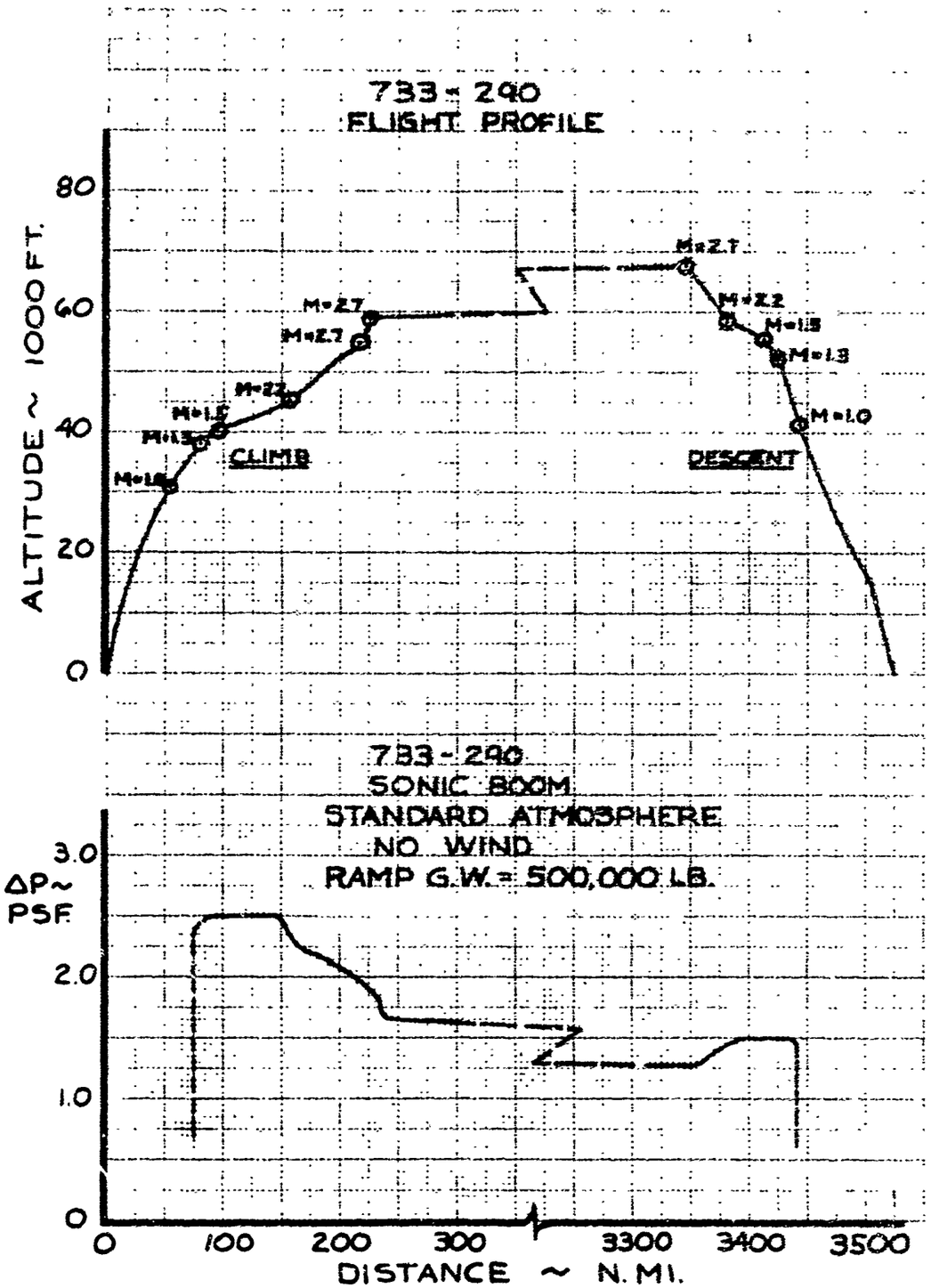


FIG. 2-1 733-290 SONIC BOOM UNDER THE FLIGHT TRACK

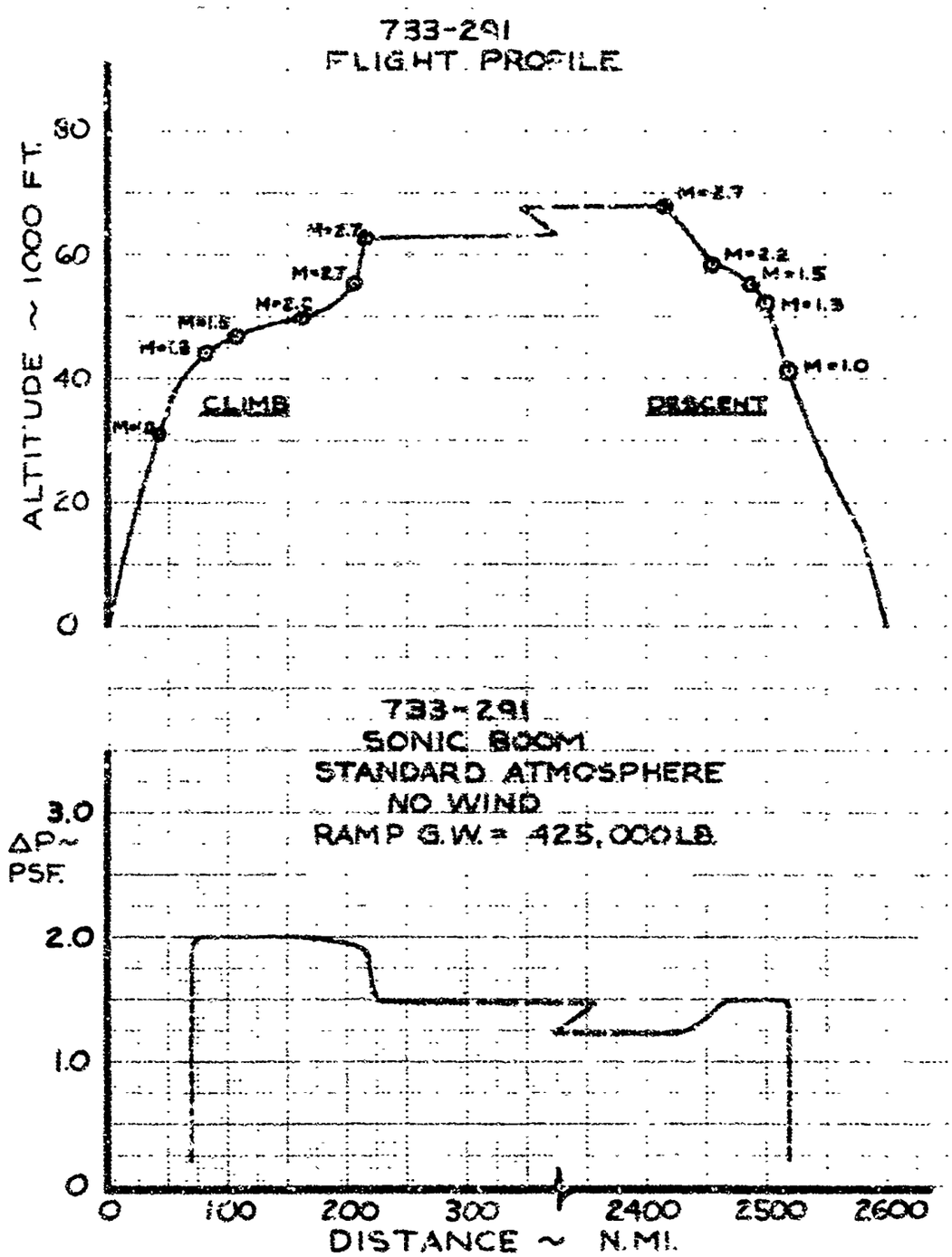


FIG. 2-2 733-291 SONIC BOOM UNDER THE FLIGHT TRACK

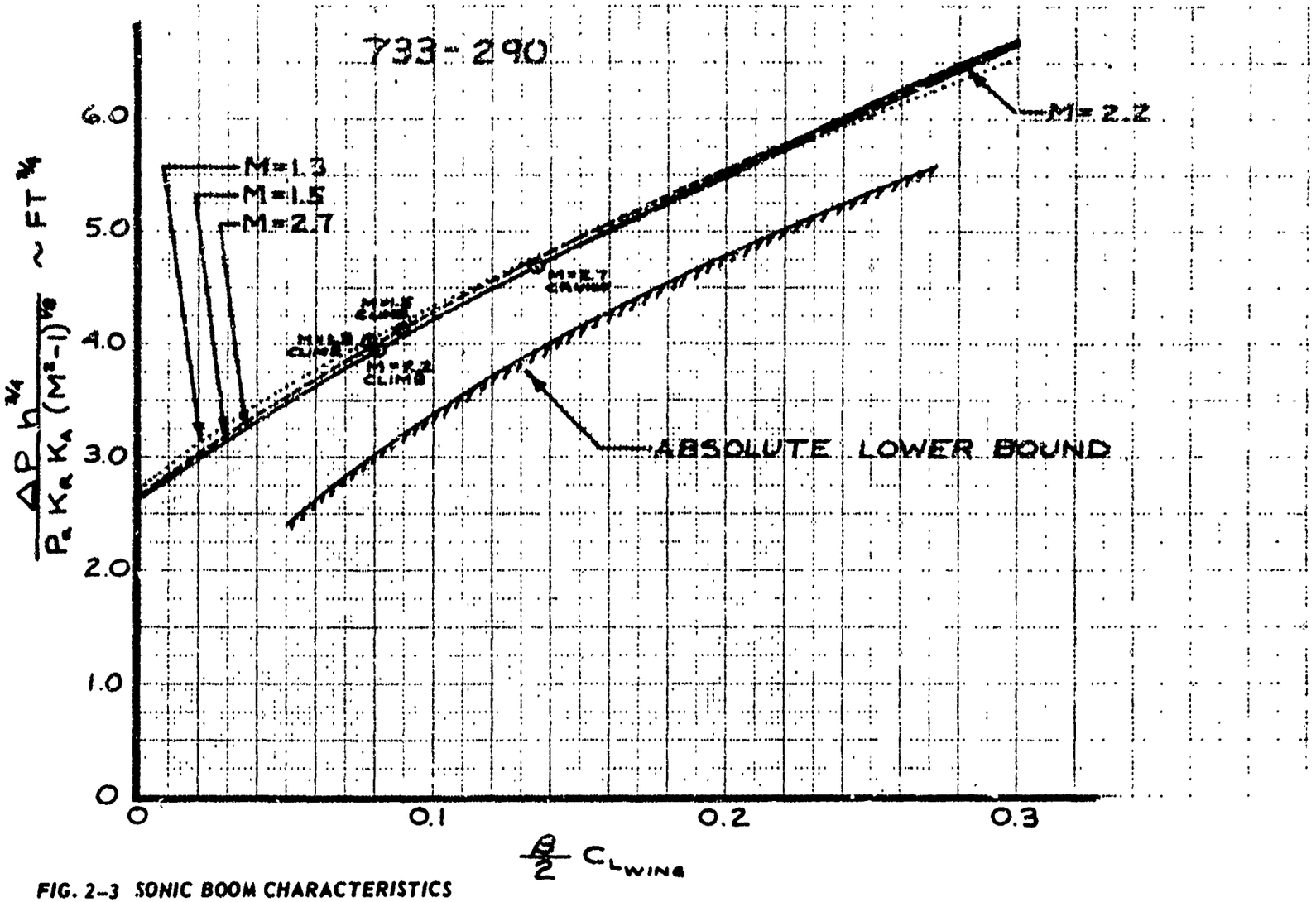


FIG. 2-3 SONIC BOOM CHARACTERISTICS

## 2.2 THEORETICAL BASIS FOR SONIC BOOM ANALYSIS

The sonic boom overpressure produced by an airplane is influenced primarily by the configuration geometry and lift distribution. The contribution of each component of the configuration, including lift, is determined by computing its F(y) function. This function was developed by G. B. Whitham and is defined in a paper published in 1952 (Ref. 2-2). The F(y) function is the key to the computation of sonic boom overpressures. It is defined by Eq. 2-1.

$$F(y) = \int_0^{\infty} \left[\frac{2}{\beta R(x)}\right]^{1/2} h\left[\frac{y - x}{\beta R(x)}\right] \frac{d\,S'(x)}{2\pi} \qquad \text{Eq. 2-1}$$

where:

$\beta = \sqrt{M^2 - 1}$

$S(x)$ = "equivalent body" area distribution

$R(x) = \sqrt{\frac{S(x)}{\pi}}$

$h\left[\frac{y - x}{\beta R(x)}\right] = h(z)$, and is a function plotted in Ref. 2-2.

$M$ = Mach number

$S'(x) = \frac{dS}{dx}$

The procedure used by The Boeing Company separates the configuration into its basic components and the lift of each: wing, fuselage, nacelles, horizontal tail, and vertical tail. An "equivalent body of revolution" is generated for each and the F(y) function is obtained. Finally, the F(y) functions are combined to obtain the sonic boom characteristics for the complete airplane.

Each component of the airplane is transferred from its own axis, X', along the appropriate Mach cutting planes to the axis of the configuration, X, where the "equivalent body" is generated (Fig. 2-4). The choice of Mach cutting planes is determined by the Mach number and angular location, $\phi$, of interest. Under the airplane, this angle is -90 degrees; to the side, it is zero degrees.

The "equivalent bodies" are obtained by defining each component of the configuration for use in a digital computer program (Ref. 2-3) which is also used to calculate the airplane wave drag. The lift induced by the nacelles is obtained by superimposing the nacelle flow field, calculated by the method of Ref. 2-2, on the wing planform. The resulting load distribution is integrated to determine the "equivalent body" for the nacelle lift. The contributions of the wing lift due to both camber and angle of attack are obtained by the use of another digital computer program (Ref. 2-4). The resulting "equivalent bodies" are transferred along the appropriate Mach plane cuts to the configuration axis.

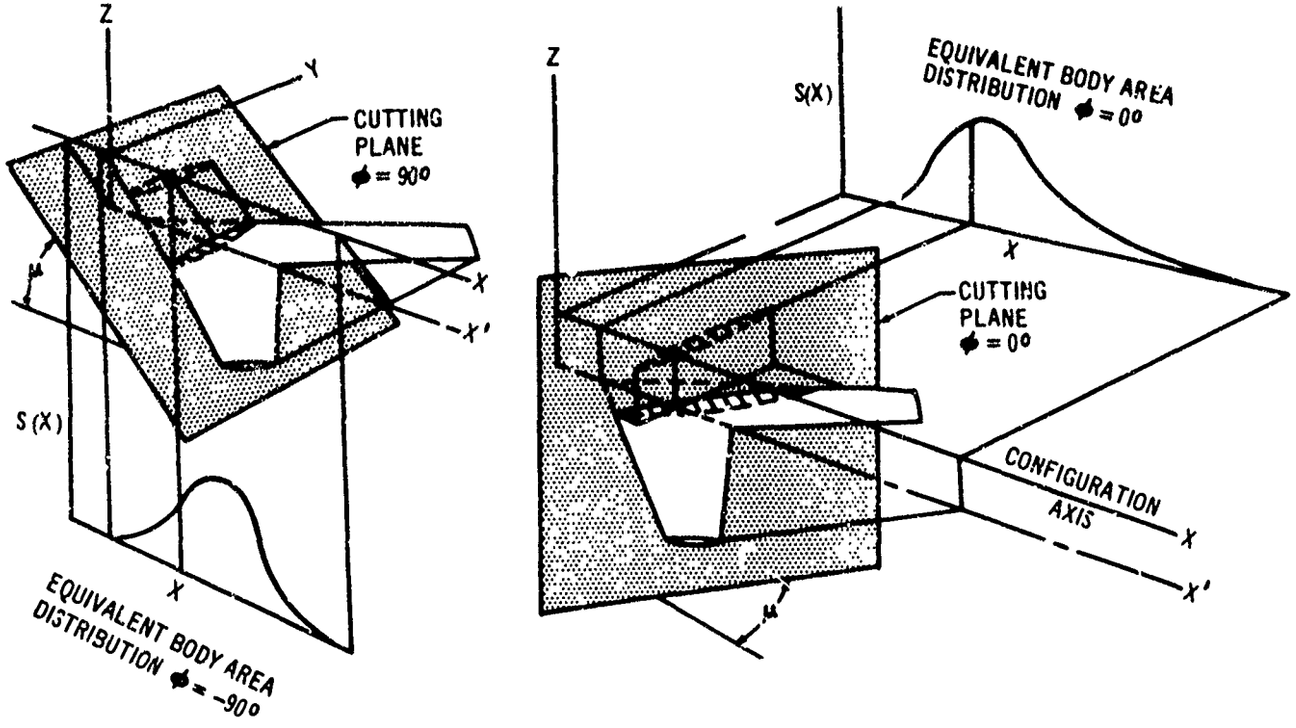


FIG. 2-4 MACH CUTTING PLANES

The expression for F(y) (Eq. 2-1) is readily amenable to digital computer analysis. The "equivalent body" of each component is converted to the individual F(y) function by the method of Ref. 2-1. The sonic boom for the complete configuration is determined by summing the individual F(y) functions and integrating the results according to Eq. 2-2.

$$I(y_o) = \int_o^{y_o} F(y)dy \qquad \text{Eq. 2-2}$$

where $y_o$ is the value of y for which I(y) is a positive maximum.

The sonic boom overpressure of the front shock on the ground is determined from Eq. 2-3.

$$\Delta P = P_a K_R K_A (M^2 - 1)^{1/8} \frac{2^{1/4}\gamma}{(\gamma + 1)^{1/2}} \frac{\left[I(y_o)\right]^{1/2}}{(h/-\sin\phi)^{3/4}} \qquad \text{Eq. 2-3}$$

where:

$P_a$ = ambient pressure at airplane altitude, psf

$K_R$ = ground reflectivity factor (1.9 in this document)

$K_A$ = atmospheric correction factor (square root of the ratio of ambient pressure at the airplane to that at the ground)

M = airplane Mach number

h = airplane altitude, ft

$\gamma$ = ratio of specific heat, 1.4

$\phi$ = Mach cutting plane angle

For $\phi$ = -90 degrees (directly under the flight path) Eq. 2-3 may be rearranged in the form below,

$$\frac{\Delta P\, h^{3/4}}{P_a K_R K_A (M^2 - 1)^{1/8}} = 1.075 \left[I(y_o)\right]^{1/2}$$

The right hand side of this equation is a function only of the configuration, Mach number, and the lift; it is the sonic boom characteristic of the airplane.

The theory (Ref. 2-2) and method have been well substantiated by both wind tunnel tests and flight tests. Examples were shown in the Phase I proposal. Subsequent comparisons with flight test data have been made during Phase II-A. These are shown in Fig. 2-5 where theoretical pressure wave signatures have been compared with observed signatures for the F-104A, F-101B, and B-58 airplanes. These comparisons show excellent agreement in detail — overpressure, signature shape, and trace length.

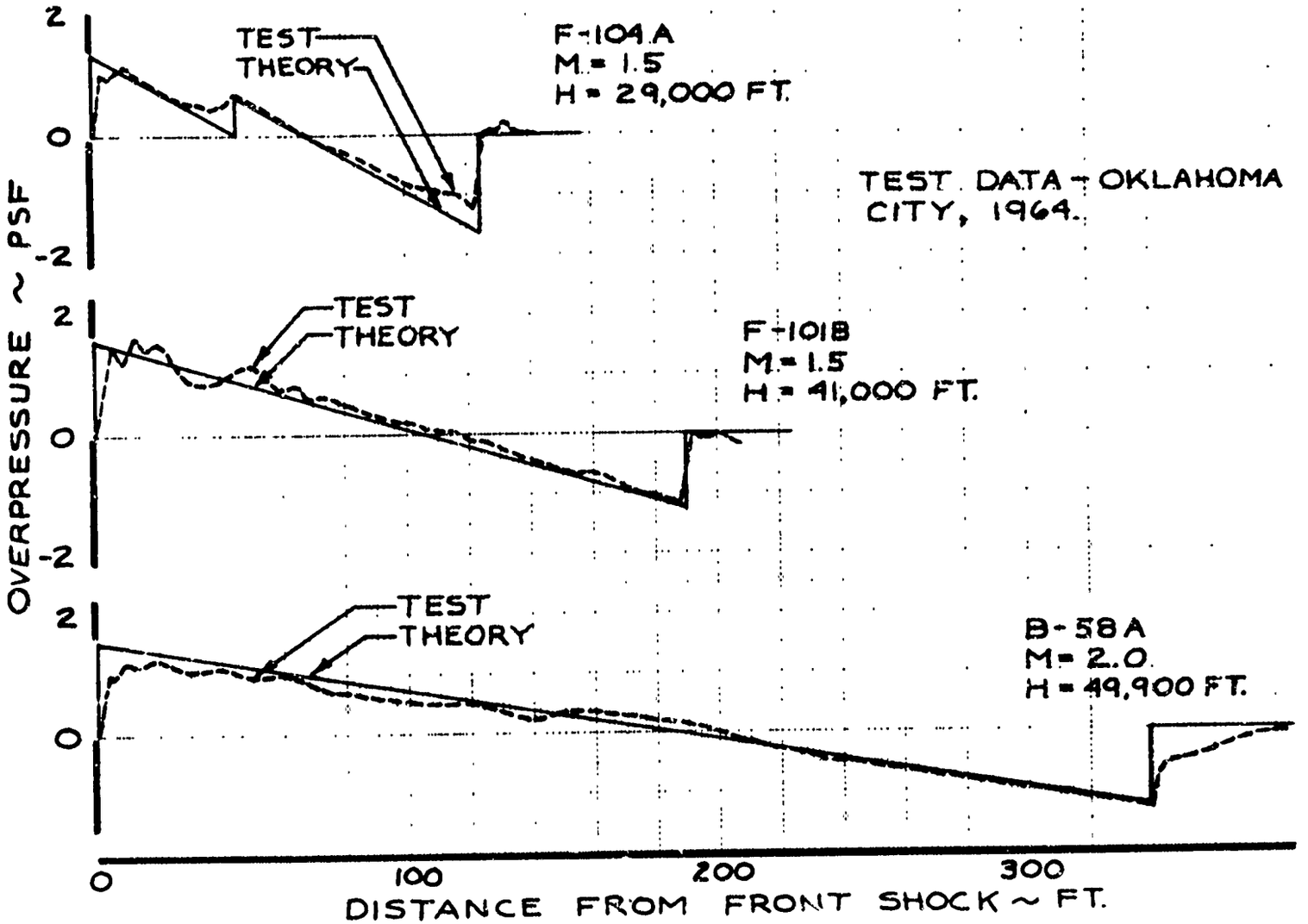


FIG. 2-5 COMPARISON OF PRESSURE WAVE SIGNATURES

## 2.3 ANALYSIS OF THE 733-290 AIRPLANE

The model 733-290 configuration is defined in Volume V-A, Book One, Aerodynamics. The geometric data provided there have been used in determining the sonic boom characteristics for the airplane. The "equivalent body" area distribution and the resulting F(y) function for each component are shown in Figs. 2-6 through 2-9 for Mach 2.7, 2.2, 1.5 and 1.3, respectively. The "volume" components which contribute to the strength of the front shock wave are the wing, fuselage, and nacelles including boundary layer diverters. The area distribution and F(y) function of each of these are shown on the left hand side of each figure. The "lift" components which contribute to the strength of the front shock wave are the wing camber and angle of attack lift, and the nacelle induced lift. The "equivalent" area distribution and F(y) function of each of these are shown on the right hand side of each figure. The lift coefficient of each component is noted.

The F(y) summations are shown in Fig. 2-10 for Mach 2.7, and in Fig. 2-11 for Mach 2.2, 1.5, and 1.3. The combination of the volume components and the combination of the volume-and-lift components are indicated in the plots. Only the components having their origin ahead of the point $y_o$ will contribute to the strength of the front shock wave (Ref. 2-2). It can be seen from the figures that the volume of the horizontal tail, vertical tail, and ventral fin as well as the horizontal tail lift do not contribute to the strength of the front shock wave. Since the tail lift does not contribute to the bow shock overpressure, the sonic boom parameters have been plotted as a function of the wing lift only. Care must be exercised to ensure that the lift of the wing alone is used in conjunction with Fig. 2-3 and the data in Par. 2.5.

It is shown in Ref. 2-6 that the effect of variations in atmospheric properties and winds are negligible for flight at the Mach numbers considered in the preceding discussion. At Mach numbers below 1.3 these variations become significant and are discussed in the following paragraphs.

## 2.4 ADDITIONAL CONSIDERATIONS

A discussion of the effects of the atmosphere on the boom for some very special circumstances, the effect of elastic deformations, and an evaluation of slight variations in calculation procedures follow.

### 2.4.1 Effect of Hot Day on Sonic Boom

Variations in atmospheric properties can affect the sonic boom overpressure at the ground. The influence of these variations has been studied for the arbitrary standard +20°F and +40°F hot days used to present performance data. The data in Fig. 2-12 show the temperature variation and resulting pressure altitude variation with tapeline altitude assumed in each of these model atmospheres. The effect of these variations from the standard conditions may be estimated from Eq. 2-4 (obtained from Ref. 2-6).

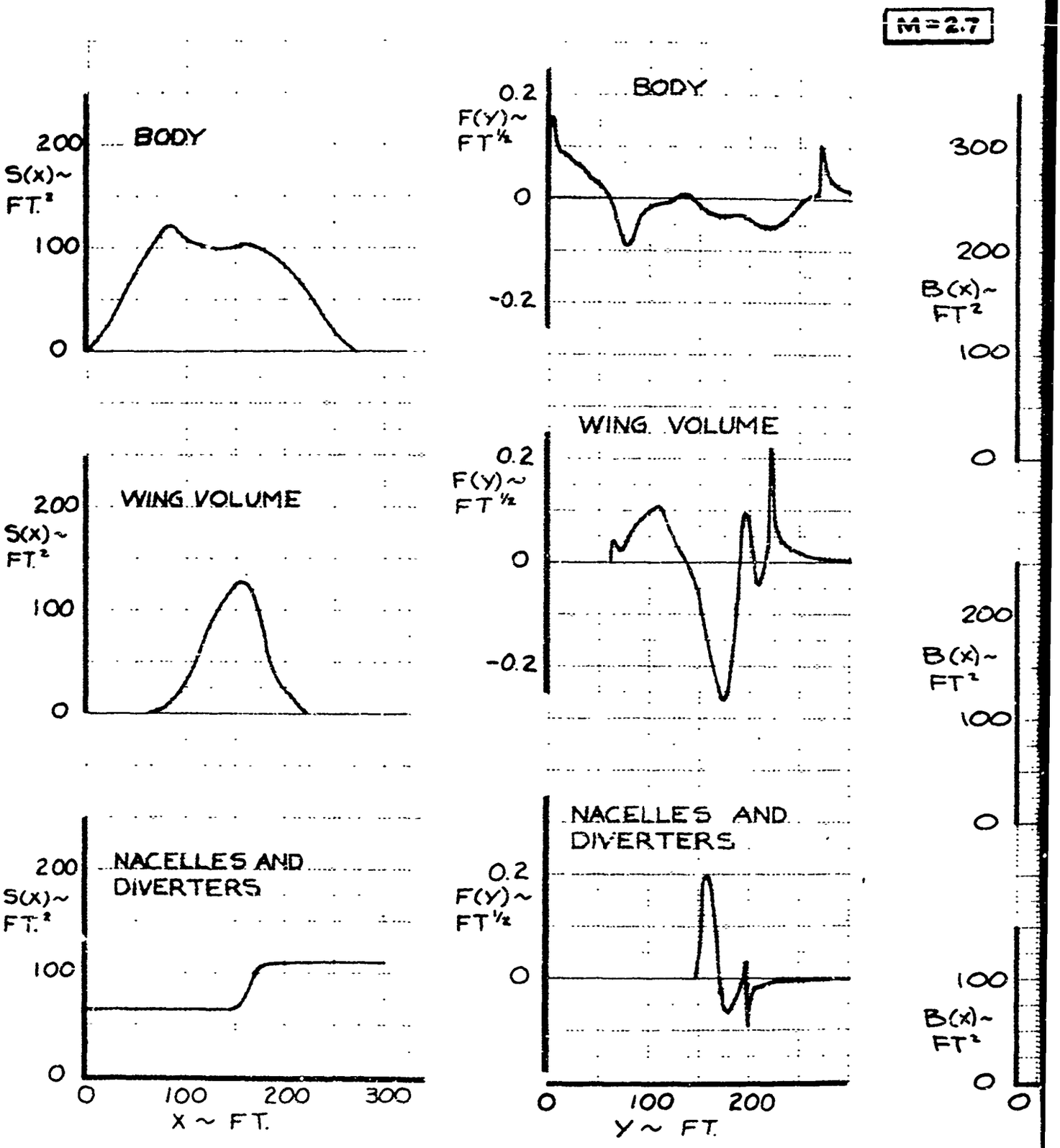


FIG. 2-6 COMPONENT AREA DISTRIBUTIONS AND F(Y) FUNCTIONS (M = 2.7)

A

M=2.7

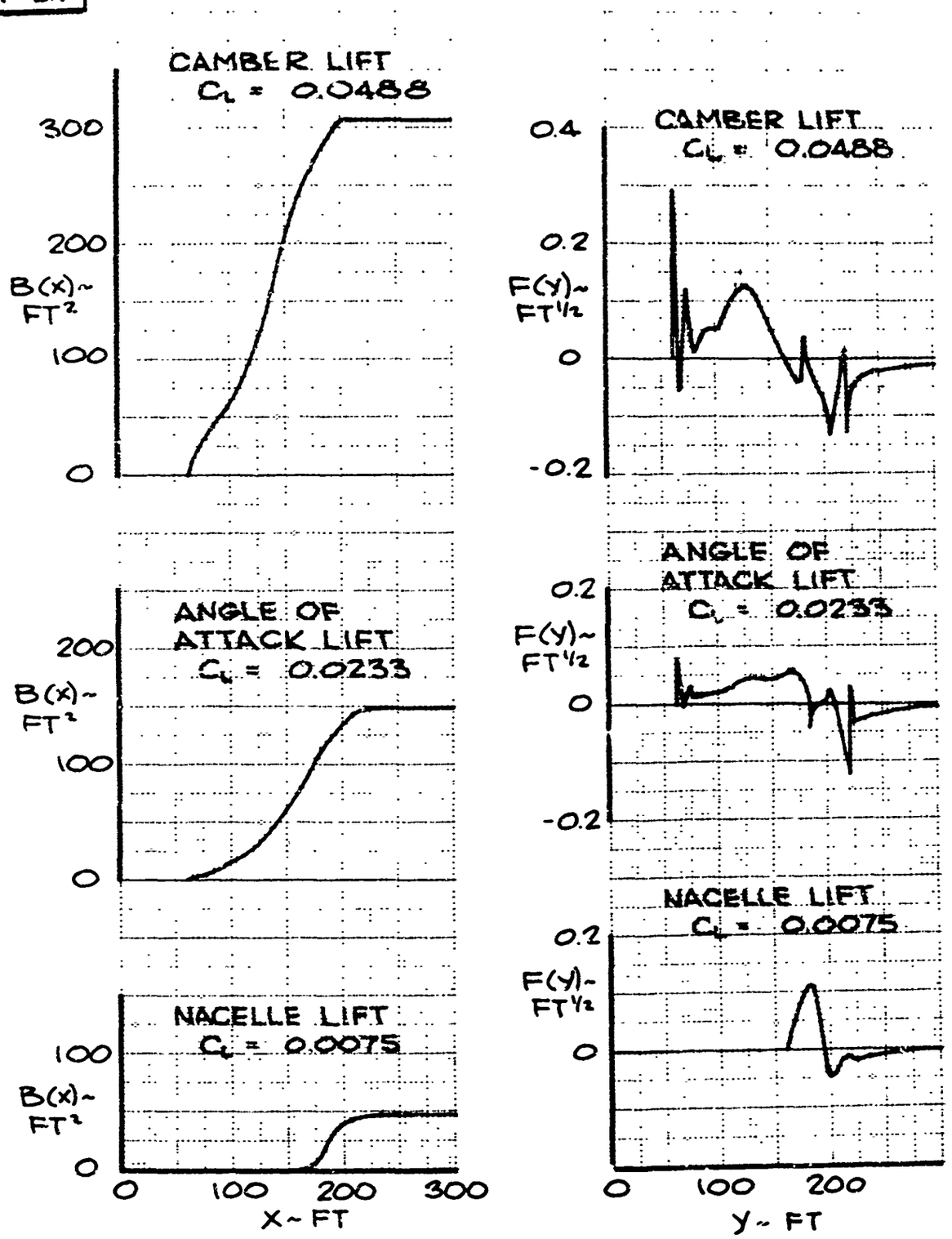
CAMBER LIFT
$C_L$ = 0.0488
300
200
B(x)~ FT²
100
0
ANGLE OF ATTACK LIFT
$C_L$ = 0.0233
200
B(x)~ FT²
100
0
NACELLE LIFT
$C_L$ = 0.0075
100
B(x)~ FT²
0
0
100
200
300
X~ FT
CAMBER LIFT
$C_L$ = 0.0488
0.4
0.2
F(y)~ FT^1/2
0
-0.2
ANGLE OF ATTACK LIFT
$C_L$ = 0.0233
0.2
F(y)~ FT^1/2
0
-0.2
NACELLE LIFT
$C_L$ = 0.0075
0.2
F(y)~ FT^1/2
0
0
100
200
y~ FT

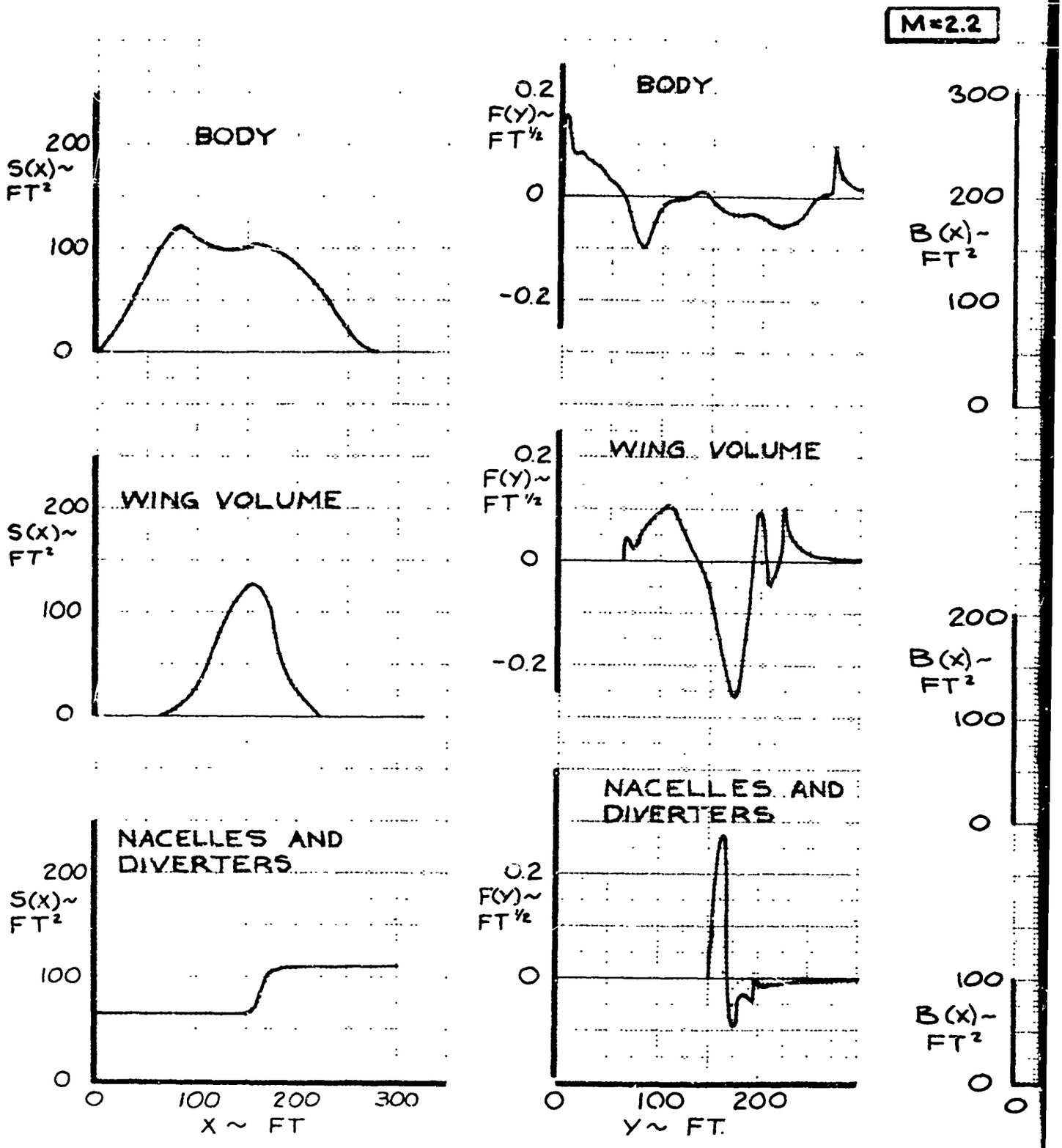


FIG. 2-7 COMPONENT AREA DISTRIBUTIONS AND F(Y) FUNCTIONS (M=2.2)

A

M=2.2

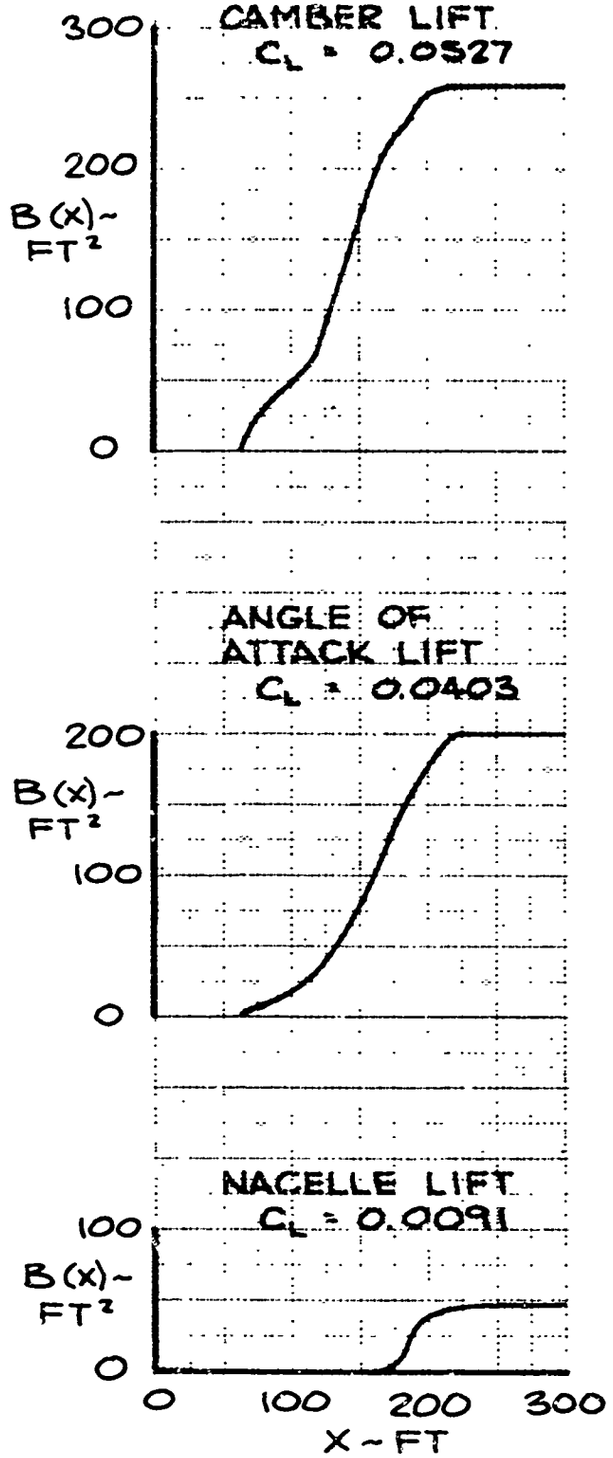
CAMBER LIFT
$C_L$ = 0.0527
300
200
100
0
B(x)~ FT²

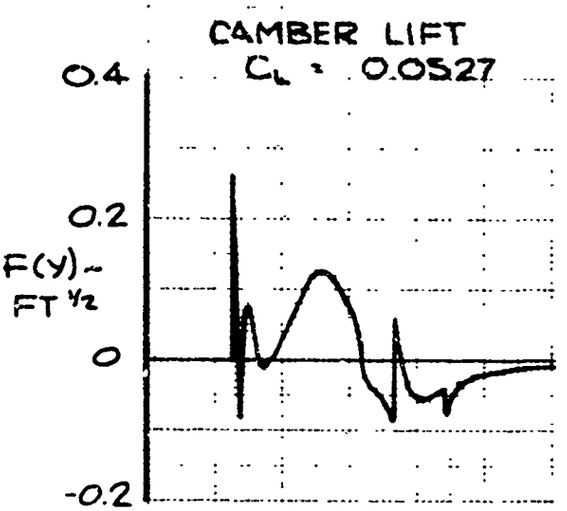
CAMBER LIFT
$C_L$ = 0.0527
0.4
0.2
0
-0.2
F(y)~ FT^1/2


ANGLE OF ATTACK LIFT
$C_L$ = 0.0403
200
100
0
B(x)~ FT²

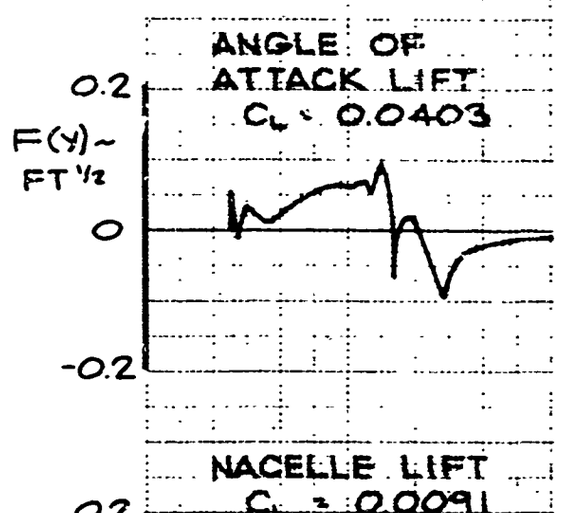
ANGLE OF ATTACK LIFT
$C_L$ = 0.0403
0.2
0
-0.2
F(y)~ FT^1/2


NACELLE LIFT
$C_L$ = 0.0091
100
0
B(x)~ FT²
0
100
200
300
X~FT

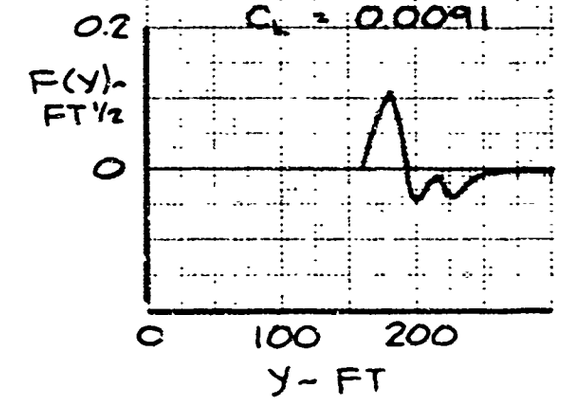
NACELLE LIFT
$C_L$ = 0.0091
0.2
0
F(y)~ FT^1/2
0
100
200
Y~FT

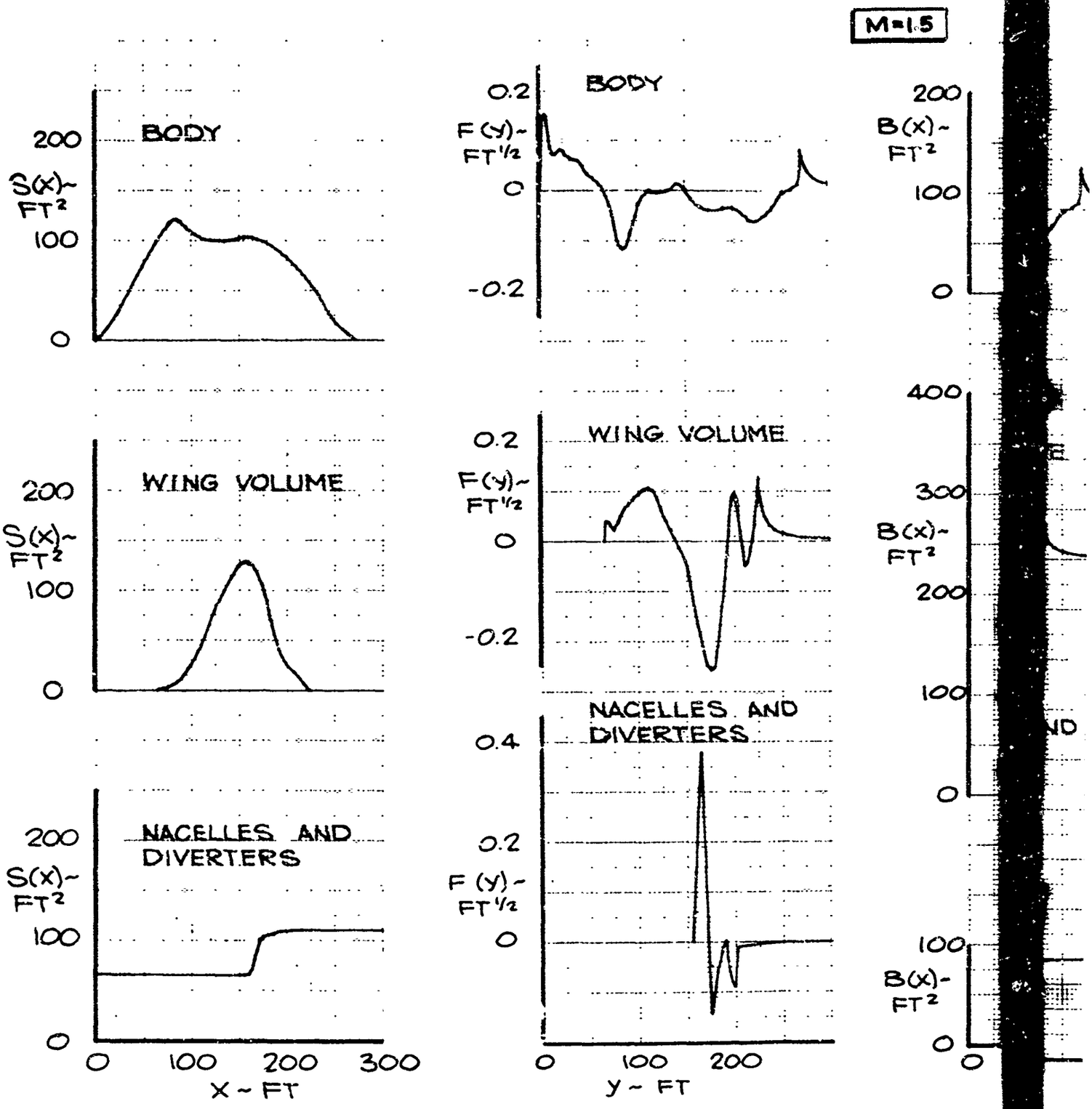


FIG. 2-8 COMPONENT AREA DISTRIBUTIONS AND F(Y) FUNCTIONS (M=1.5)

A

M=1.5

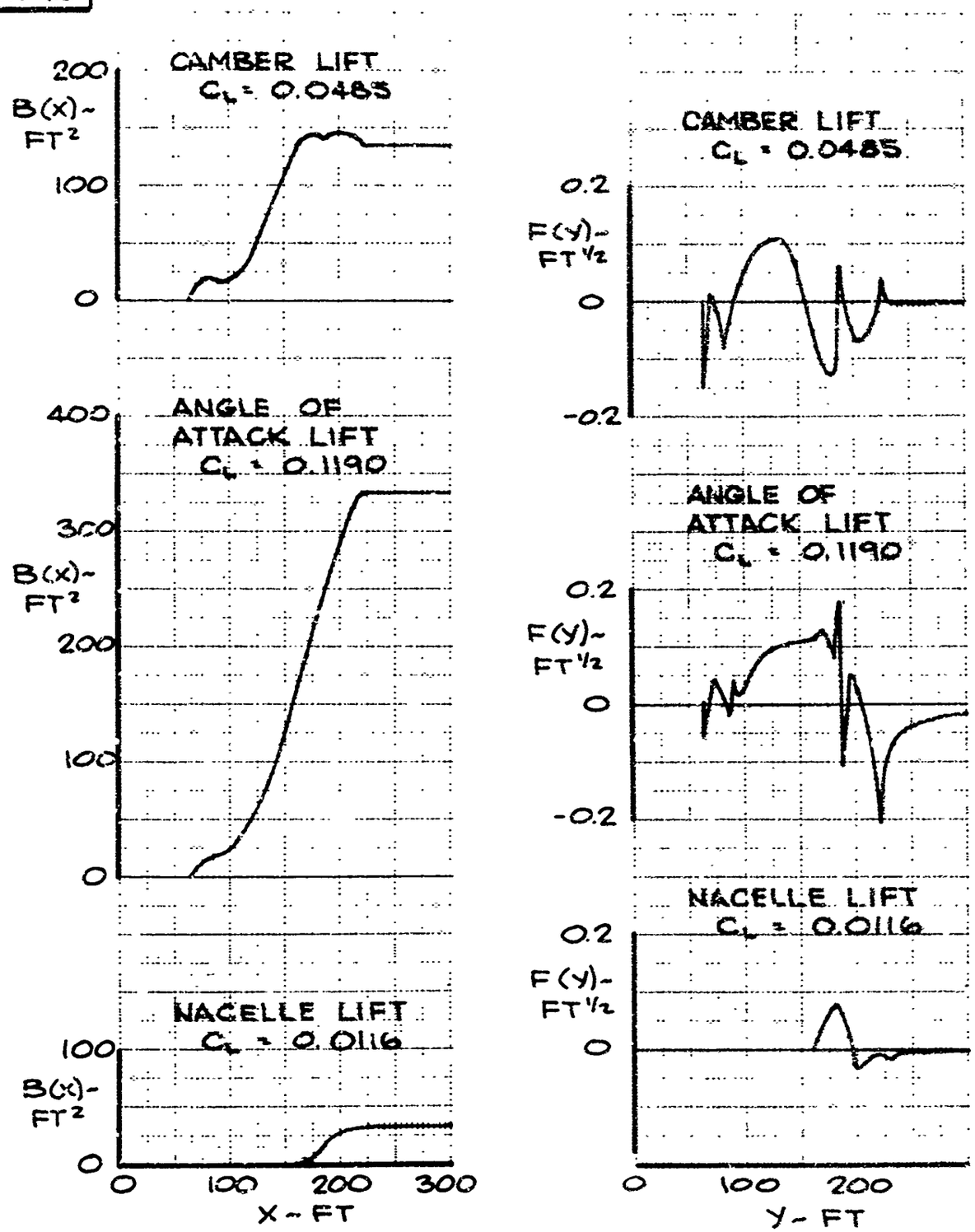
CAMBER LIFT
$C_L$ = 0.0485
B(x)-
FT²
200
100
0
ANGLE OF
ATTACK LIFT
$C_L$ = 0.1190
400
300
200
100
0
NACELLE LIFT
$C_L$ = 0.0116
100
0
0
100
200
300
X-FT
CAMBER LIFT
$C_L$ = 0.0485
F(y)-
FT^1/2
0.2
0
-0.2
ANGLE OF
ATTACK LIFT
$C_L$ = 0.1190
0.2
0
-0.2
NACELLE LIFT
$C_L$ = 0.0116
0.2
0
0
100
200
Y-FT

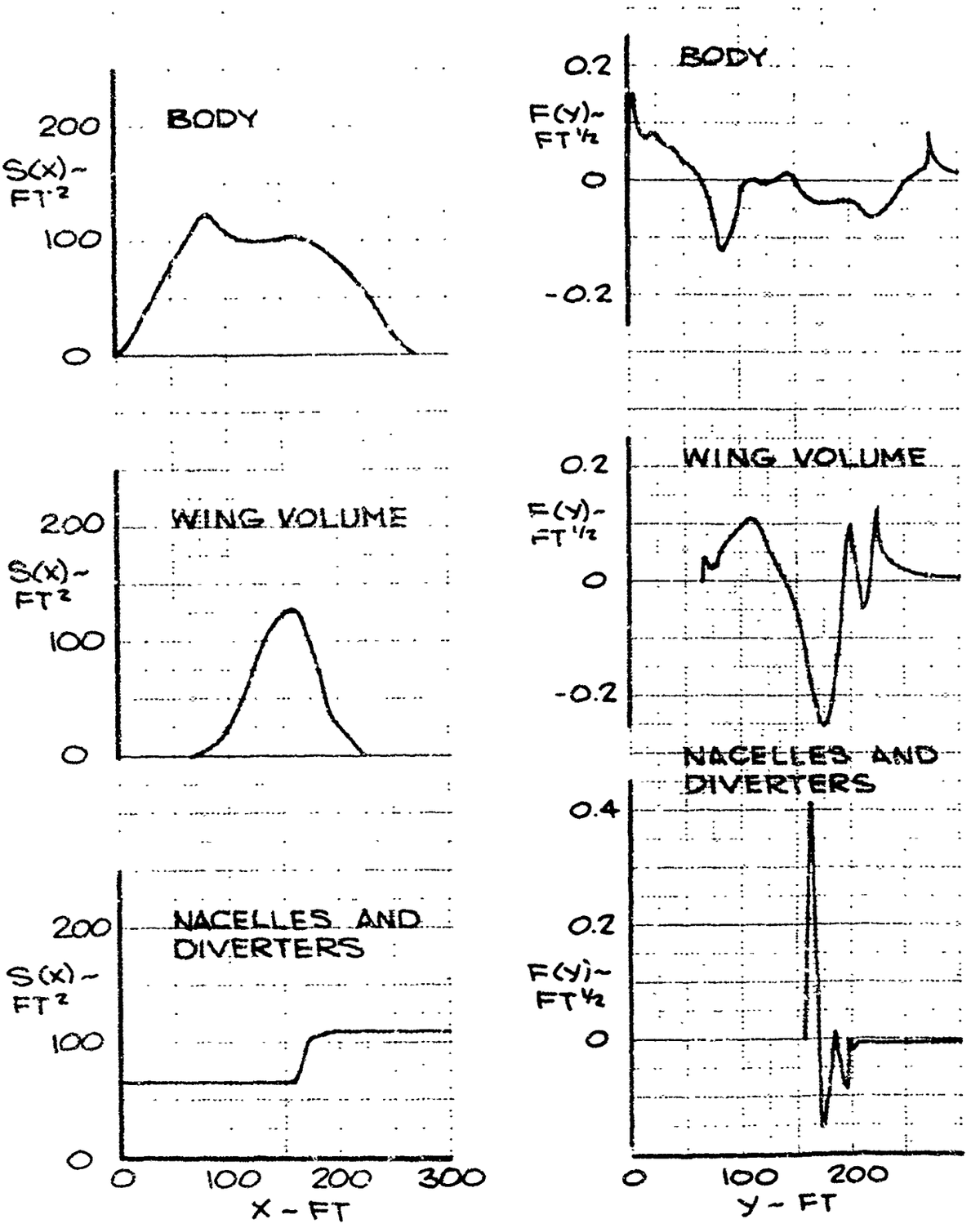


FIG. 2-9 COMPONENT AREA DISTRIBUTIONS AND F(y) FUNCTIONS (M = 1.3)

A

M=1.3

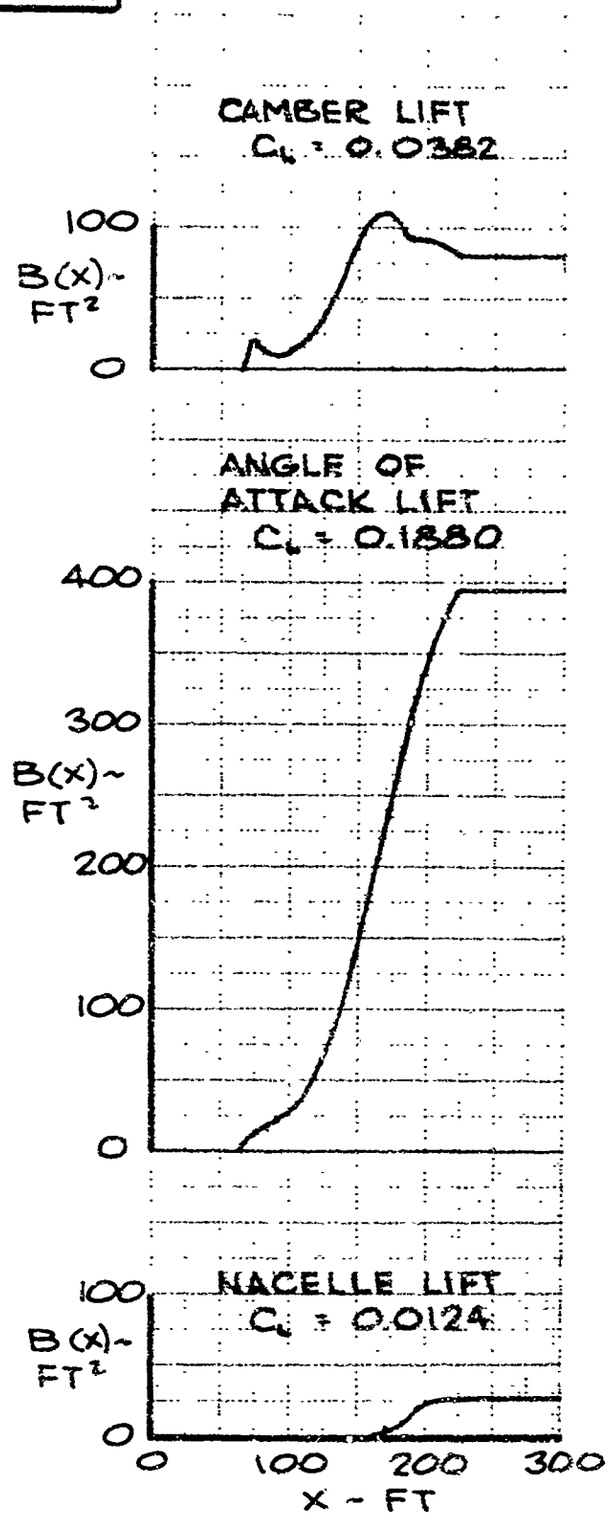
CAMBER LIFT
$C_L$ = 0.0382
100
B(X)-
FT²
0
ANGLE OF
ATTACK LIFT
$C_L$ = 0.1880
400
300
B(X)-
FT²
200
100
0
NACELLE LIFT
$C_L$ = 0.0124
100
B(X)-
FT²
0
0
100
200
300
X - FT

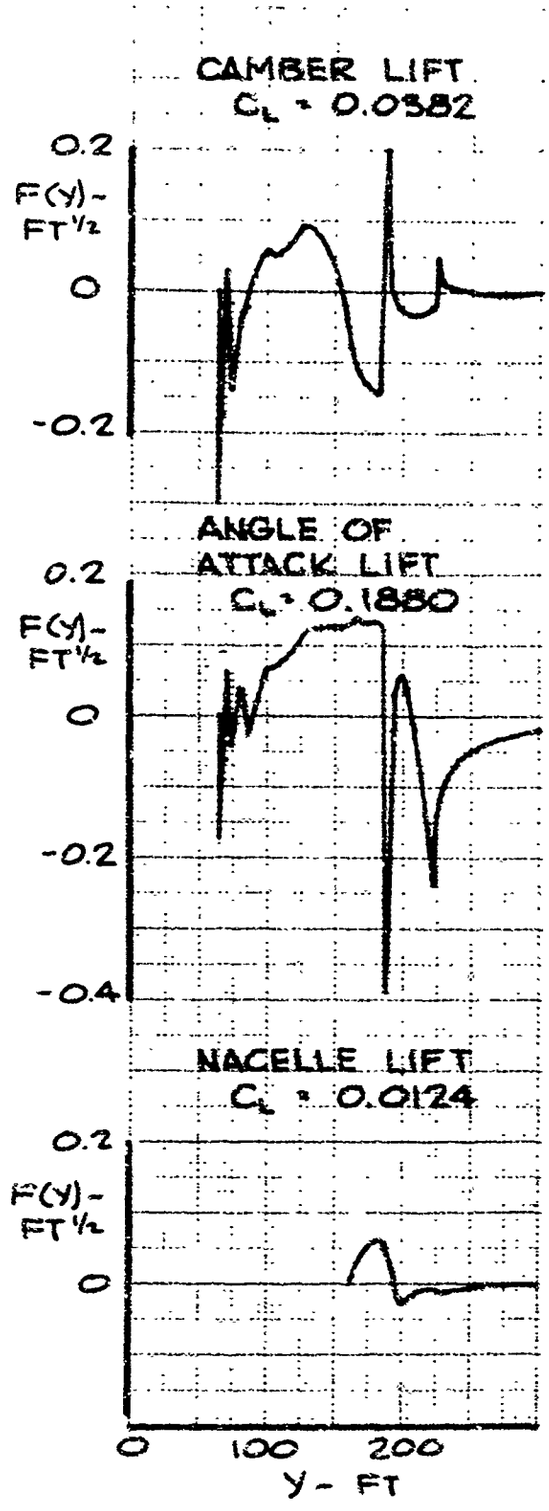
CAMBER LIFT
$C_L$ = 0.0382
0.2
F(Y)-
FT½
0
-0.2
ANGLE OF
ATTACK LIFT
$C_L$ = 0.1880
0.2
F(Y)-
FT½
0
-0.2
-0.4
NACELLE LIFT
$C_L$ = 0.0124
0.2
F(Y)-
FT½
0
0
100
200
Y - FT

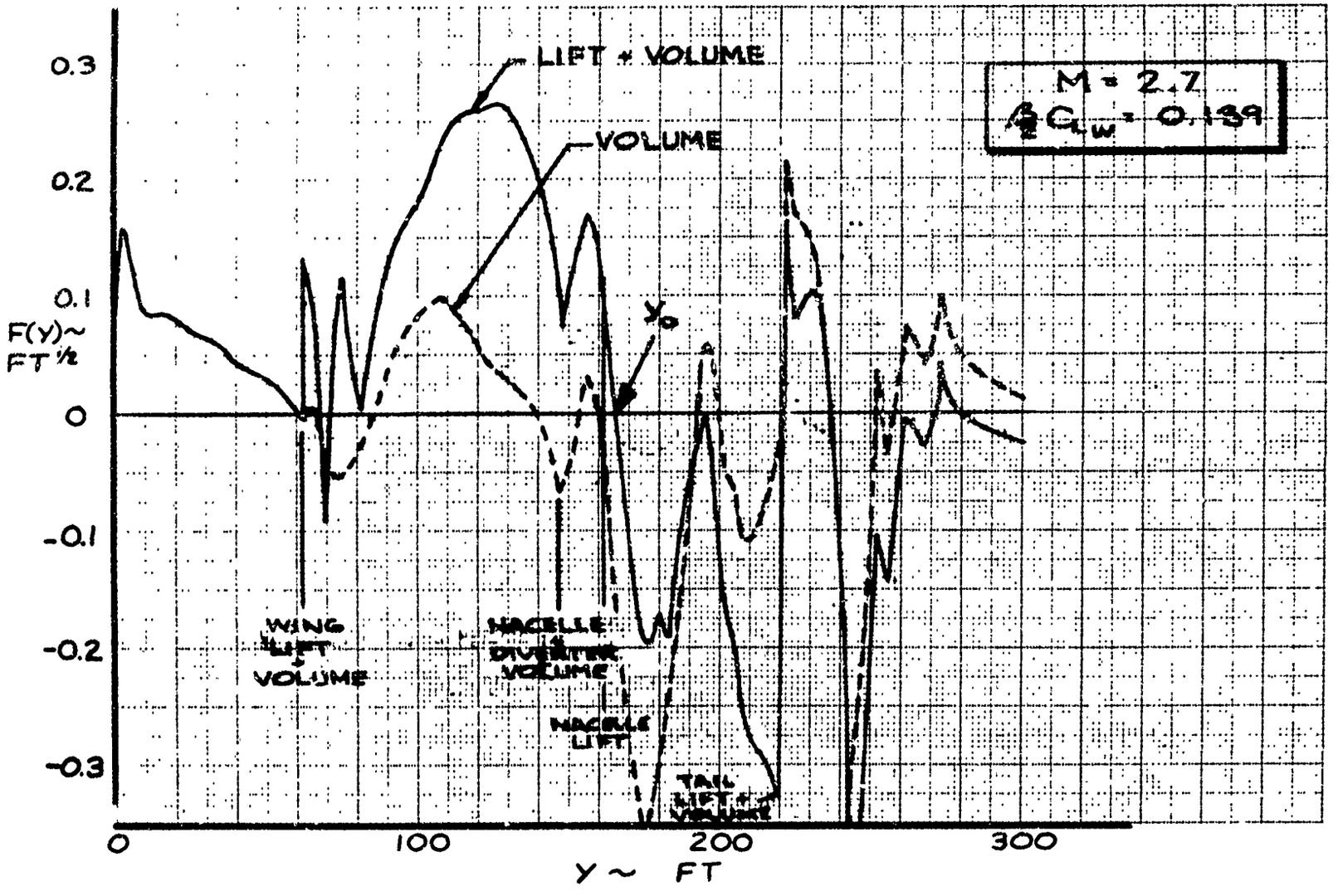


FIG. 2-10 COMBINED F(Y) FUNCTION M=2.7

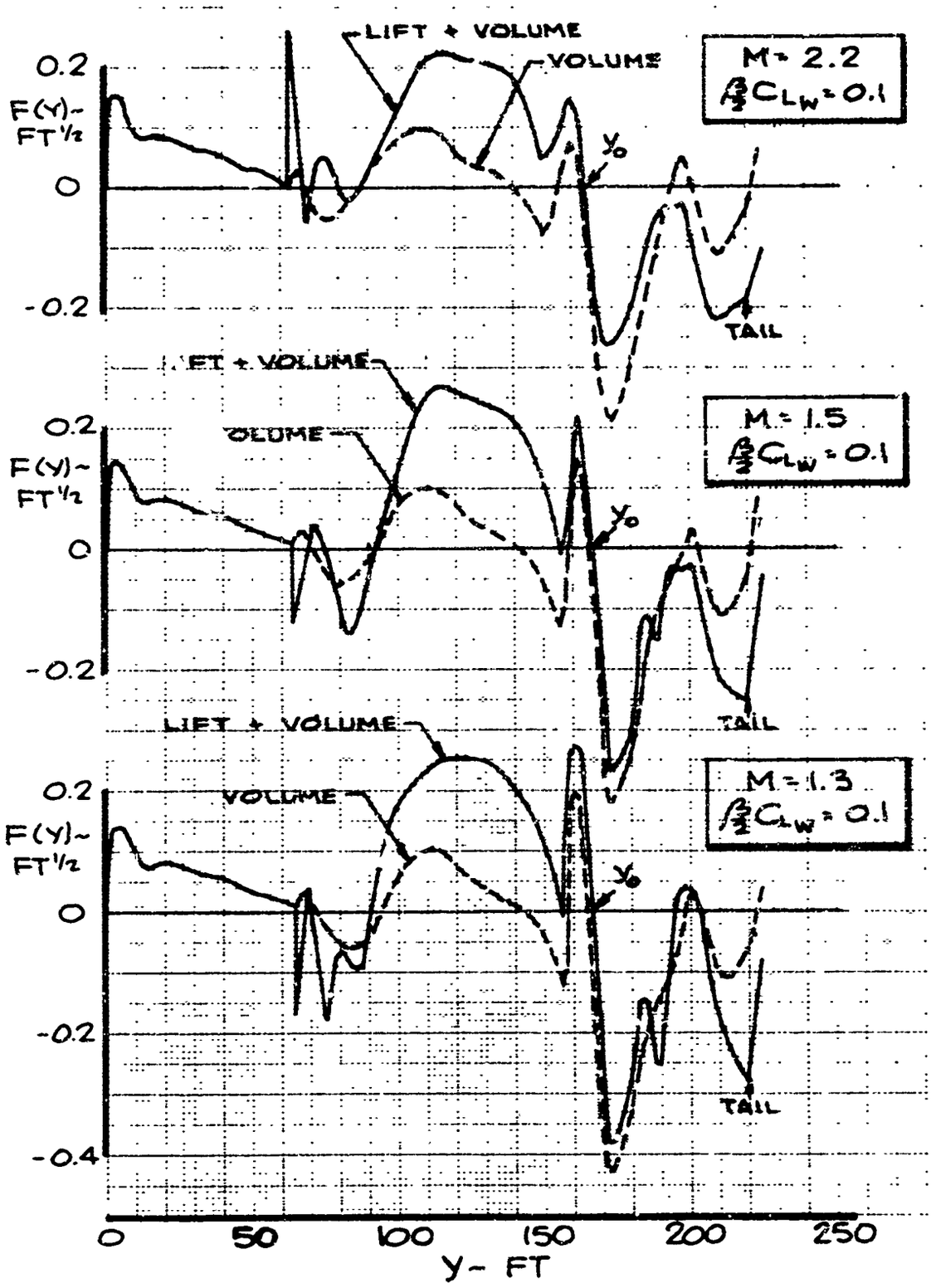


*FIG. 2-11 COMBINED F(Y) FUNCTION, M=2.2, 1.5, AND 1.3*

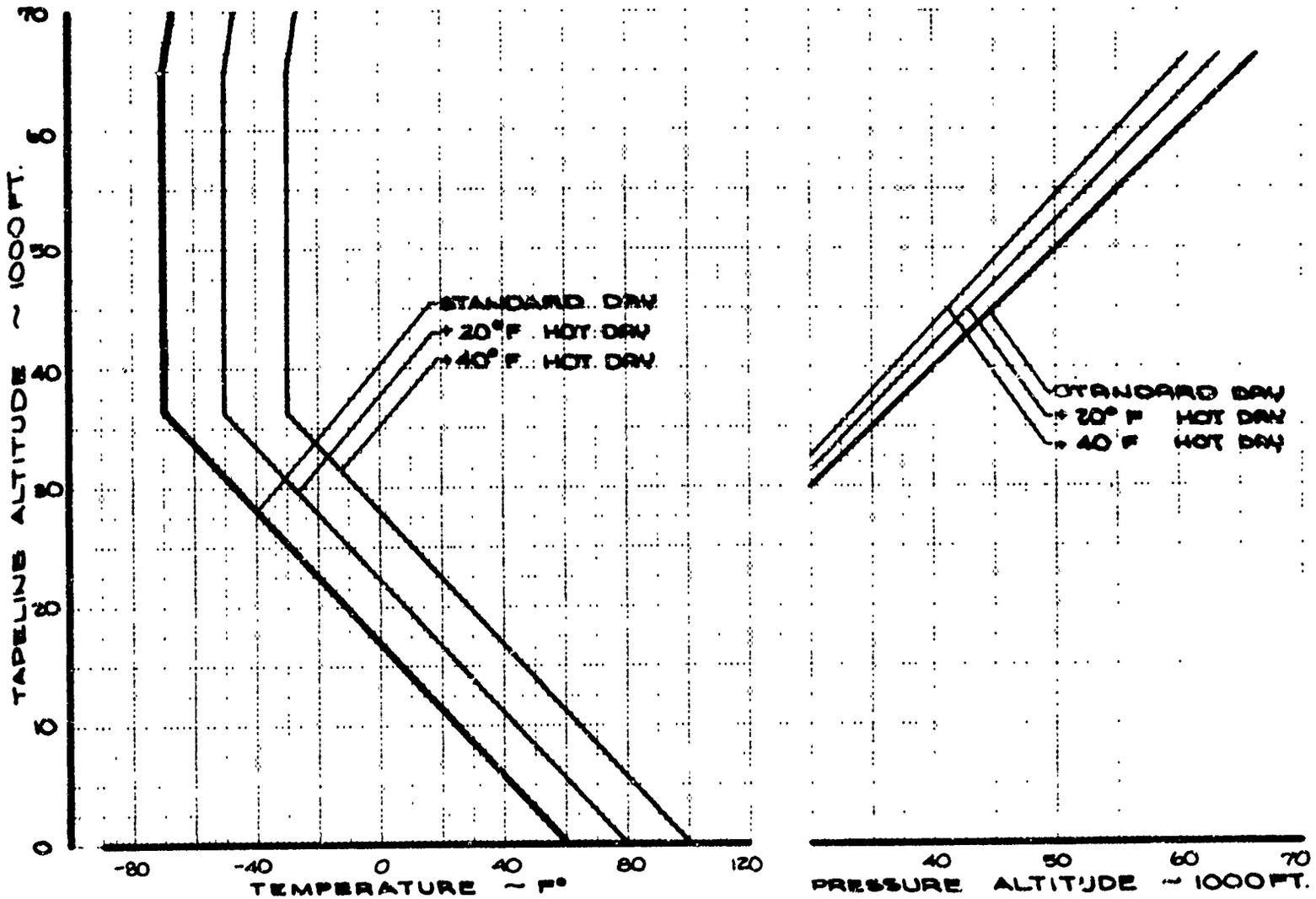


FIG. 2-12 HOT DAY MODEL ATMOSPHERES

$$\frac{\Delta P}{\Delta P_{std}} = \left[\frac{P_g}{(P_g)_{std}}\right]^{1/2} \left[\frac{P_a}{(P_a)_{std}}\right]^{1/4} K_T \frac{\left[I(y_o)\right]^{1/2}}{\left[I(y_o)_{std}\right]^{1/2}} \frac{(h_{std})^{3/4}}{(h)^{3/4}}$$

Eq. 2-4

where

$\Delta P$ = overpressure in model atmosphere

$\Delta P_{std}$ = overpressure in standard atmosphere

$P_g$ = ambient pressure at ground in model atmosphere

$(P_g)_{std}$ = ambient pressure at ground in standard atmosphere

$P_a$ = ambient pressure at airplane in model atmosphere

$(P_a)_{std}$ = ambient pressure at airplane in standard atmosphere

$K_T$ = temperature correction factor (Ref. 2-6)

$\left[I(y_o)\right]^{1/2}$ = sonic boom characteristic in model atmosphere

$\left[I(y_o)_{std}\right]^{1/2}$ = sonic boom characteristics in standard atmosphere

$h$ = height of airplane above the ground in model atmosphere

$h_{std}$ = height of airplane above the ground in standard atmosphere

The ambient pressure at the ground has been assumed to be 2116.22 psf in these atmospheric models. The airplane has been assumed to fly along a profile of fixed tapeline altitude versus Mach number independent of temperature. The sonic boom characteristics were taken as those in Fig. 2-3. The effect of the pressure and temperature variation is illustrated in Fig. 2-13 for various tapeline altitudes. Variations in $\left[I(y_o)\right]^{1/2}$ occur because of the ambient pressure change at the airplane and because of the variation in fuel consumption. The data in Fig. 2-14 illustrate the combination of these effects on the sonic boom as compared to that in the standard atmosphere for a number of Mach numbers during the initial phases of supersonic flight. These data show that the effect of hot day on the boom is quite small.

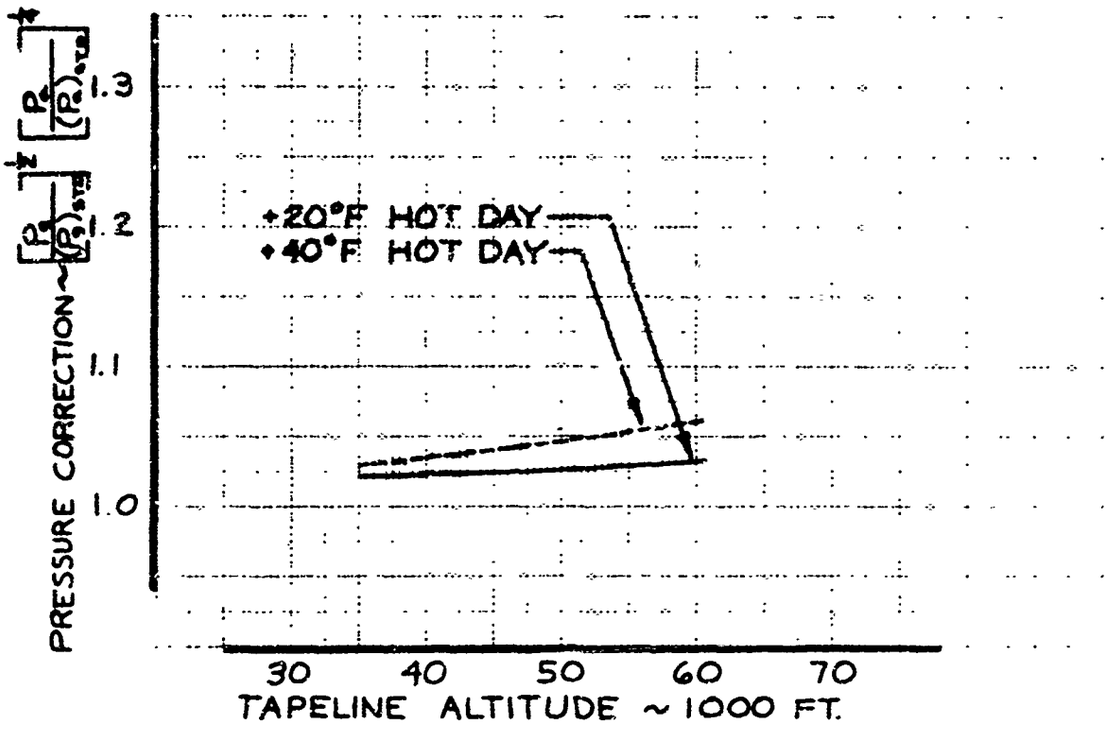


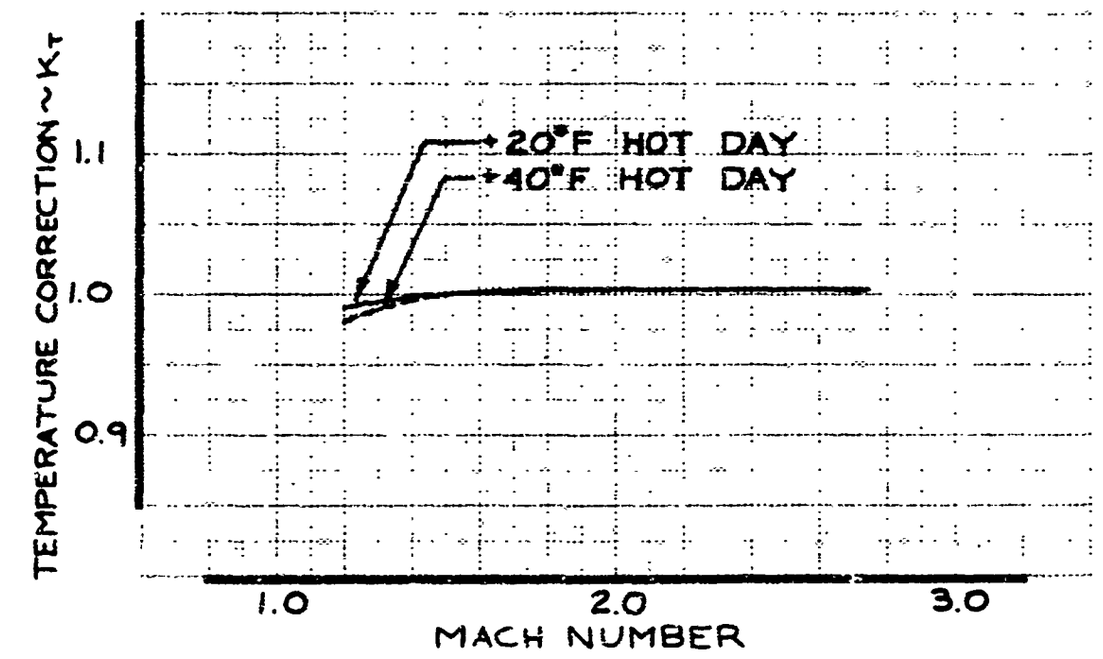


*FIG. 2-13 PRESSURE AND TEMPERATURE CORRECTIONS*

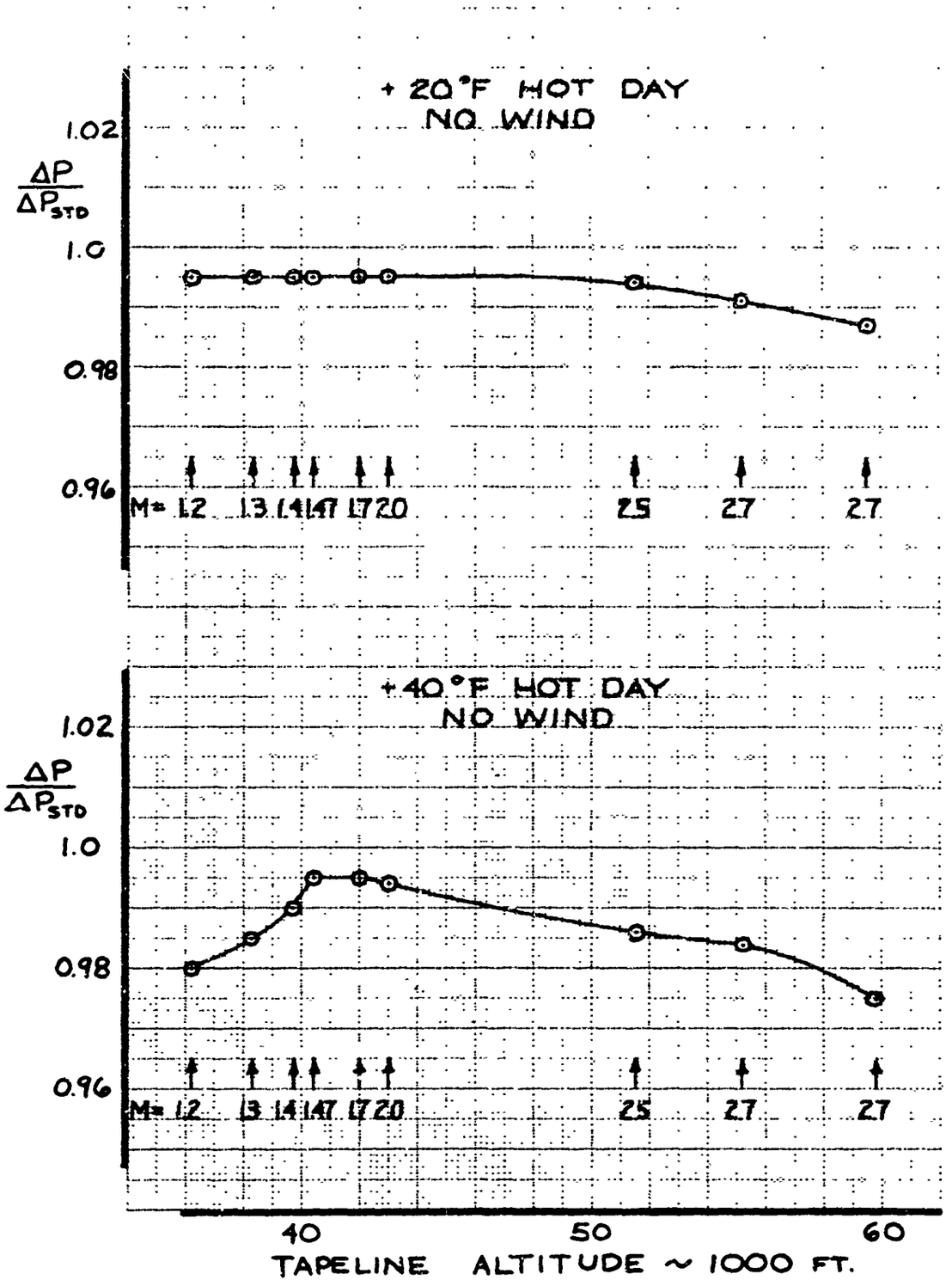


FIG. 2-14 EFFECT OF HOT DAY ON SONIC BOOM

A more general study of atmospheric effects on sonic boom, made over the range of conditions encountered in the northern hemisphere, is given in Ref. 2-6. The results of that study, when applied to the SST, show variations in overpressure from that in the standard atmosphere of ±3% at low Mach numbers and ±1% at Mach numbers above 1.5.

2.4.2 Sonic Boom at Mach Numbers Near 1.0

The sonic boom generated during flight at supersonic Mach numbers near 1.0 can reach the ground under special circumstances. For example, flight at Mach 1.02 at 31,000 feet in the standard atmosphere with a tailwind of 70 knots will result in the boom reaching the ground. The overpressure at the ground generated under these conditions has been calculated for the 733-290 to be 1.55 psf.

The shock wave produced at these low Mach numbers may be only one of several to reach a given point on the ground since the airplane is accelerating. The sketch in Fig. 2-15 illustrates the history of the shock front as it is developed during the acceleration through Mach 1.0. The figure shows that the shock wave generated at the cut-off Mach number will reach the ground after a shock wave generated at some higher Mach number. It can also be seen that the location of the cut-off ray on the ground determines the point beyond which only one pressure wave will be observed. The phenomena of two pressure signatures being recorded at the same point on the ground under an accelerating airplane has been observed during the tests discussed in Ref. 2-7.

2.4.3 Effect of Elasticity

The wing of the airplane is designed to have the required camber and twist at the average supersonic cruise condition. At off-design Mach numbers, the applied loads being approximately the same, the wing shape does not differ significantly from its shape at cruise. A check has been made of the effect on sonic boom due to the incremental variations in wing shape caused by changes in load distribution. The effect has been investigated for Mach 1.5 at representative weight and altitude. The comparison is shown in Fig. 2-16 and indicates that the aeroelastics effects are small. The assumption used in the sonic boom calculation herein is that the wing shape does not change with Mach number.

2.4.4 Comparison of Calculation Procedures

The calculation of the function F(y) for the airplane following the method outlined in Ref. 2-1 may be considered in a number of ways. The procedure used in this document has been to calculate this function individually from the area distribution of each component of the airplane and then to sum these functions to calculate the shock wave strength. Another approach is to superimpose the individual area distributions of all the components and then to calculate the F(y) function from the combined area distribution. The first of these methods is equivalent to superimposing in the farfield the perturbation velocities calculated for

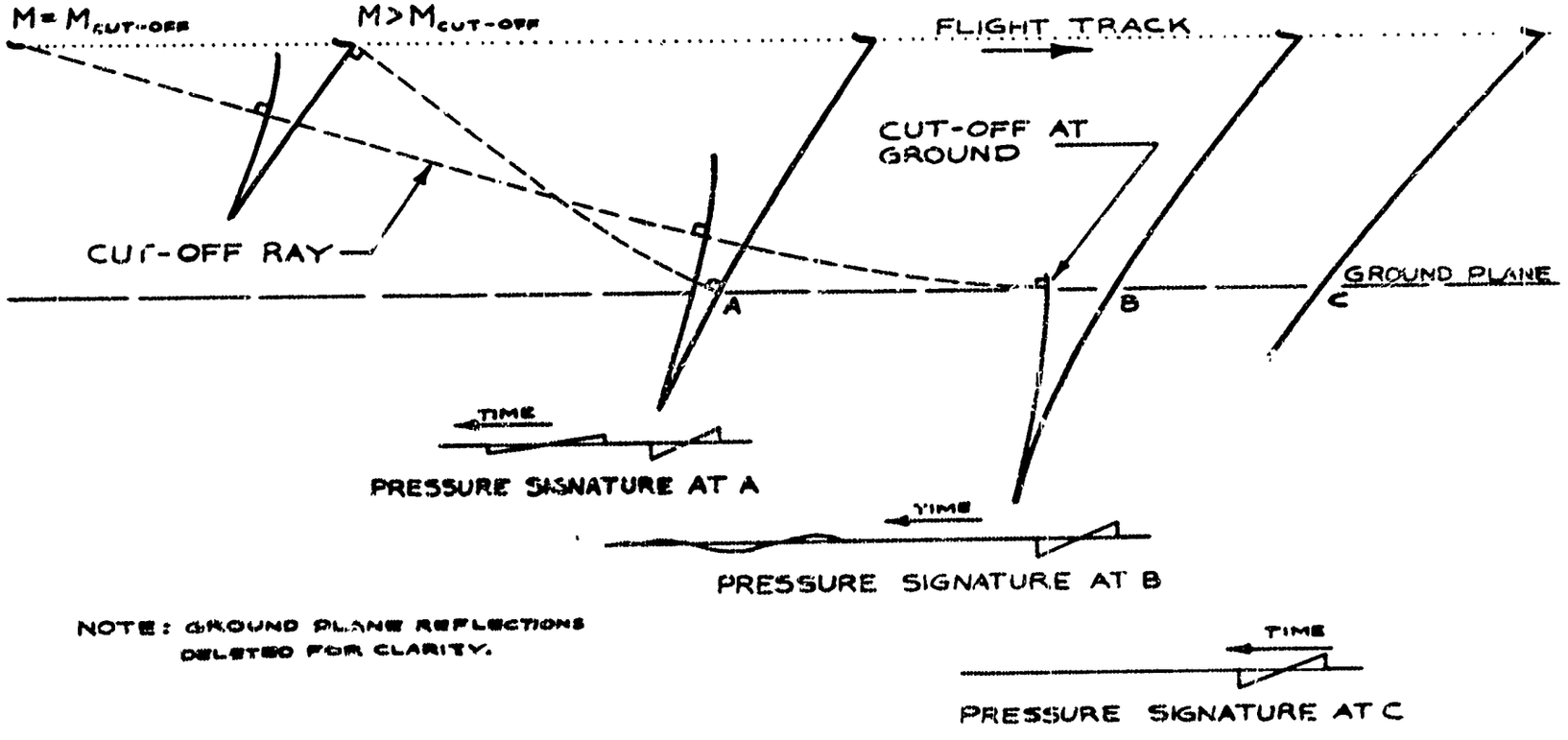


NOTE: GROUND PLANE REFLECTIONS DELETED FOR CLARITY.

D6-8560-7



FIG. 2-15 SHOCK PATTERNS DURING INITIAL ACCELERATION

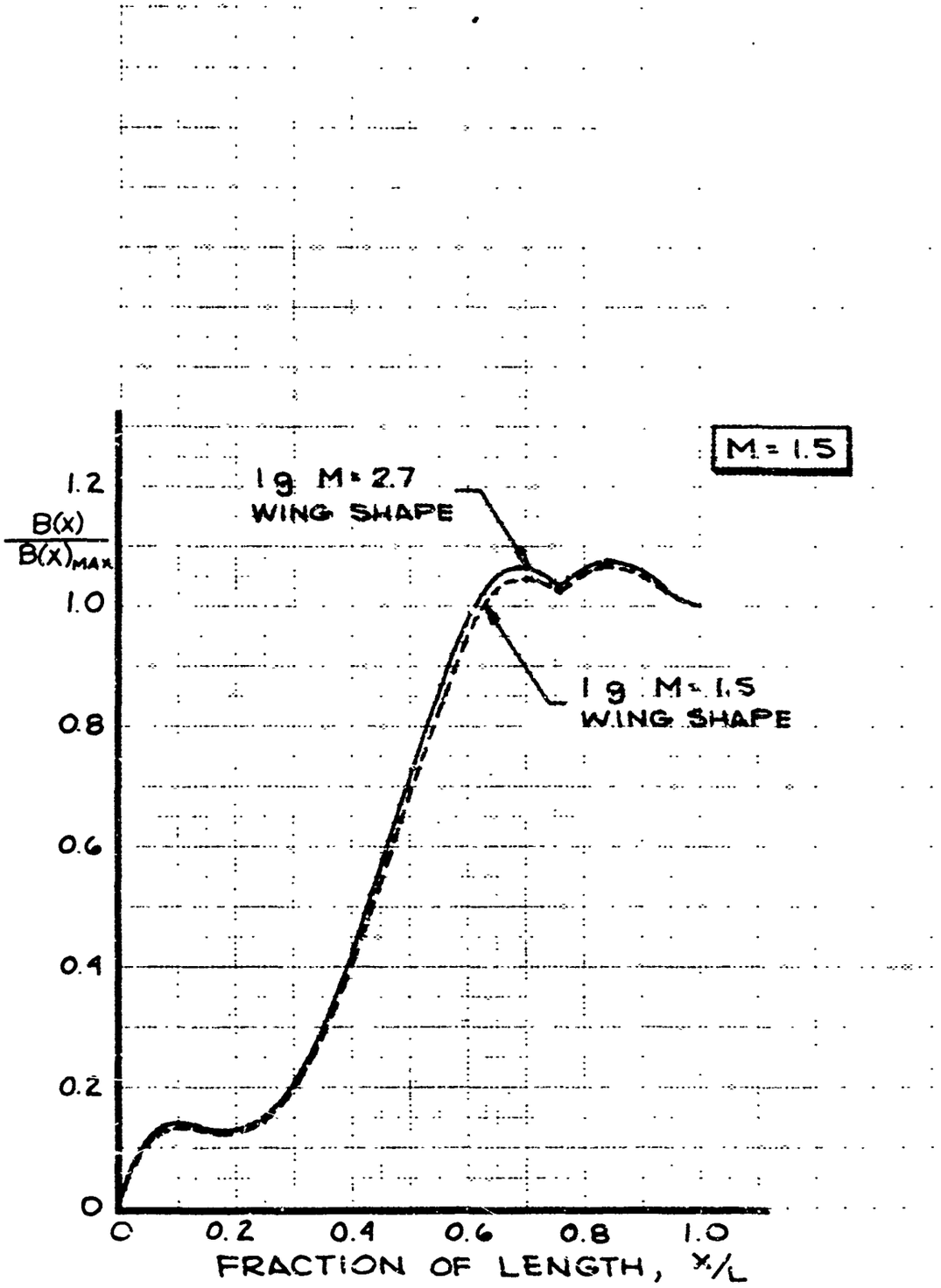


FIG. 2-16 EFFECT OF WING AEROELASTICITY AT MACH 1.5 $C_L$ WING = 0.158

every component of the aircraft. In the second method the singularities that are used in the analysis to define the airplane are superimposed to produce a combined "equivalent body." Velocity perturbations due to this "equivalent body" are then computed. These two methods have been compared. The Mach 1.0 area distribution of the configuration was used and is shown in Fig. 2-17. The resulting F(y) functions obtained by the two methods are compared in Fig. 2-18. The two curves are similar in most respects. The sonic boom characteristics differ by less than 1 percent, which is negligible.

## 2.5 TABULATED COMPUTER DATA

The digital computer program inputs used in determining the area distributions of the volume components are shown in Fig. 2-19. These are in a form suitable for use in the NASA Langley Computer Program P7120. The computer input data for the program which computes the "equivalent lift" area distributions for the wing are shown in Fig. 2-20. These are in a form suitable for use in the NASA Langley Computer Program P916.C.

The sonic boom characteristics for the Model 733-290 airplane have been put in nondimensional form. These are plotted and tabulated in Fig. 2-21 for Mach 2.7, 2.2, 1.5 and 1.3.

## 2.6 REFERENCES

Copies of the following referenced data may be obtained by making a request to either:

The Boeing Company
Suite 120 Commonwealth Building
1625 K Street
Washington 6, D.C.

or

The Boeing Company
Airplane Division
P.O. Box 707
Renton, Washington
Attn: M. L. Pennell, Organization 6-2000, Mail Stop 73-60


2-1 FAA Letter to Mr. M. L. Pennell from Mr. Gordon Bain, dated September 8, 1964, concerning "Sonic Boom Calculation Methods to be Used for the Phase II-A Evaluation."

2-2 Whitham, G. B., "The Flow Pattern of a Supersonic Projectile," Communications on Pure and Applied Mathematics. Vol. V, pages 301 to 348, 1952.

2-3 Palmer, R. L., "Two Computer Programs for Finding the Generalized Wave Drag of Wings and/or Wing Body Combinations." Boeing Document D6-6507 TN, 1963.

2-4 Carlson, H. and Middleton, W., "A Numerical Method of Estimating and Optimizing the Supersonic Aerodynamic Characteristics of Wings of Arbitrary Planform." AIAA Preprint No. 64-590, Aug. 1964.

2-5 Brown, J. R., "Influence of Non-Smooth Geometrics on Sonic Boom." Boeing Document D6-2430, 1964.

2-6 Kane, E. J., and Palmer, T. Y., "Meteorological Aspects of Sonic Boom." FAA SRDS Report (number to be assigned), 1964.

2-7 Hubbard, H. H., Maglieri, D. J., Huckel, V. and Hilton, D. A., "Ground Measurement of Sonic Boom Pressures for the Altitude Range of 10,000 to 75,000 Feet." NASA TR R-198, 1964.

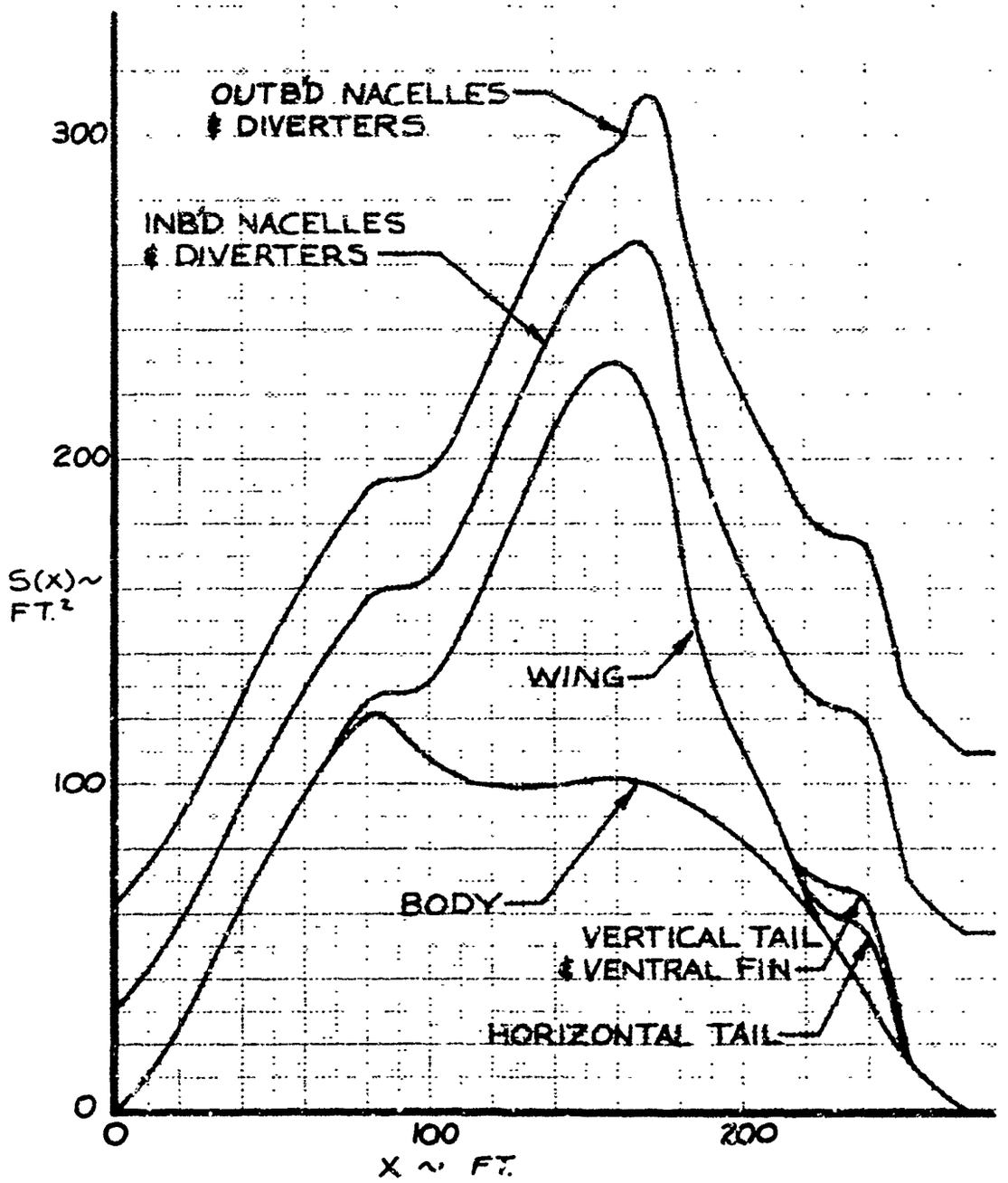


FIG. 2-17 MACH 1.0 AREA DISTRIBUTION

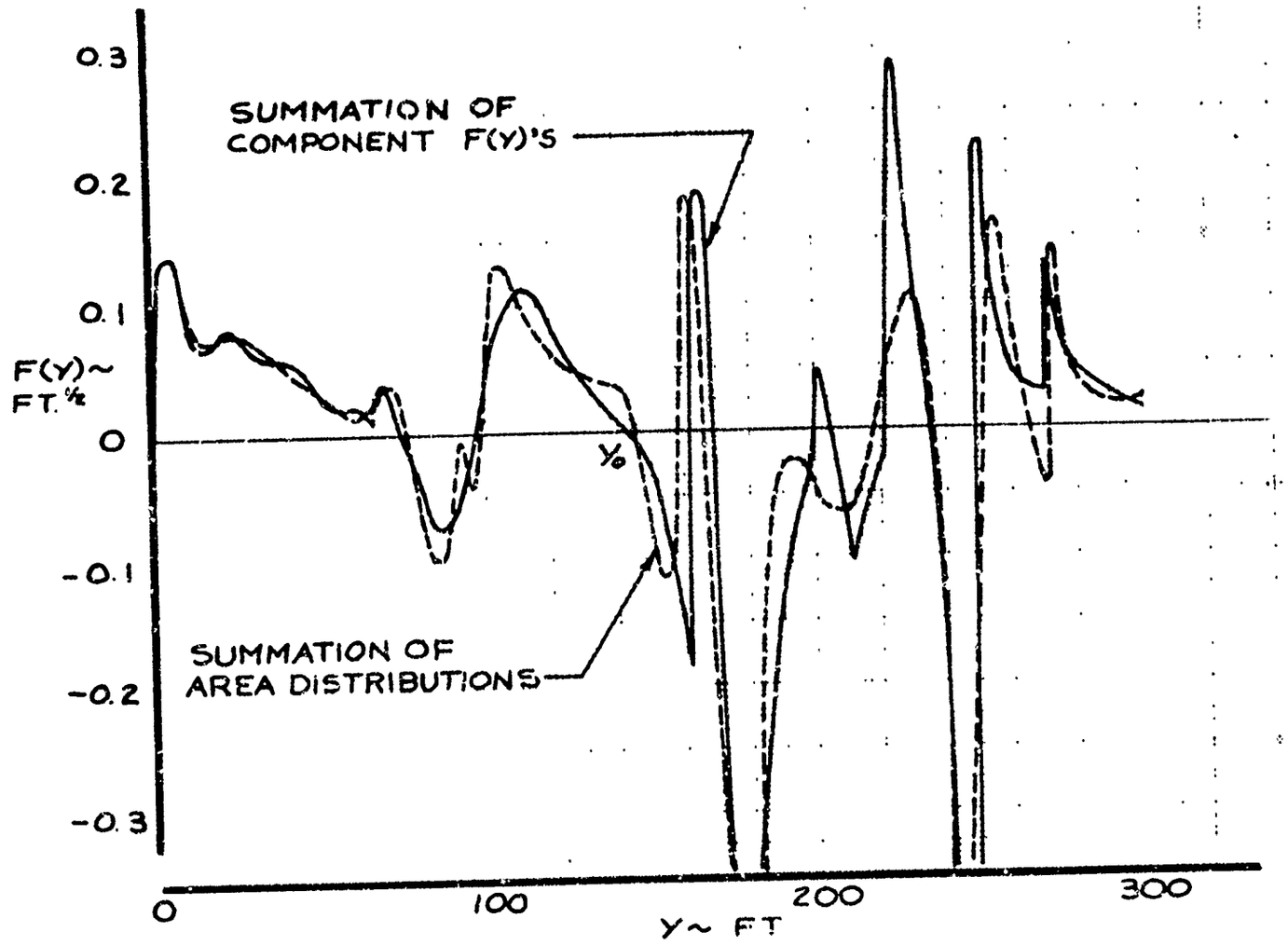


FIG. 2-18 COMPARISON OF F(Y) FUNCTIONS (M=1.0)

733-290 AREA DISTRIBUTION INPUTS

| | | | | | | | | | | |
|---|---|---|---|---|---|---|---|---|---|---|
| 0.0 | 0.5 | 2.5 | 5.0 | 10.0 | 15.0 | 20.0 | 25.0 | 30.0 | 35.0 | XAF1 |
| 40.0 | 45.0 | 50.0 | 55.0 | 60.0 | 65.0 | 70.0 | 75.0 | 80.0 | 85.0 | XAF2 |
| 90.0 | 95.0 | 100.0 | | | | | | | | XAF3 |
| 66.254 | 5.625 | -2.5 | 121.917 | | | | | | | WORG1 |
| 83.333 | 7.792 | -2.5 | 104.838 | | | | | | | WORG2 |
| 92.00 | 8.250 | -2.5 | 96.171 | | | | | | | WORG3 |
| 100.0 | 10.965 | -2.5 | 80.171 | | | | | | | WORG4 |
| 130.492 | 20.872 | -2.5 | 57.679 | | | | | | | WORG5 |
| 188.482 | 39.714 | -2.5 | 36.631 | | | | | | | WORG6 |
| 217.695 | 46.206 | -2.5 | 0.0 | | | | | | | WORG7 |
| 0.0 | .117 | .329 | .494 | .732 | .929 | 1.102 | 1.249 | 1.382 | 1.507 | WAF1-1 |
| 1.623 | 1.693 | 1.716 | 1.715 | 1.706 | 1.647 | 1.555 | 1.406 | 1.215 | .971 | WAF1-2 |
| .679 | 0.357 | 0.0 | | | | | | | | WAF1-3 |
| 0.0 | .181 | .399 | .580 | .873 | 1.129 | 1.363 | 1.548 | 1.687 | 1.786 | WAF2-1 |
| 1.845 | 1.875 | 1.882 | 1.876 | 1.837 | 1.751 | 1.622 | 1.464 | 1.260 | .997 | WAF2-2 |
| .706 | .361 | 0.0 | | | | | | | | WAF2-3 |
| 0.0 | .197 | .464 | .708 | 1.055 | 1.330 | 1.543 | 1.700 | 1.826 | 1.912 | WAF3-1 |
| 1.952 | 1.968 | 1.960 | 1.947 | 1.889 | 1.802 | 1.653 | 1.480 | 1.275 | 1.012 | WAF3-2 |
| .708 | .346 | 0.0 | | | | | | | | WAF3-3 |
| 0.0 | .326 | .631 | .899 | 1.251 | 1.505 | 1.691 | 1.833 | 1.940 | 2.007 | WAF4-1 |
| 2.040 | 2.050 | 2.047 | 2.027 | 1.965 | 1.863 | 1.719 | 1.535 | 1.310 | 1.045 | WAF4-2 |
| .736 | .389 | 0.0 | | | | | | | | WAF4-3 |
| 0.0 | .36 | .693 | .986 | 1.373 | 1.652 | 1.856 | 2.012 | 2.129 | 2.203 | WAF5-1 |
| 2.239 | 2.250 | 2.246 | 2.225 | 2.156 | 2.045 | 1.886 | 1.635 | 1.438 | 1.147 | WAF5-2 |
| .808 | .427 | 0.0 | | | | | | | | WAF5-3 |
| 0.0 | .20 | .385 | .548 | .763 | .918 | 1.031 | 1.118 | 1.183 | 1.224 | WAFT-1 |
| 1.244 | 1.250 | 1.248 | 1.236 | 1.198 | 1.136 | 1.048 | .936 | .799 | .637 | WAFT-2 |
| .449 | .237 | 0.0 | | | | | | | | WAFT-3 |
| 0.0 | .20 | .385 | .548 | .763 | .918 | 1.031 | 1.118 | 1.183 | 1.224 | WAFT-1 |
| 1.244 | 1.250 | 1.248 | 1.236 | 1.198 | 1.136 | 1.048 | .936 | .799 | .637 | WAFT-2 |
| .449 | .237 | 0.0 | | | | | | | | WAFT-3 |
| 0.0 | 10.0 | 20.0 | 30.0 | 40.0 | 50.0 | 60.0 | 75.0 | 83.2 | 90.0 | XFUS |
| 100.0 | 120.0 | 135.0 | 145.0 | 157.0 | 170.0 | 185.0 | 200.0 | 215.0 | 230.0 | XFUS |
| 250.0 | 260.0 | 271.0 | | | | | | | | XFUS |
| 0.0 | 10.5 | 25.0 | 42.5 | 60.8 | 79.4 | 95.9 | 116.5 | 121.5 | 118.3 | FUSA |
| 108.0 | 100.8 | 99.6 | 100.2 | 102.9 | 101.5 | 93.9 | 83.0 | 69.5 | 49.2 | FUSA |
| 19.8 | 9.0 | 0.0 | | | | | | | | FUSA |
| 161.2 | 7.5 | -3.33 | 161.0 | 18.17 | -1.67 | 161.2 | 7.5 | -3.08 | 161.0 | PODORG1 |
| 18.17 | -0.83 | | | | | | | | | PODORG2 |
| 0.0 | 9.10 | 13.267 | 30.20 | 34.003 | | | | | | XPOD1 |
| 2.275 | 2.7625 | 2.833 | 2.9583 | 2.9583 | | | | | | PODR1 |
| 0.0 | 9.10 | 13.267 | 30.20 | 34.003 | | | | | | XPOD2 |
| 2.275 | 2.7625 | 2.833 | 2.9583 | 2.9583 | | | | | | PODR2 |
| 0.0 | 4.0 | 8.0 | 12.0 | 20.0 | | | | | | XPOD3 |
| 0.0 | 0.418 | 0.465 | 0.431 | 0.0 | | | | | | PODR 3 |
| 0.0 | 4.0 | 8.0 | 12.0 | 20.0 | | | | | | XPOD 4 |
| 0.0 | 0.316 | 0.356 | 0.333 | 0.0 | | | | | | PODR 4 |
| 212.0 | 0.0 | 3.98 | 31.9 | 244.5 | 0.0 | 25.85 | 8.1 | | | FINORG |
| 0.0 | 10.0 | 25.0 | 40.0 | 50.0 | 60.0 | 75.0 | 90.0 | 100.0 | | XFIN |
| 0.0 | 0.54 | 1.125 | 1.44 | 1.5 | 1.44 | 1.125 | 0.54 | 0.0 | | FINORD |
| 220.0 | 3.0 | 0.0 | 29.4 | 243.0 | 25.9 | -6.0 | 5.88 | | | CANORG |
| 0.0 | 10.0 | 25.0 | 40.0 | 50.0 | 60.0 | 75.0 | 90.0 | 100.0 | | XCAN |
| 0.0 | 0.54 | 1.125 | 1.44 | 1.5 | 1.44 | 1.125 | 0.54 | 0.0 | | CANORD |

*FIG. 2-19 LANGLEY COMPUTER PROGRAM P7120 INPUTS*

MACH NO.= 1.70000 XMAX= 24.40000 NCN= 19 CBAR= 9.15000

JAYMAX= 9 NOPCT= 13 RATIO= 6.5

| | TPCT | | TYB2 |
|---|---|---|---|
| 1 | 0. | 1 | 0. |
| 2 | 5.000000 | 2 | 0.120200 |
| 3 | 10.000000 | 3 | 0.273800 |
| 4 | 15.000000 | 4 | 0.424200 |
| 5 | 20.000000 | 5 | 0.566600 |
| 6 | 30.000000 | 6 | 0.618000 |
| 7 | 40.000000 | 7 | 0.729500 |
| 8 | 50.000000 | 8 | 0.807100 |
| 9 | 60.000000 | 9 | 1.000000 |
| 10 | 70.000000 | | |
| 11 | 80.000000 | | |
| 12 | 90.000000 | | |
| 13 | 100.000000 | | |

XLEO= 0. XTEO= 18.750000

| | TXLE | TXTE |
|---|---|---|
| 1 | 0. | 18.750000 |
| 2 | 0. | 18.750000 |
| 3 | 2.136000 | 18.750000 |
| 4 | 4.272000 | 18.750000 |
| 5 | 6.409000 | 18.750000 |
| 6 | 7.612000 | 18.750000 |
| 7 | 8.815000 | 18.750000 |
| 8 | 10.018000 | 18.750000 |
| 9 | 11.221000 | 19.410000 |
| 10 | 12.424000 | 20.240000 |
| 11 | 13.626000 | 21.074000 |
| 12 | 14.829000 | 21.906000 |
| 13 | 16.032000 | 22.737000 |
| 14 | 17.235000 | 23.569000 |
| 15 | 18.438000 | 24.400000 |
| 16 | 19.641000 | 24.112000 |
| 17 | 20.844000 | 23.825000 |
| 18 | 22.047000 | 23.537000 |
| 19 | 23.250000 | 23.250000 |

TZORD

| | | | | | | | |
|---|---|---|---|---|---|---|---|
| 0.922600 | 0.749006 | 0.636732 | 0.541376 | 0.455248 | 0.298372 | 0.153800 | 0.026146 |
| -0.115350 | -0.249156 | -0.369120 | -0.446020 | -0.487546 | 0.507540 | 0.436792 | 0.392190 |
| 0.364506 | 0.335294 | 0.261460 | 0.153800 | 0.026146 | -0.115350 | -0.249156 | -0.369120 |
| -0.446020 | -0.487546 | 0.063827 | 0.077669 | 0.096125 | 0.101816 | 0.089665 | 0.058905 |
| 0.019994 | -0.025377 | -0.073209 | -0.125501 | -0.160106 | -0.182407 | -0.195018 | -0.011535 |
| 0. | 0.026146 | 0.029068 | 0.027838 | 0.021532 | 0.010151 | -0.005691 | -0.025069 |
| -0.048140 | -0.067518 | -0.069819 | -0.112889 | -0.013688 | -0.002615 | 0.002615 | 0.006613 |
| 0.009613 | 0.009689 | 0.006306 | 0. | -0.009613 | -0.019840 | -0.033375 | -0.049216 |
| -0.066535 | -0.044294 | -0.032144 | -0.023839 | -0.017841 | -0.012919 | -0.005383 | -0.001846 |
| 0. | -0.001077 | -0.003230 | -0.007536 | -0.013227 | -0.013996 | -0.064288 | -0.051831 |
| -0.042141 | -0.034144 | -0.027376 | -0.015995 | -0.007152 | 0. | 0.005075 | 0.008920 |
| 0.011341 | 0.012765 | 0.012612 | -0.080745 | -0.067364 | -0.056906 | -0.047678 | -0.039527 |
| -0.024300 | -0.011320 | 0. | 0.010381 | 0.019379 | 0.027376 | 0.034528 | 0.040603 |
| -0.080745 | -0.067364 | -0.056906 | -0.047678 | -0.039527 | -0.024300 | -0.011320 | 0. |
| 0.010381 | 0.019379 | 0.027376 | 0.034528 | 0.040603 | | | |

*FIG. 2-20 LANGLEY COMPUTER PROGRAM P916C INPUTS*

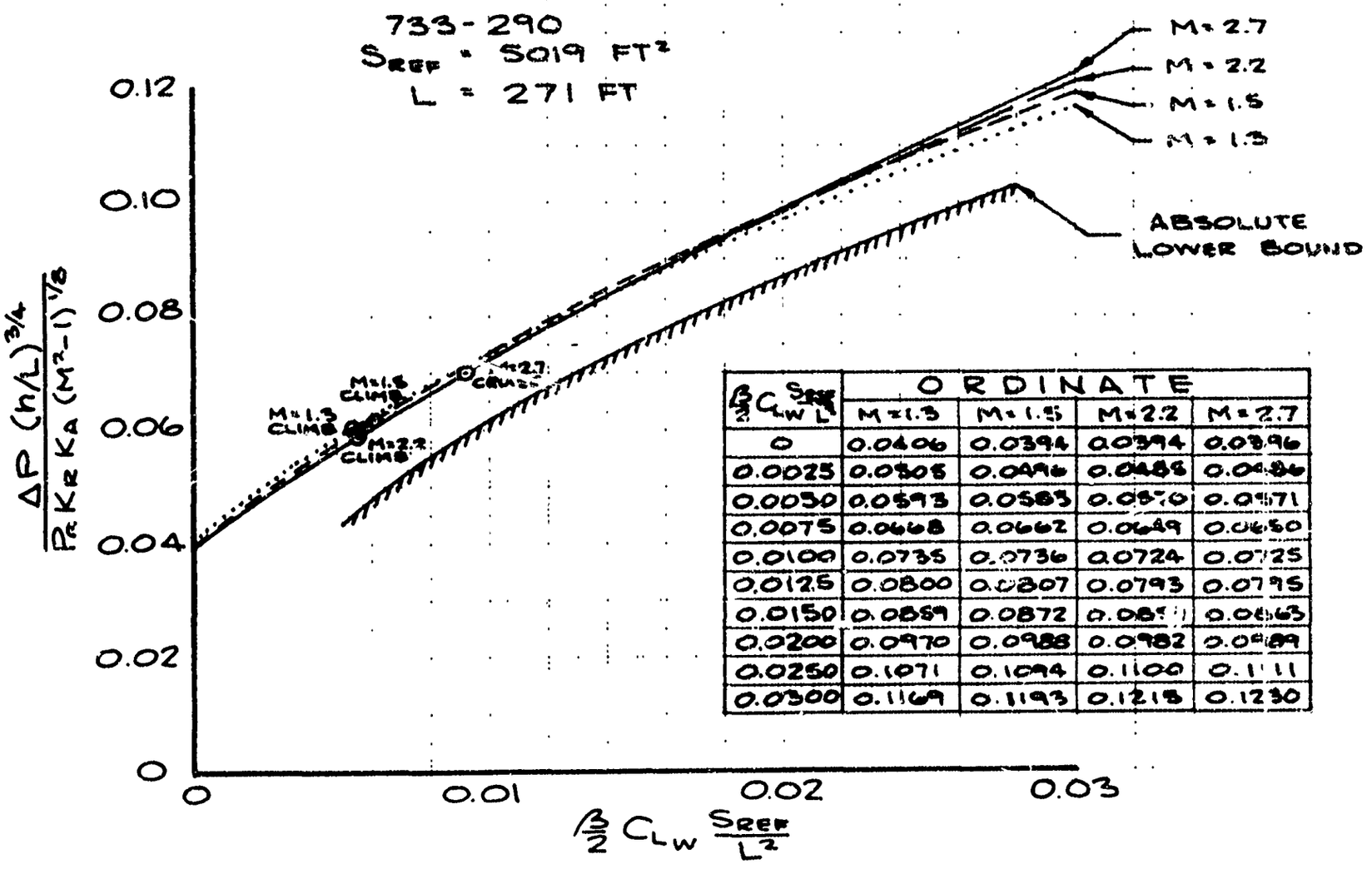


| $\frac{B}{2} C_{L_W} \frac{S_{REF}}{L^2}$ | ORDINATE | | | |
|---|---|---|---|---|
| | M=1.3 | M=1.5 | M=2.2 | M=2.7 |
| 0 | 0.0406 | 0.0394 | 0.0394 | 0.0396 |
| 0.0025 | 0.0505 | 0.0496 | 0.0488 | 0.0486 |
| 0.0050 | 0.0593 | 0.0583 | 0.0570 | 0.0571 |
| 0.0075 | 0.0668 | 0.0662 | 0.0649 | 0.0650 |
| 0.0100 | 0.0735 | 0.0736 | 0.0724 | 0.0725 |
| 0.0125 | 0.0800 | 0.0807 | 0.0793 | 0.0795 |
| 0.0150 | 0.0859 | 0.0872 | 0.0859 | 0.0863 |
| 0.0200 | 0.0970 | 0.0988 | 0.0982 | 0.0989 |
| 0.0250 | 0.1071 | 0.1094 | 0.1100 | 0.1111 |
| 0.0300 | 0.1169 | 0.1193 | 0.1218 | 0.1230 |



FIG 2-21 NONDIMENSIONAL SONIC BOOM CHARACTERISTICS

## 3.0 ENGINE NOISE

Noise levels produced by the Boeing SST proposed in Phase II-A are below the objectives stated in the standards. The predicted noise levels are based on (1) Phase II-A engine and airplane performance, (2) sound suppression as verified by test, and (3) standardized procedures for predicting jet noise.

### 3.1 ENGINE NOISE CHARACTERISTICS

The engine noise levels predicted for the GE4/J5G engine as installed on the Boeing SST are presented in Figs. 3-1, 3-2, and 3-3 for ground operations and for takeoff and landing operations. These data provide the basis for all noise analysis.

#### 3.1.1 Airport and Community Noise

The predicted GE4/J5G engine noise characteristics have been combined with the performance characteristics of the Boeing SST airplane to predict the noise environment at the airport and in the community during takeoff and landing. The noise levels below and to the side of the airplane takeoff path resulting from recommended noise abatement techniques on a standard day are presented in Figs. 3-4 and 3-5 for 425,000 pound and 500,000 pound gross weight airplanes, respectively. The maximum perceived noise level (PNL), 1,500 feet to the side of the runway as the airplane passes on its takeoff run, is 116 PNdb with all engines operating at maximum dry thrust. The community noise levels shown in Figs. 3-4 and 3-5 are based on a thrust reduction that results in an unaccelerated rate of climb of 500 feet per minute at a point one statute mile beyond the departure end of the runway. After thrust reduction for noise abatement, the noise level in the community is reduced to 96.8 PNdb for the airplane at 425,000 pounds gross weight and 105.5 PNdb for the 500,000 pound airplane. The trade between airport and community noise that is available through variation in takeoff power setting is shown in Fig. 3-6.

The noise levels below and to the side of the airplane landing approach path are presented in Figs. 3-7 and 3-8 at landing weights of 302,000 and 320,000 pounds. At 1 statute mile from the runway threshold, the predicted noise levels are 111.3 PNdb and 112.0 PNdb for the light and heavy gross weight airplanes, respectively.

Several noise abatement approach procedures are being considered in order to achieve even lower community noise levels. These make use of the all-weather automatic landing throttle controls. An approach is made at a controlled deceleration rate, with reduced thrust, on a 3 degree glide slope to reach the inner marker at final approach speed. The automatic throttles increase thrust to stabilize at final approach speed until the landing flare is initiated. With the engine inlet choked and the nozzle throat open, the community noise level is 107 PNdb with a deceleration rate of 1 knot per second. Using idle thrust, the community noise is 105 PNdb with a deceleration rate of 2.6 knots per second. The operational aspects of these procedures are described in Volume X-A, Flight Operations, and Volume V-A, Aerodynamics.

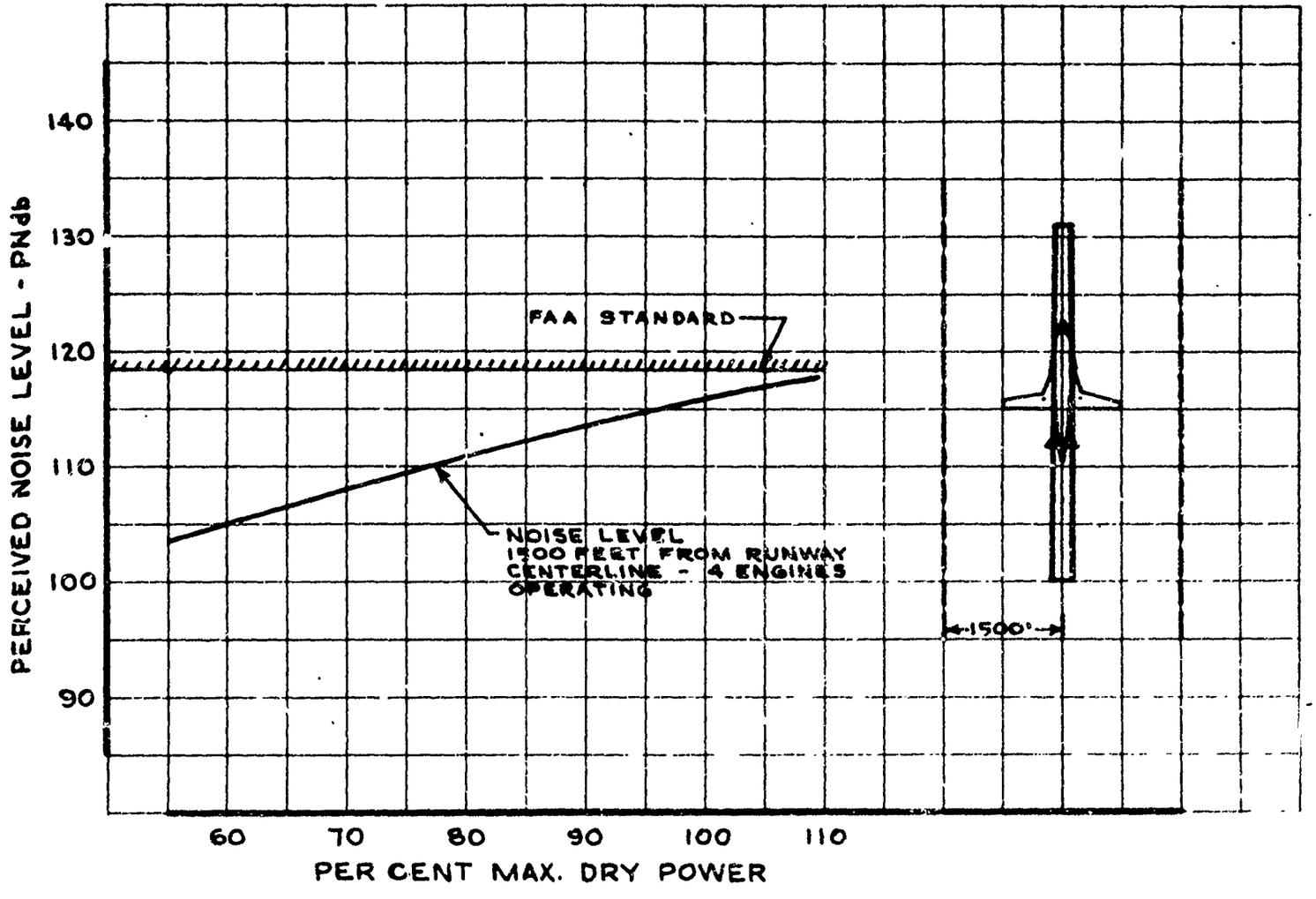


*FIG. 3-1 AIRPORT NOISE DURING STATIC GROUND OPERATIONS*

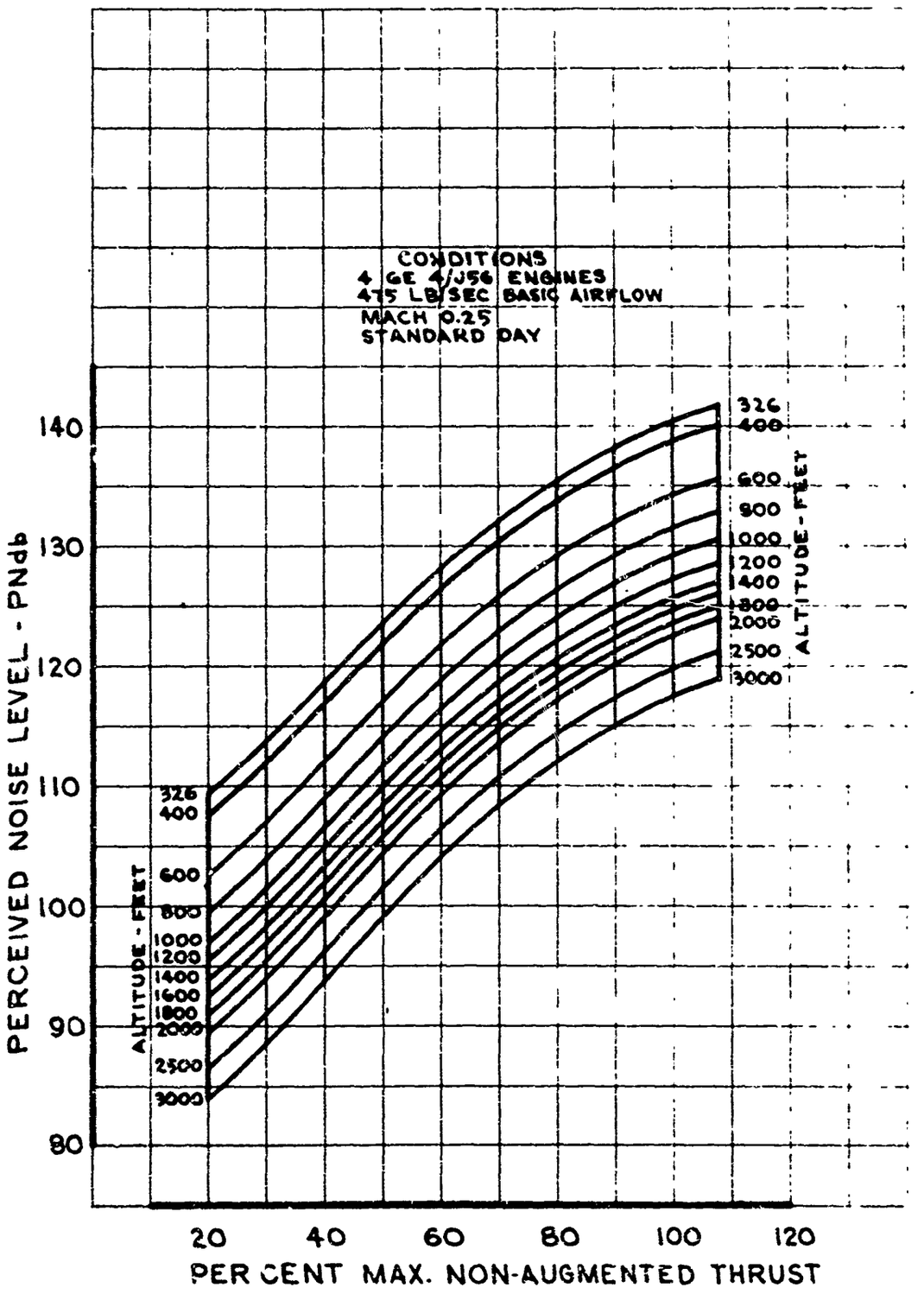


*FIG. 3-2 FAR FIELD NOISE LEVELS DURING TAKEOFF AND LANDING*

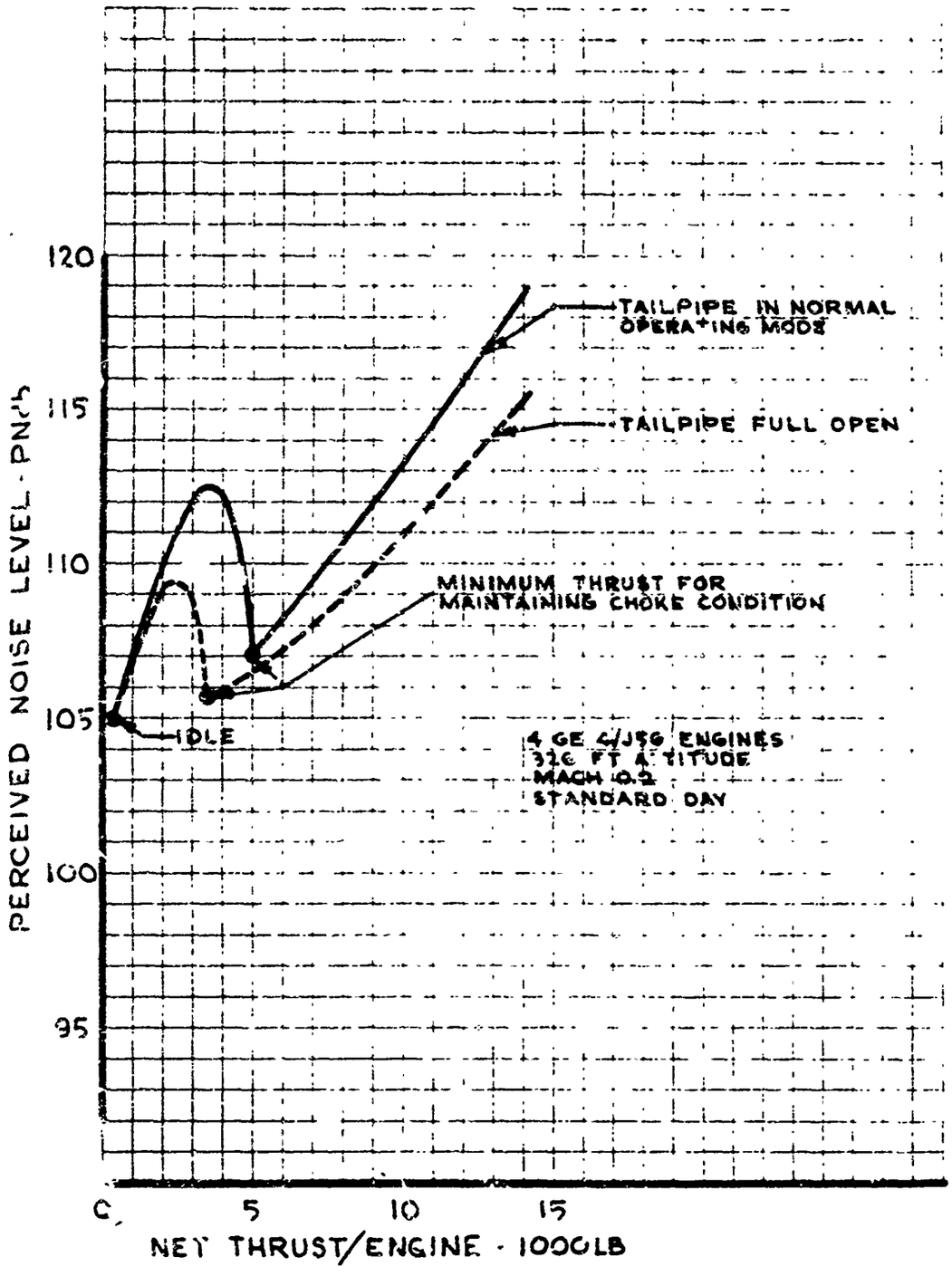


FIG. 3-3 NOISE LEVEL FOR VARIOUS OPERATING PROCEDURES DURING LANDING APPROACH

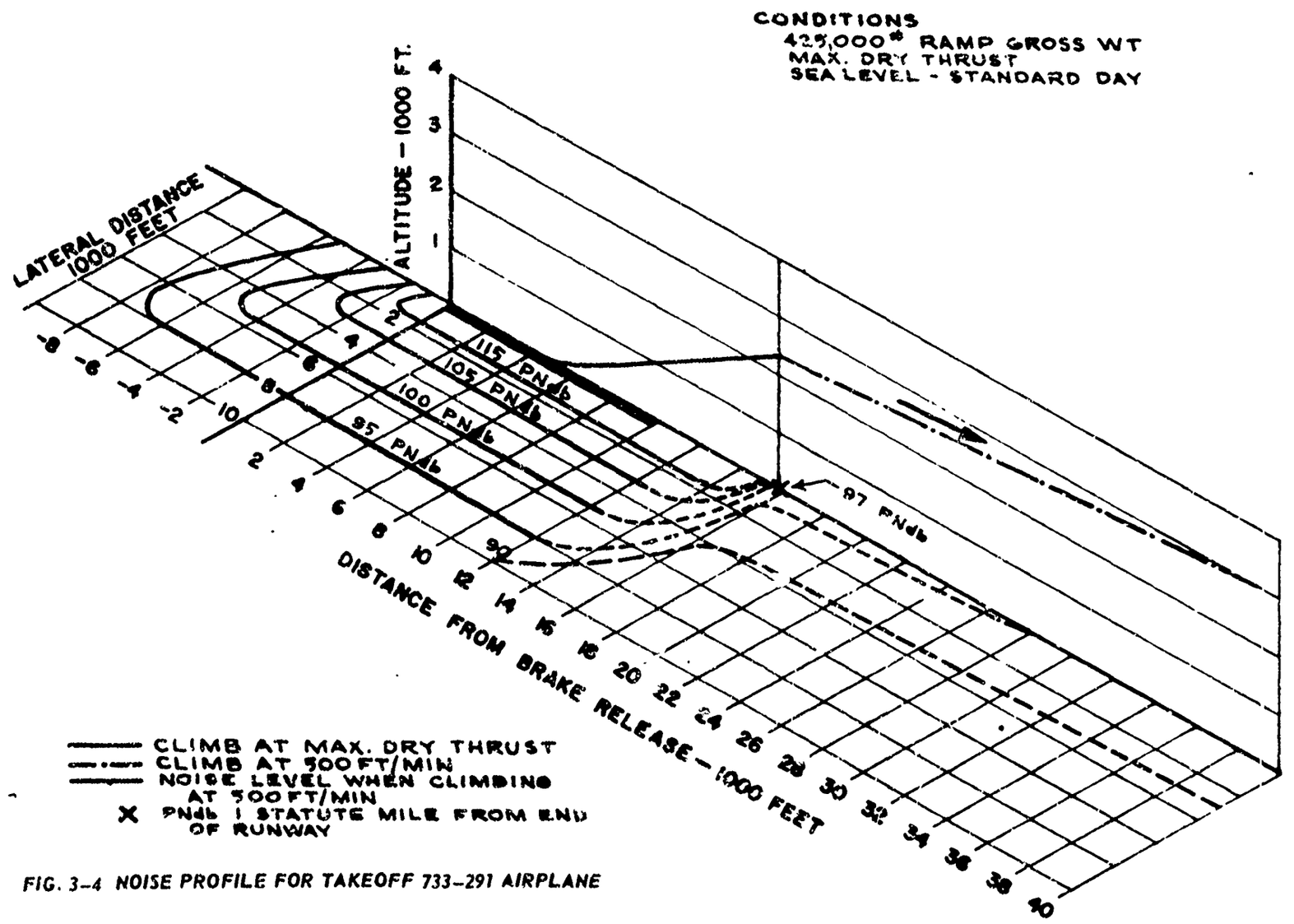


D6-8680-7

FIG. 3-4 NOISE PROFILE FOR TAKEOFF 733-291 AIRPLANE

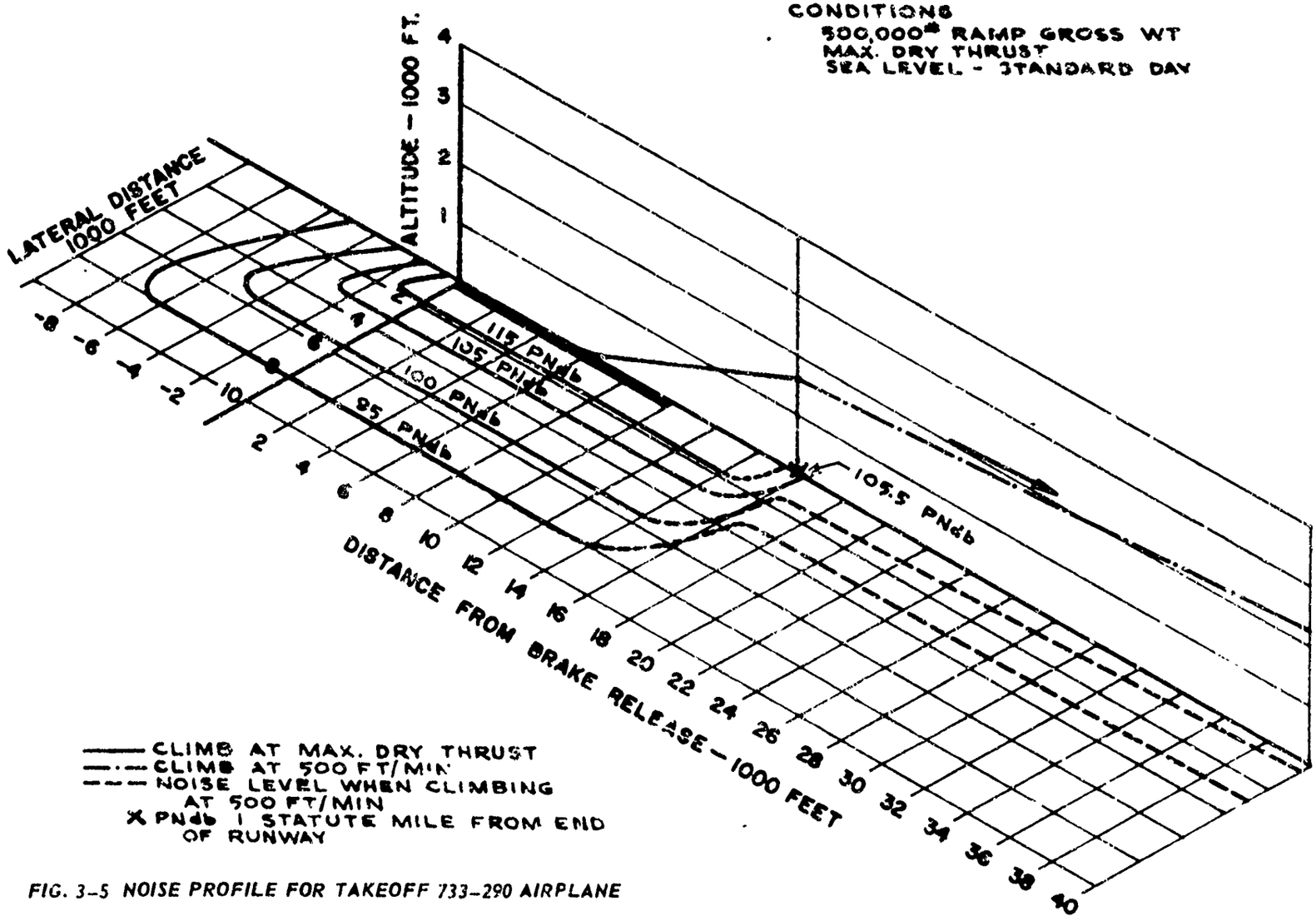


*FIG. 3-5 NOISE PROFILE FOR TAKEOFF 733-290 AIRPLANE*

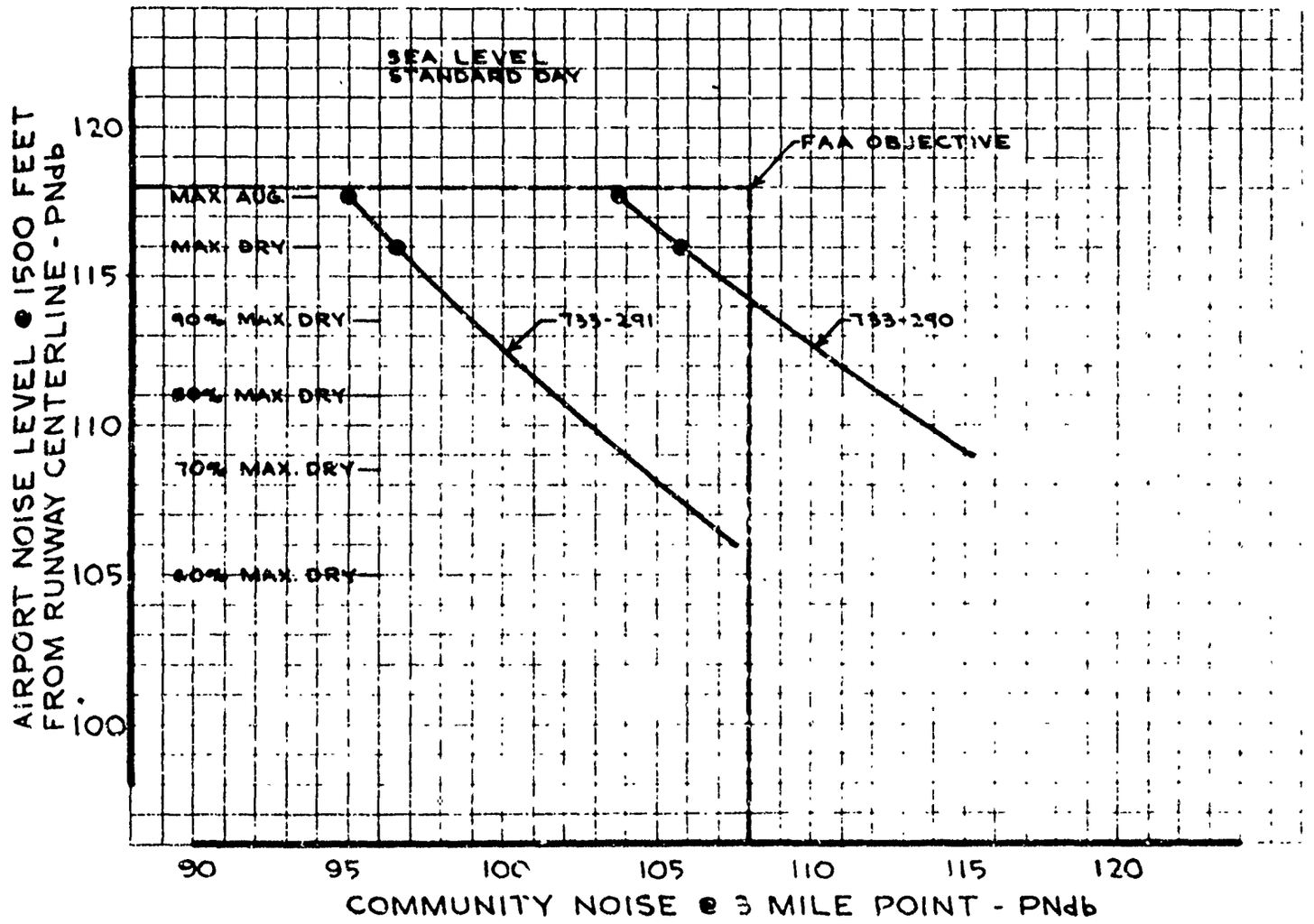


D6-8880-7

FIG. 3-6 AIRPORT/COMMUNITY NOISE TRADES

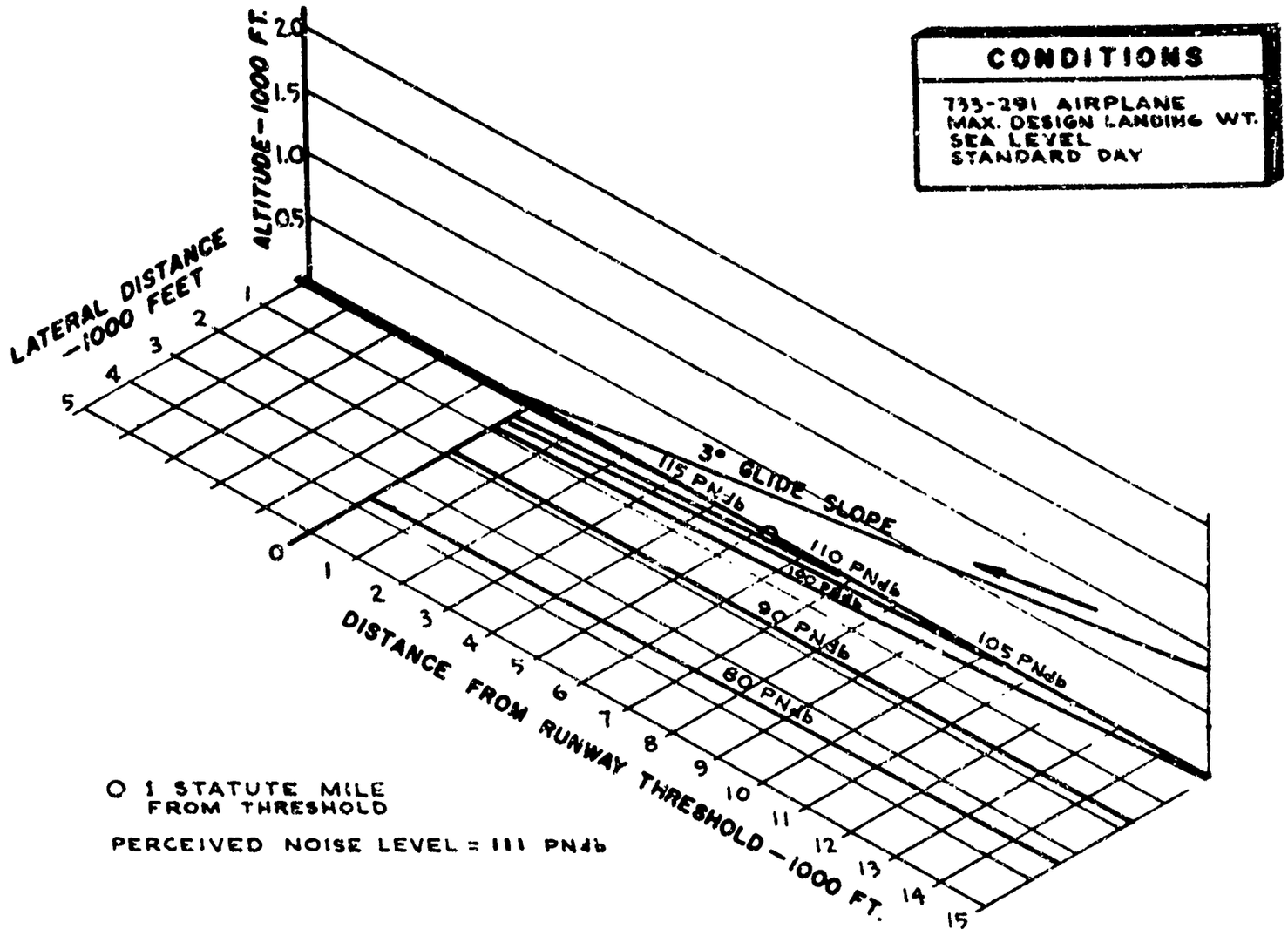


FIG. 3-7 NOISE PROFILE FOR LANDING APPROACH 733-291 AIRPLANE

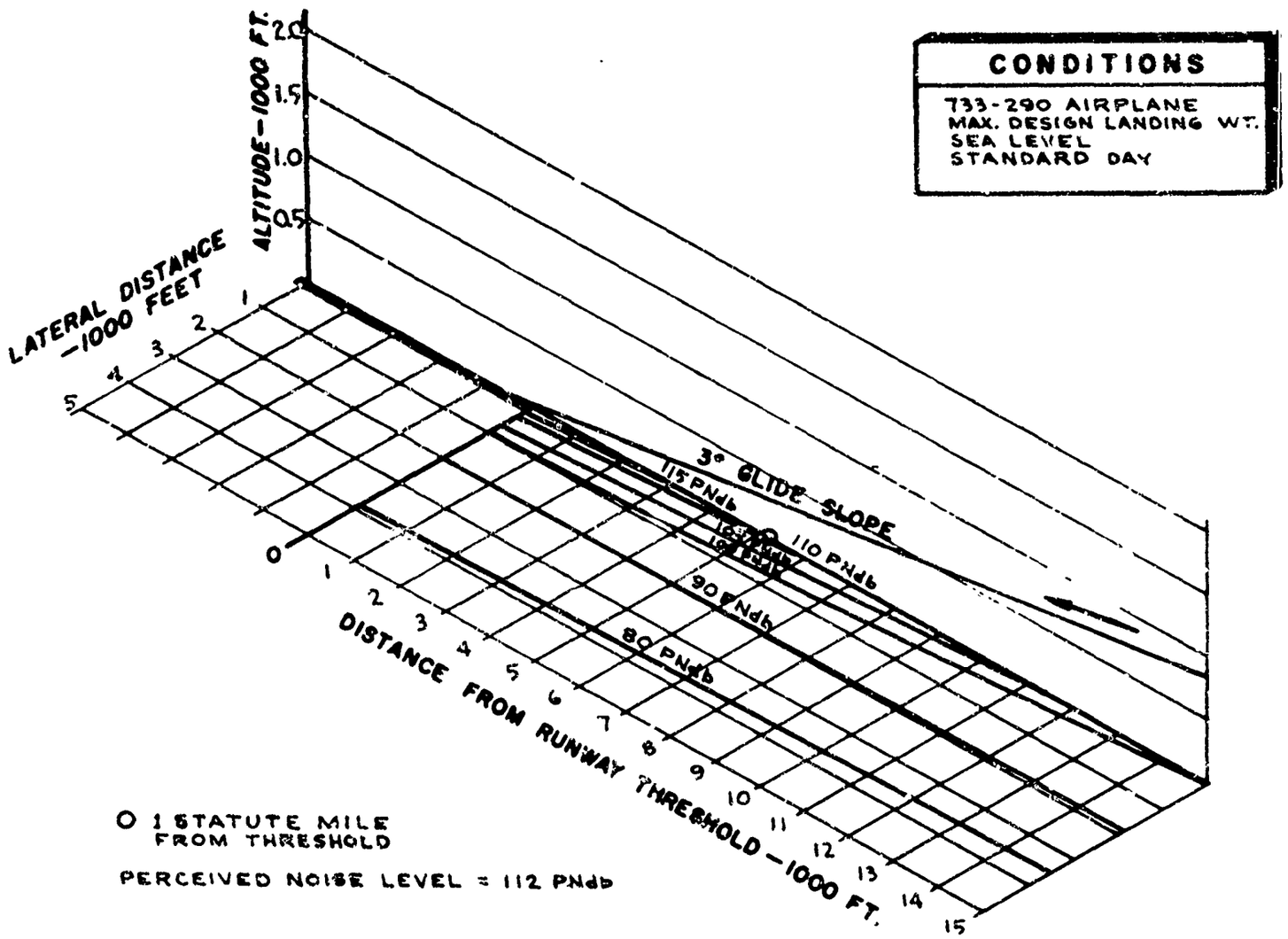


D6-8880-7

FIG. 3-8 NOISE PROFILE FOR LANDING APPROACH 733-290 AIRPLANE

3.1.2 Ground Operations and Maintenance Runups

3.1.2.1 Ramp Noise

The noise levels resulting from ground operations near the airport terminal (taxi, etc.) are predicted to be no greater than those presently experienced during similar subsonic jet operations. The levels predicted for the Boeing SST during taxi operation are presented in Fig. 3-9. The PNL's are predicted to be between 105 and 120 PNdb at 200 feet from the airplane. These levels are based on a taxi thrust requirement of 3 percent of the gross weight of the airplane.

3.1.2.2 Maintenance Runups

Without ground sound suppression, noise levels due to operations of the GE4/J5G engine at maximum augmentation are 123 db on a 1500 foot radius and 160 db at a point 20 feet downstream of the nozzle. Current ground runup noise suppressors of a portable type afford a reduction of 20 to 25 db at these locations (Ref. 3-1). Compatitility of a suppressor of this type with the Boeing SST engine and airplane is shown in Section 2.0 of Volume VII-A, Ground Operations. No problems beyond the reach of current technology are anticipated.

With a suppressor of this type the maximum perceived noise level is 100 PNdb at 1500 feet from the engine during maximum afterburning condition. Maintenance personnel stationed in the immediate vicinity of the airplane during engine runup will be subjected to levels no greater than 135 db OA SPL and 127 db SIL with the suppressor installed.

3.2 SUBSTANTIATION OF NOISE DATA

3.2.1 Unsuppressed Engine Noise

The unsuppressed engine noise characteristics for the GE4/J5G have been predicted by using:

- installed performance characteristics of the engine, Appendix A Volume VIII-A, Propulsion
- compressor noise characteristics based on Boeing test data, Fig. 3-10
- procedures for jet noise prediction, Ref. 3-2

The octave band and overall sound pressure levels obtained by these methods are shown in Figs. 3-11 and 3-12 for several engine throttle settings. These data have been used as a baseline for predicting the jet and compressor suppressed noise levels.

3.2.2 Inlet and Exhaust Noise Suppression

The noise suppression characteristics of the GE4/J5G engine as installed on the Boeing SST have been determined from many acoustic tests run on a J-75 test engine and a 1/8th scale model of the GE4/J5G engine exhaust nozzle. Inlet noise suppression tests were run on a J-75 engine for both choked and unchoked airflow conditions. Exhaust noise tests

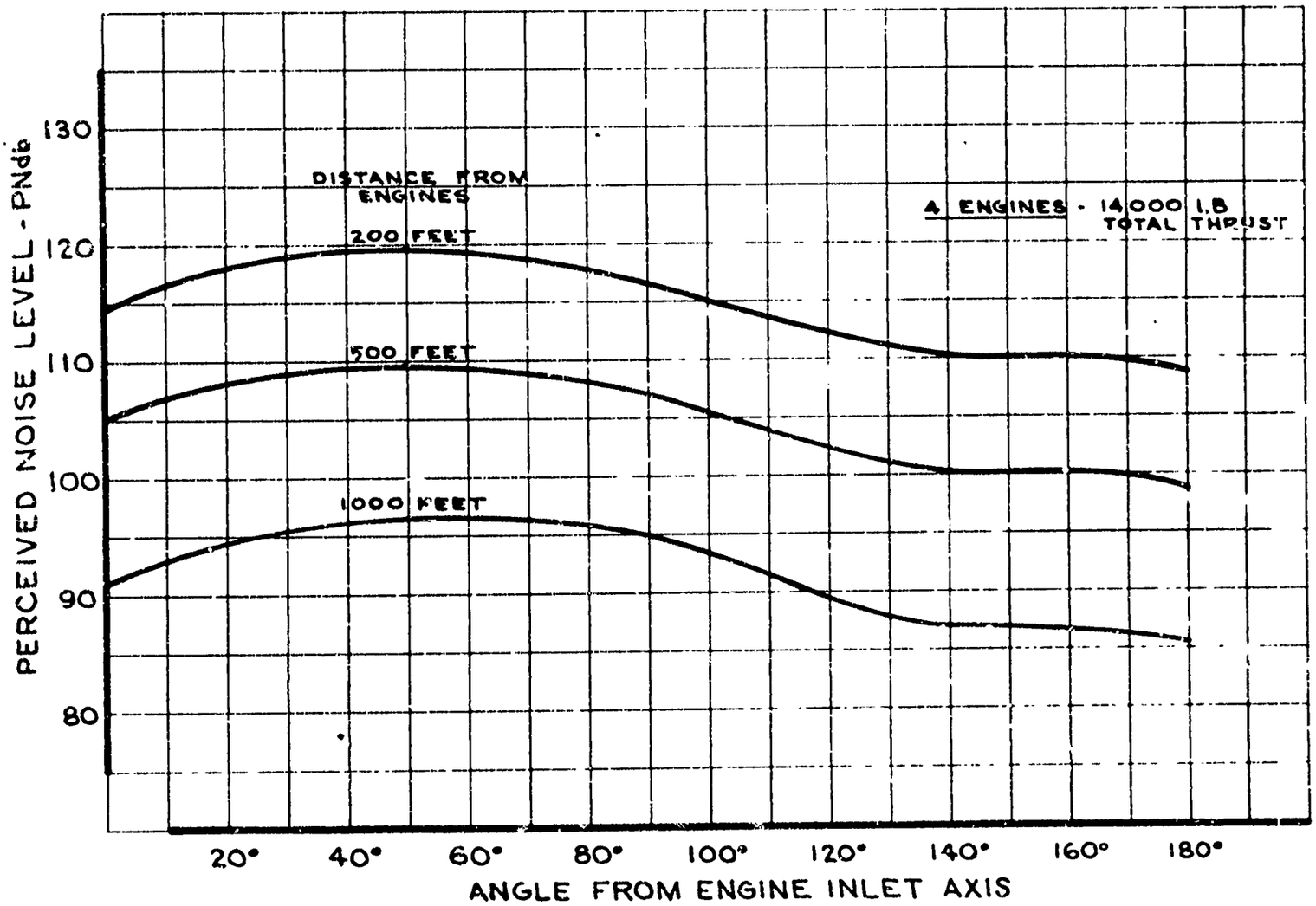


D6-8888-7

*FIG. 3-9 NOISE DURING TAXI MANEUVERS*

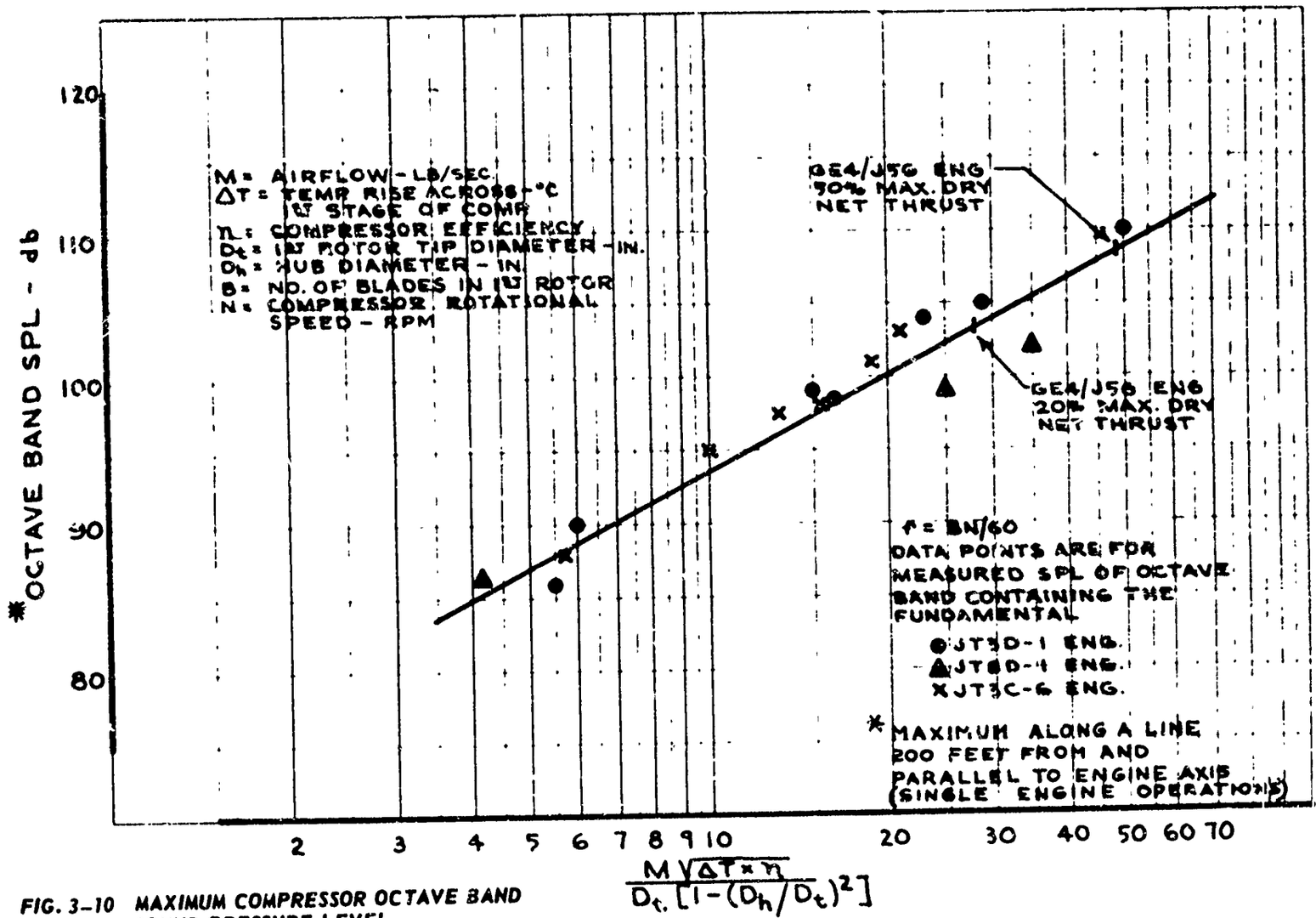


FIG. 3–10 MAXIMUM COMPRESSOR OCTAVE BAND SOUND PRESSURE LEVEL

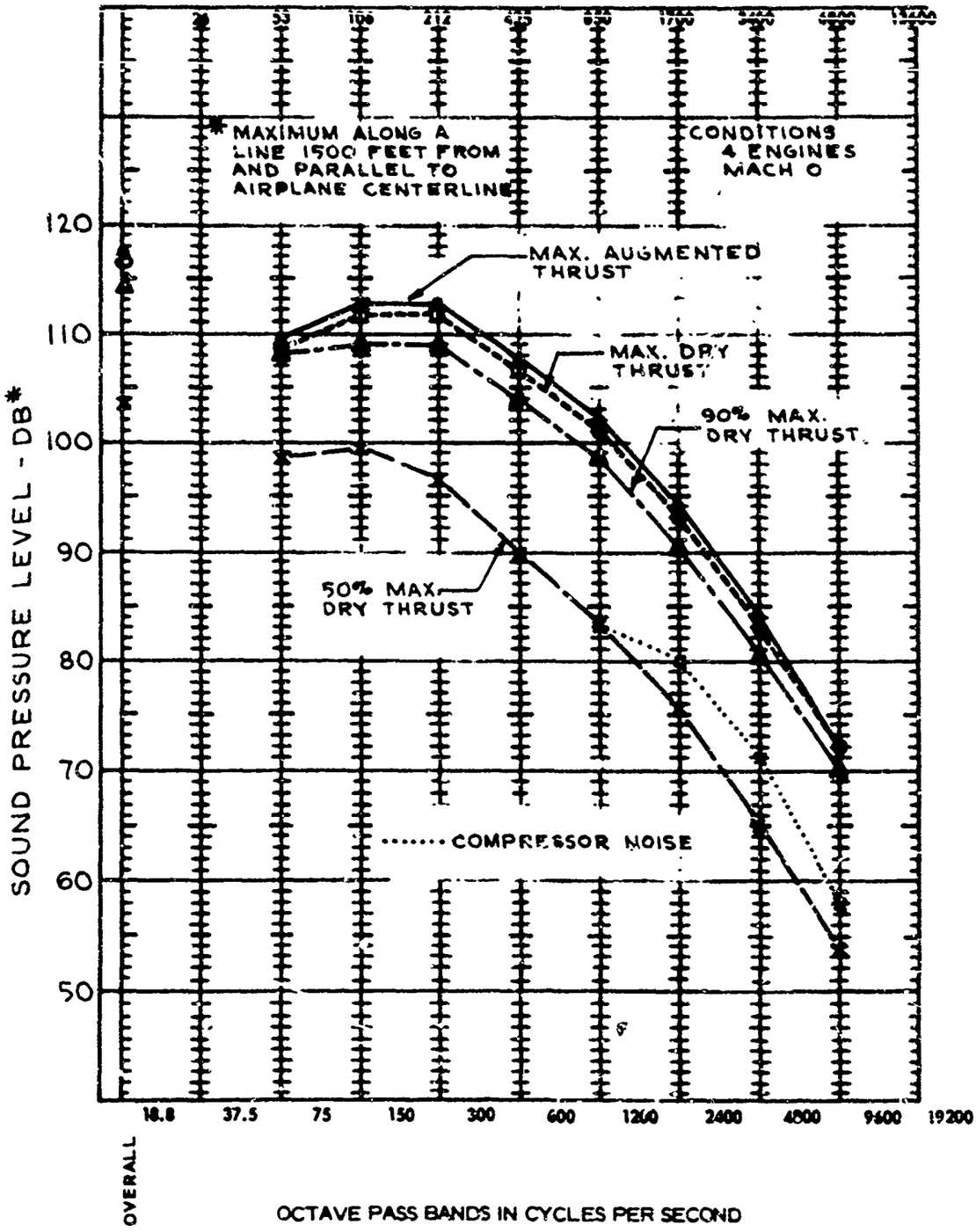


*FIG. 3-11 UNSUPPRESSED NOISE LEVELS FOR STATIC ENGINE OPERATIONS*

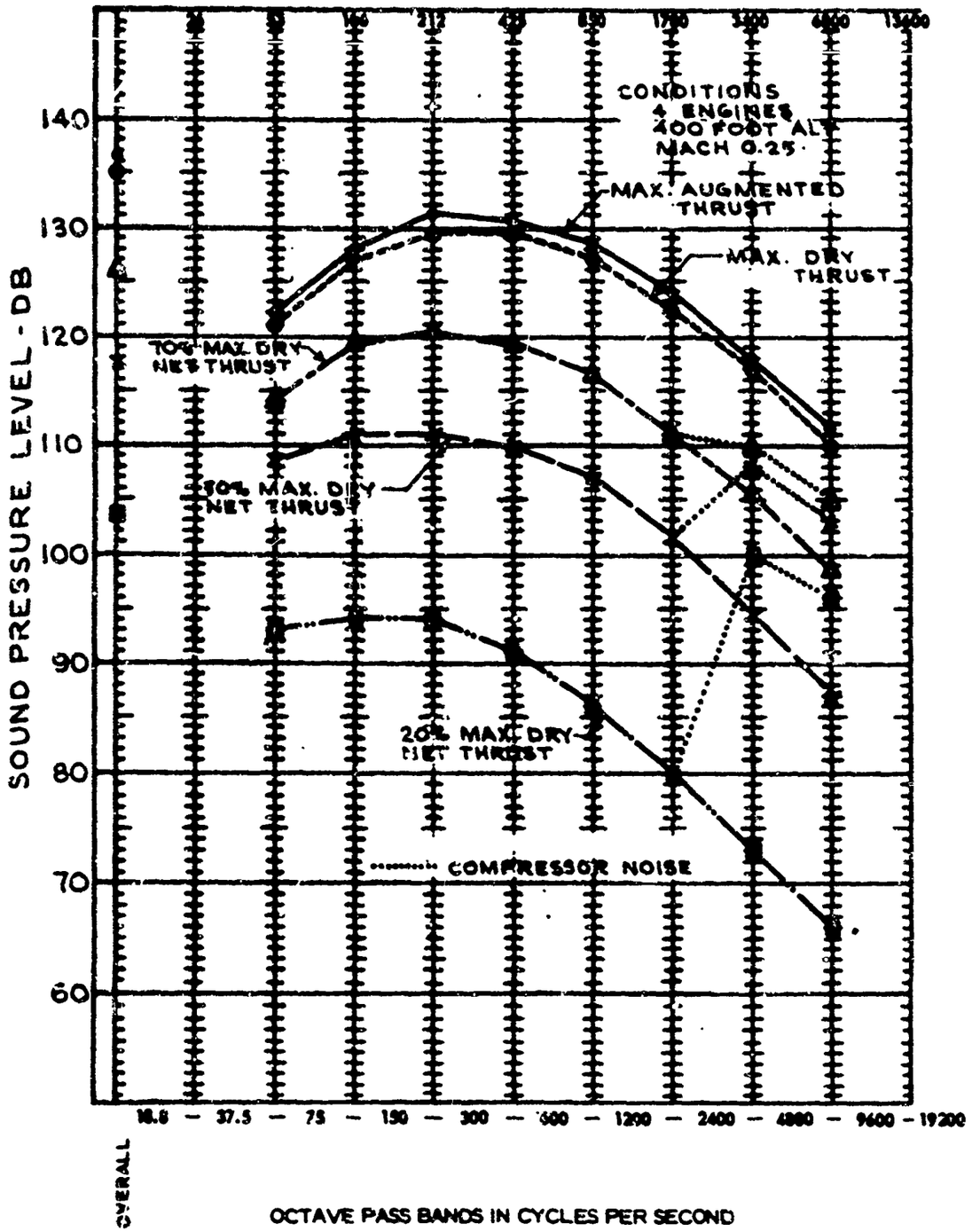


*FIG. 3-12 UNSUPPRESSED NOISE LEVELS FOR IN-FLIGHT ENGINE OPERATIONS*

were conducted with a standard round nozzle as well as with the "star shaped" primary throat and nozzle configuration proposed for the GE4/J5G engine.

3.2.2.1 Exhaust Noise Suppression

The exhaust noise suppression predicted for the GE4/J5G engine exhaust nozzle configuration is shown in Fig. 3-13. The maximum attenuation is 3 PNdb at thrust settings from maximum dry thrust to 70 percent of maximum dry thrust. As jet velocity is reduced, the nozzle configuration is predicted to become less effective. This prediction is based on noise suppression characteristics of tested jet suppression nozzles such as are presently in use on 707 airplanes. Reduction in suppression efficiency is predicted for the maximum augmented operating condition because of the reduction in star shaping as the throat opens.

3.2.2.2 Inlet Noise Suppression

Engine compressor noise suppression for the Boeing SST has been achieved by establishing a choked flow condition in the inlet. It is possible to achieve this choked condition at thrust settings below 50 percent of maximum dry power and at Mach numbers below 0.3 (see Section , Volume VIII-A, Propulsion).

The octave band noise levels predicted for the Boeing SST during a typical landing approach under choked inlet flow conditions are shown in Fig. 3-14. The noise spectrum predicted for an unchoked condition is also shown in Fig. 3-14. The attenuation shown is based on J-75 choked inlet test data obtained at Boeing using a simulated Boeing SST inlet. The effect of inlet choking on the single frequency compressor noise generated by the J-75 engine is shown in Fig. 3-15. Predicted GE4/J5G inlet noise has been superimposed on the spectra to indicate the reduction the choked inlet will give this engine.

J-75 data indicate that with the inlet choked, the noise that will determine the maximum PNdb during airplane flyover at low power conditions will radiate at angles between 40 degrees to 90 degrees to the exhaust axis. The predicted spectrum is not "pure jet exhaust" in nature. High frequency noise from the turbine is predicted to be dominant in the last two or three octave bands. This turbine noise contributes strongly to the perceived noise level. Tests will continue during Phase II-B with the J-75 to develop additional understanding of the turbine noise.

A tape recorded demonstration of the effect of choking the inlet has been forwarded to the FAA by The Boeing Company.

3.3 DESCRIPTION OF MODEL TESTS

Tests have been conducted to aid in defining the basic noise characteristics of the SST engines and to develop means of suppressing noise from these engines. Both turbofan and turbojet engines have been included in these studies.

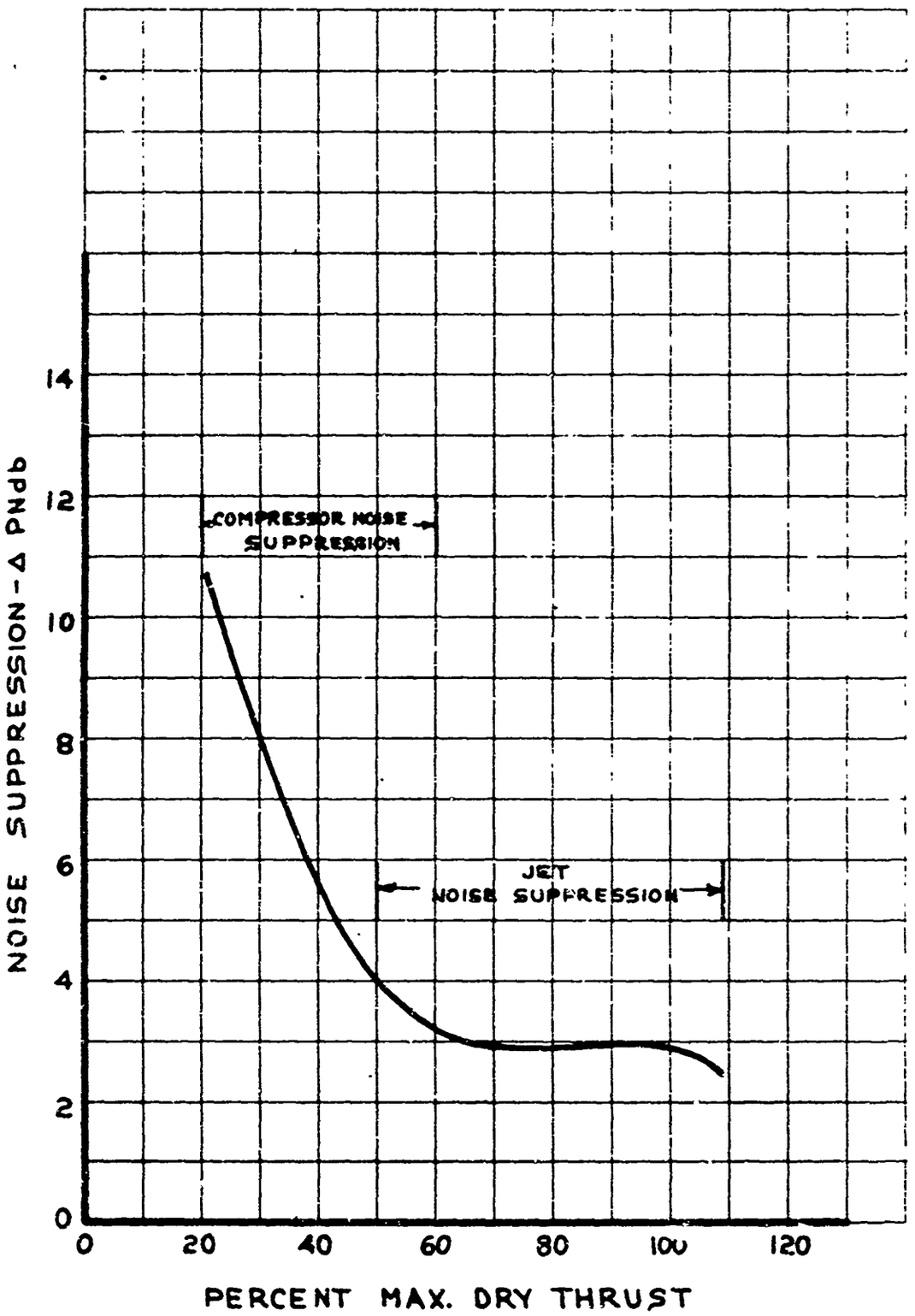


*FIG. 3-13 GE4/J5G ENGINE NOISE SUPPRESSION*

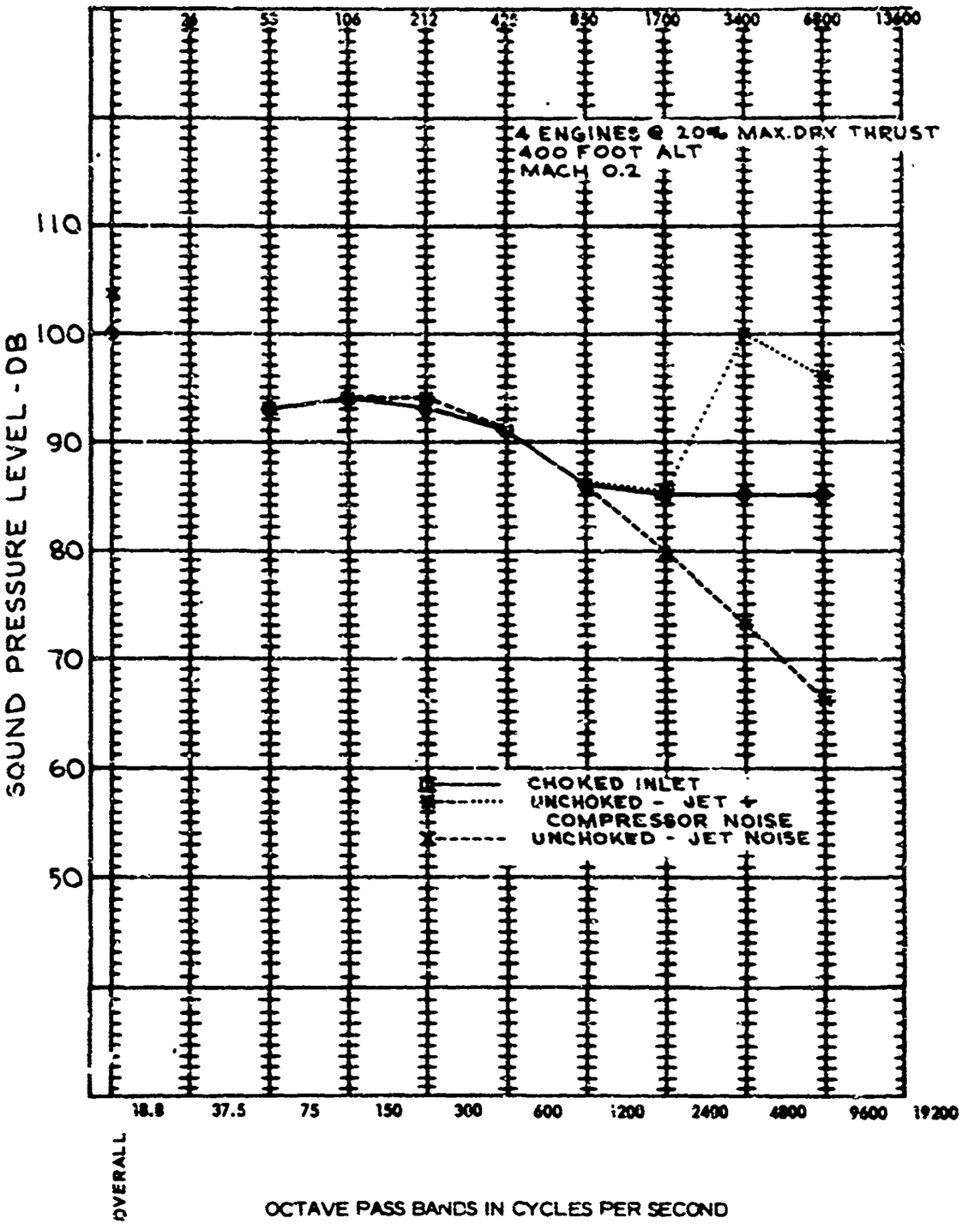


*FIG. 3-14 LANDING APPROACH NOISE LEVELS FOR CHOKED AND UNCHOKED INLET*

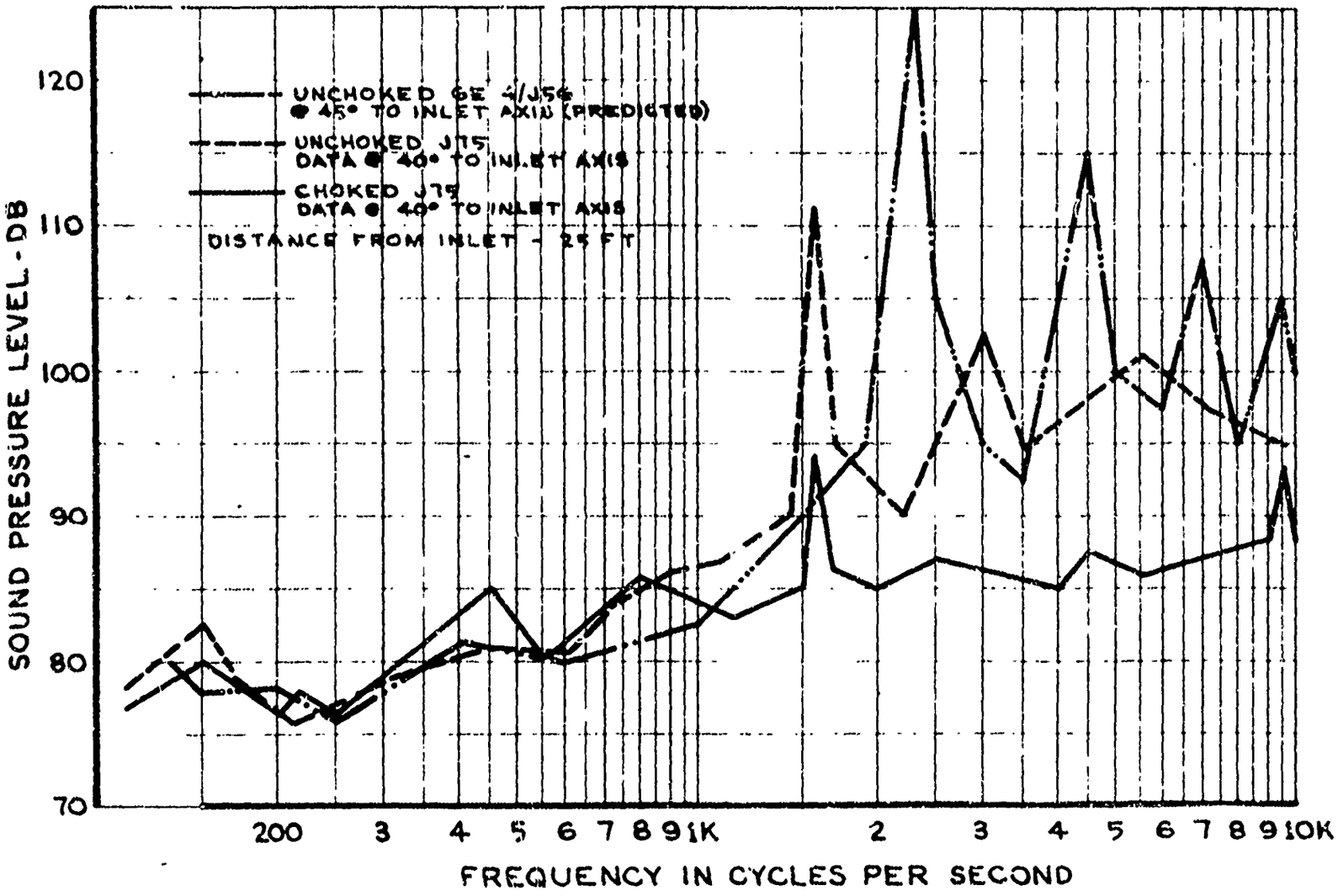


FIG. 3-15 EFFECT OF INLET CHOKING ON DISCRETE FREQUENCY COMPRESSOR NOISE RADIATION

3.3.1 Small Scale Model Jet Tests

The exhaust noise characteristics of the General Electric and Pratt & Whitney SST engine offerings were determined by means of tests in the Boeing acoustic model jet facility. One-eighth scale models of the GE4/J5G and P&W STF-219 exhaust nozzle configurations were built and tested at several design operating conditions. The nozzle configurations tested are shown in Figs. 3-16 and 3-17.

The far field noise characteristics of the GE4/J5G and the P&W STF-219 engines were determined for engine operations at maximum augmentation, maximum dry thrust, and approximately 70 percent of maximum dry thrust. As required by the procedures established in Ref. 3-2, the noise characteristics of the two proposal engine exhaust systems were determined by comparing their measured characteristics with those of a standard round nozzle when both were operating at the same conditions of tailpipe pressure ratio and exhaust temperature. The acoustic difference found between the two test nozzles was then applied to the noise characteristics established for the full scale round nozzle through application of the standardized procedures. Noise comparisons were made over an arc of 19 feet radius (150 feet full scale) centered on the nozzle exhaust plane. Data were obtained at 10 degree intervals from 30 degrees to 90 degrees to the jet exhaust axis. The data were then extrapolated to give perceived noise level differences along a line 25 feet (200 feet full scale) from and parallel to the jet axis. PNL's for the GE4/J5G nozzle configuration were 3 to 4 PNdb lower than the levels obtained with the standard nozzle (Fig. 3-18). The noise level for the P&W STF-219 nozzle configuration was 3 PNdb less than that of the standard nozzle at maximum augmentation, and 2 PNdb less at maximum dry thrust (Fig. 3-19). A detailed report of the test and the results may be found in Ref. 3-3.

3.3.2 Full Scale Engine Tests

3.3.2.1 Suppression of Fan Noise from Secondary Exhaust

To determine if suppression of fan discharge noise is feasible in the high velocity duct system of a turbofan engine, an acoustically treated extension of the fan discharge duct of a JT8D engine was tested. The extension consisted of an annular duct with acoustic treatment on both walls for a length of 5 feet; the hot primary gases were conducted through the hard-walled center, joining the fan-discharge air about 18 inches ahead of the nozzle exit (Fig. 3-20). Engine thrusts ranged from a little above idle to maximum static thrust (13,400 pounds).

Results showed large attenuations of discrete-frequency (spike) noise in the regions of maximum radiation: more than 20 db at intermediate thrusts, and more than 13 db at maximum thrust. "Hash" or white noise between spikes also was reduced 4 to 8 db at low thrust, indicating that this component of compressor noise is at least that much greater than jet noise at the same frequency. Octave-band analysis showed only

(a) NOZZLE CONFIGURATION

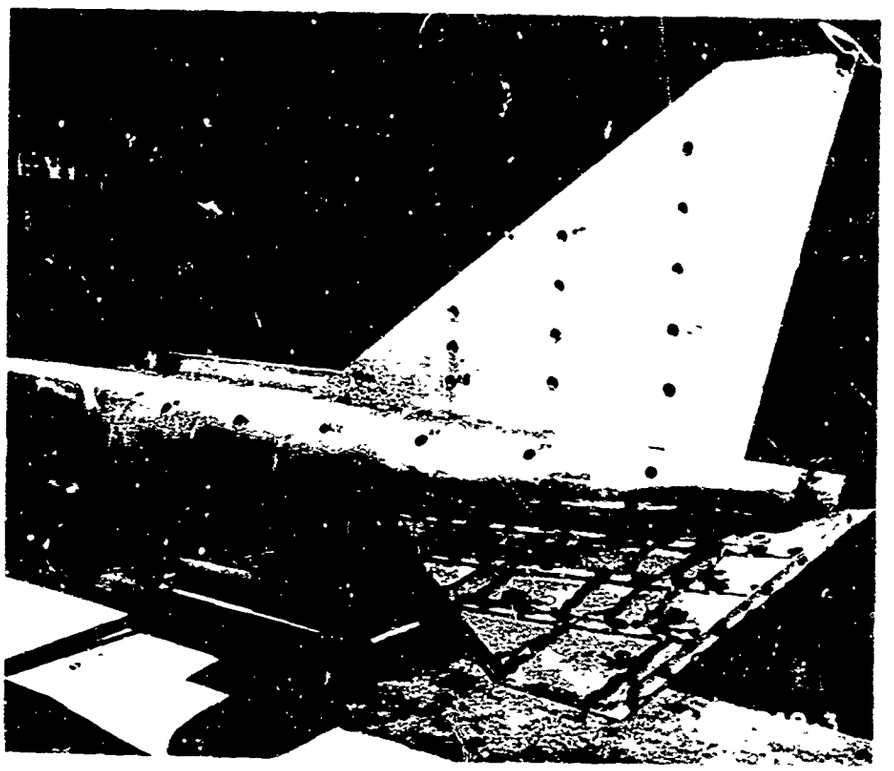

(b) ENGINE – AIRPLANE TEST MODEL

*FIG. 3-16 MODEL ACOUSTIC TEST CONFIGURATIONS FOR THE GE4/J5G*

(a) NOZZLE CONFIGURATION

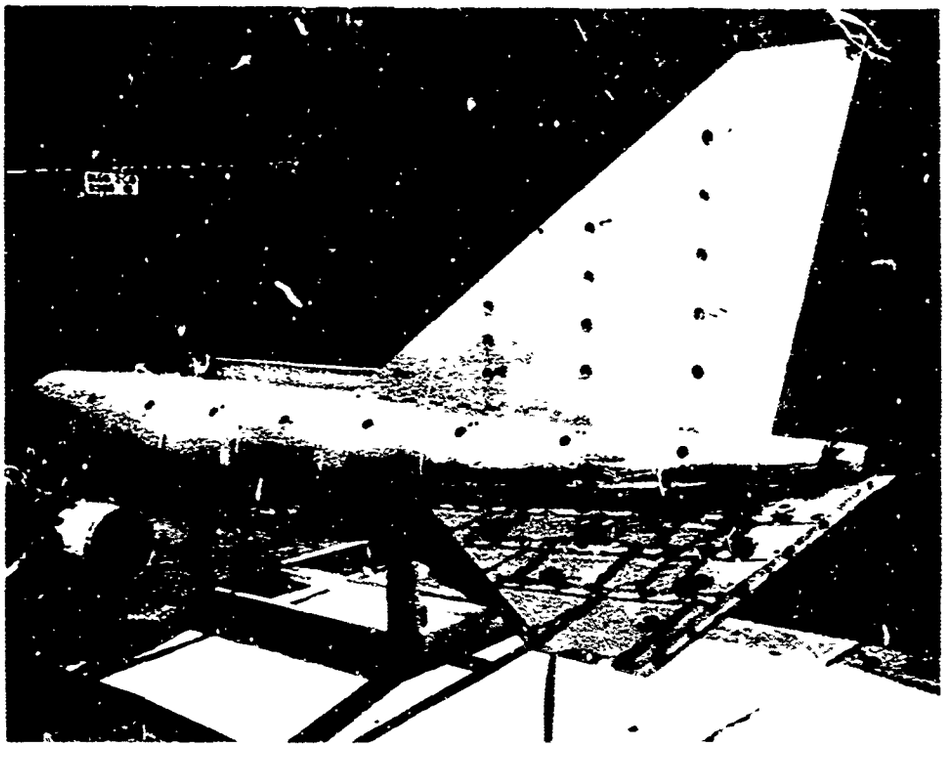

(b) ENGINE – AIRPLANE TEST MODEL

*FIG. 3-17 MODEL ACOUSTIC TEST CONFIGURATIONS FOR THE P&W STF219 ENGINE*

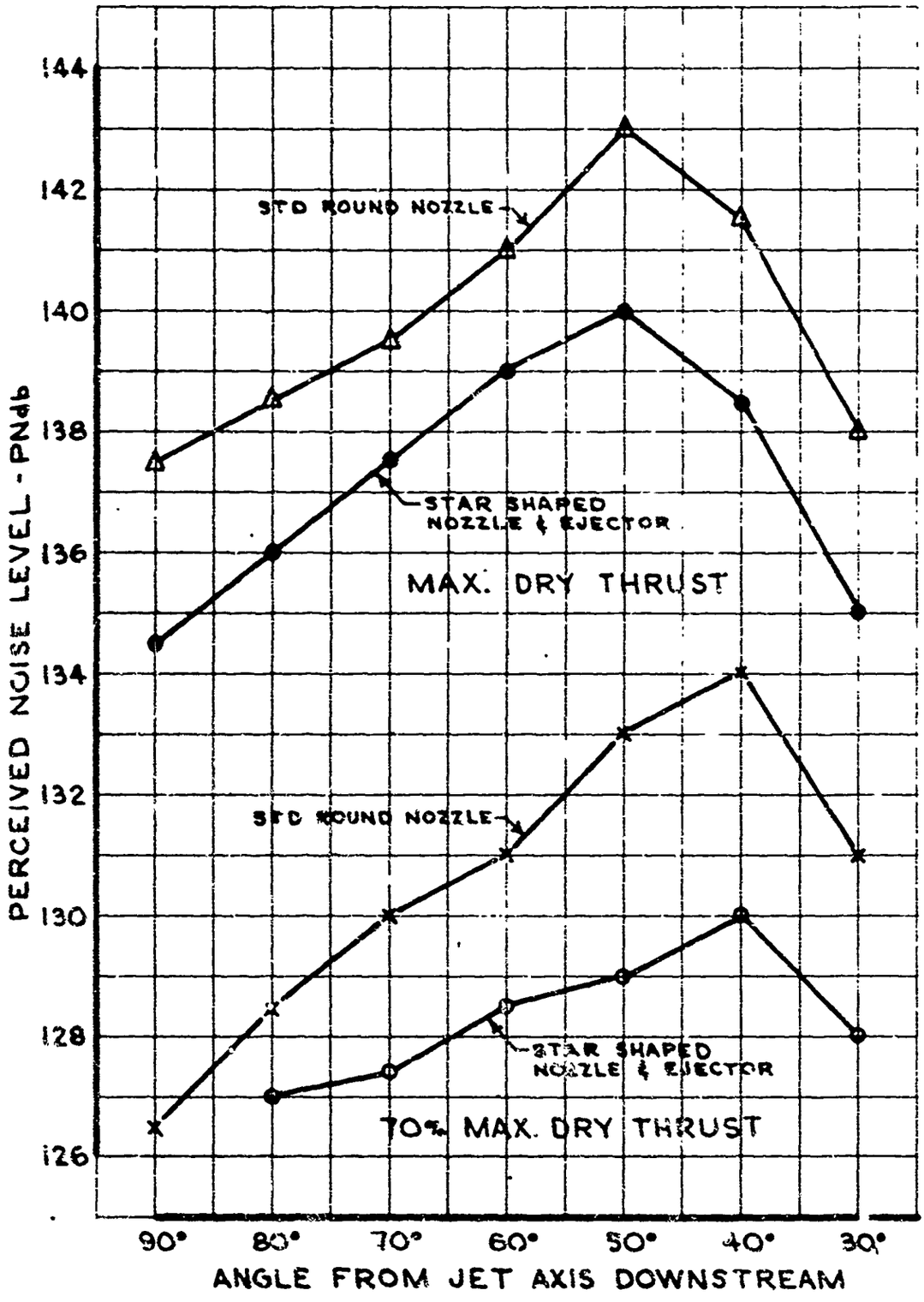


*FIG. 3-18 JET NOISE SUPPRESSION FROM MODEL TESTS OF GE4/J5G ENGINE*

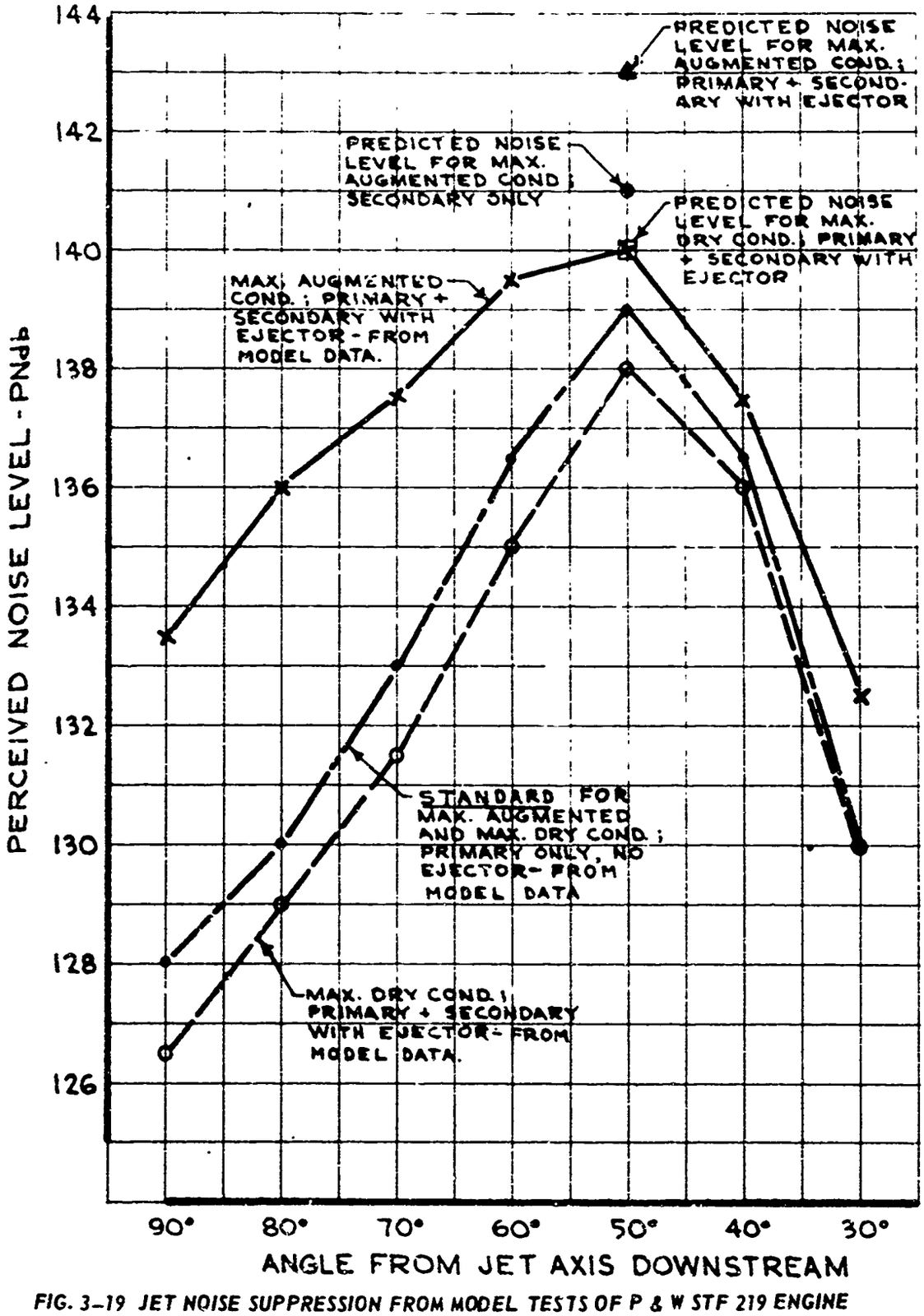


*FIG. 3–19 JET NOISE SUPPRESSION FROM MODEL TESTS OF P & W STF 219 ENGINE*

slightly less attenuation at low thrust than the values listed above. Covering the inner wall acoustic lining did not significantly affect the noise reduction from those values attained with both walls acoustically treated.

A more detailed report of the test and the results may be found in Ref. 3-4.

3.3.2.2 Inlet Noise Suppression Devices

Three devices for reducing compressor or fan noise radiated from the inlet were tested on a J-75 turbojet engine: (1) sonic throat, (2) absorbent inlet lining, and (3) absorbent inlet guide vanes. The basic inlet design simulated a 733-290 supersonic inlet with expandable spike. The first device, the sonic throat, was formed by setting the spike in its fully-expanded, supersonic-cruise position, and then advancing the throttle until choking occurred (Fig. 3-21). The absorbent inlet lining consisted of acoustic material extending along the inside of the inlet diffuser for a length of about one diameter. The absorbent guide vanes, twenty in number, were placed directly upstream of the engine's fixed inlet guide vanes. All three acoustic devices could be replaced with nonacoustic equivalent structures. Sound level measurements were made with the engine simulating landing approach with and without inlet choked.

Results showed that the most effective device was the sonic throat; attenuations directly forward of the inlet were 10 db or more on an octave band basis, and somewhat higher at the discrete frequencies of compressor noise generation.

Acoustic treatment of the inlet guide vanes showed attenuations of about 3 db directly ahead, decreasing to 0 at right angles. The maximum attenuation with the diffuser lining was approximately 2 db. Using both treatments simultaneously produced maximum attenuations of 5 to 6 db.

Use of acoustic lining with the expanded spike increased the lining's effectiveness at air flows too small to produce choking in the sonic throat. Upon reaching choke, no difference could be detected.

The possibility of reducing jet noise at low thrusts by increasing the exhaust nozzle area while holding the inlet choked was also tested on the J-75. With the afterburner in the closed position, engine speed was increased until choking occurred in the inlet and the compressor noise became inaudible. With the compressor speed held constant, the afterburner was then expanded to its full position, an area increase of about 50 percent; this reduced the thrust by approximately 30 percent and the jet noise dropped approximately 10 db. However, turbine noise showed a slight increase giving a PNL reduction of 3 to 4 PNdb. Further testing to reduce total noise from the turbine during low-thrust, choked-inlet, conditions will be conducted in Phase II-B.

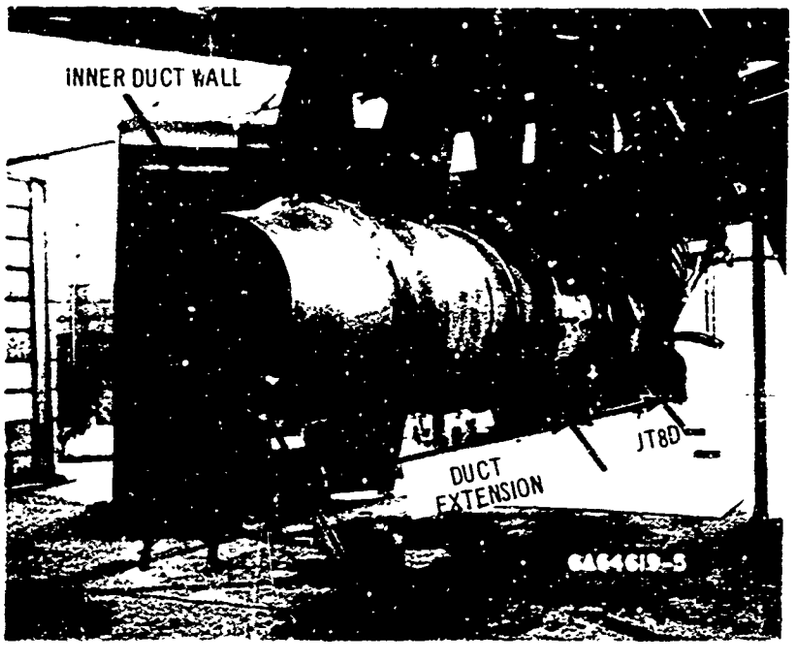


(A) COMPLETE INSTALLATION

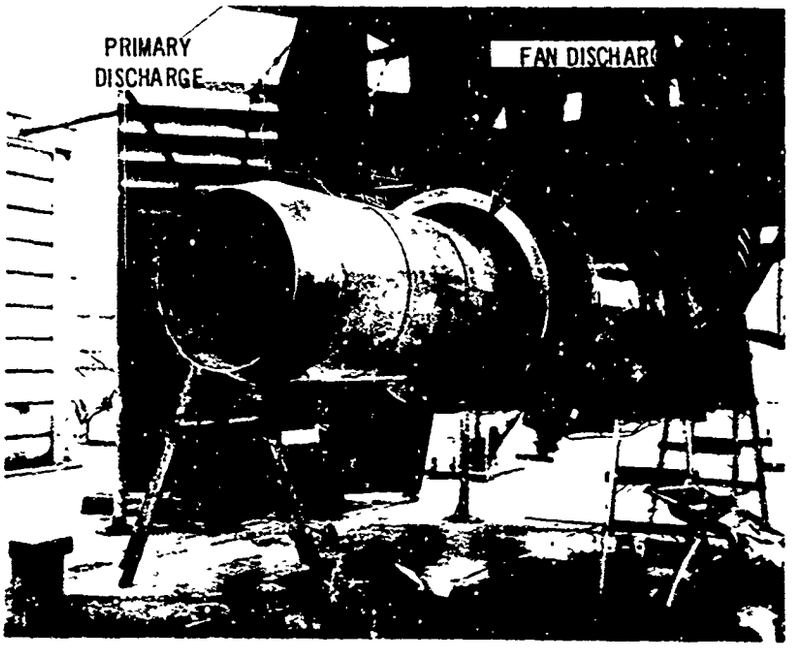


(B) INNER DUCT WALL, WITH TREATED OUTER WALL REMOVED

*FIG. 3–20 JT8D TURBOFAN ENGINE WITH ACOUSTICALLY-TREATED EXTENSION OF FAN DUCT*

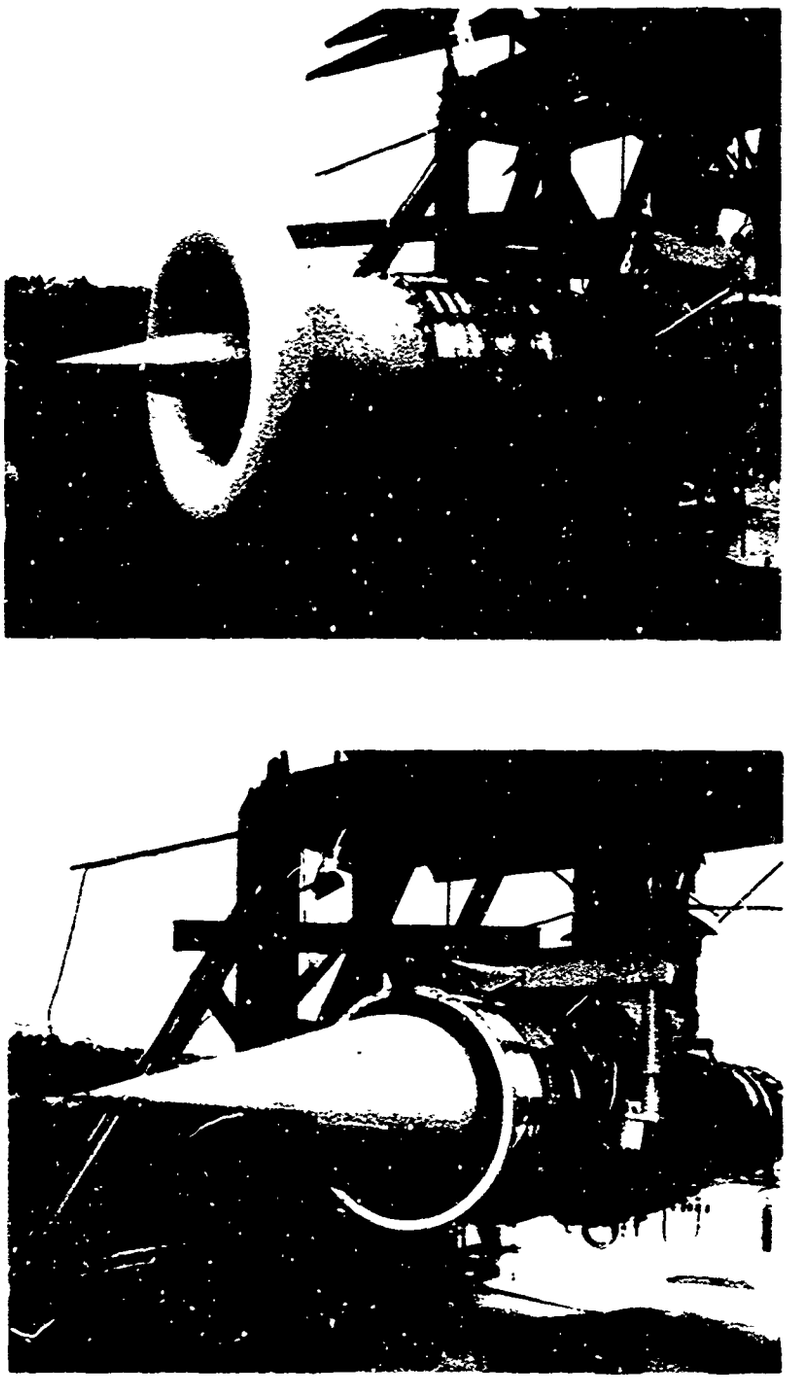

FIG. 3-21 CENTER PLUG INSTALLATION ON J-75 ENGINE FOR ACOUSTIC EVALUATION OF CHOKED FLOW

## 3.4 REFERENCES

Copies of the following referenced data may be obtained by making a request to either:

The Boeing Company
Suite 1200 Commonwealth Building
1625 K Street N. W.
Washington 6, D. C.

or

The Boeing Company
Airplane Division
P.O. Box 707
Renton, Washington
Attn: M. L. Pennell, Organization 6-2000, Mail Stop 73-60


3-1 Sawhill, R. H., "Evaluation of Koppers Ground Suppressor," Boeing Test Report T6-3174, October 1964

3-2 FAA letter to Mr. M. L. Pennell from Mr. Gordon Bain, dated October 5, 1964 concerning "Procedures for Predicting Jet Noise."

3-3 Sawhill, R. H., and Zable, D., "1/8th Scale Model Far-Field Acoustic Tests of SST Engine Nozzle Configurations," Boeing Test Report T6-3178, October 1964

3-4 McKaig, M. B., "Fan-Discharge Noise Suppression Test on JT8D Engine," Boeing Test Report T6-3166, October 1964

3-5 McKaig, M. B., "Acoustic Testing of Inlet Noise Suppression Devices for the SST," Boeing Test Report T6-3173, October 1964

## 4.0 INTERNAL NOISE

Figs. 4-1 and 4-2 present estimated 733-290 cruise and takeoff sound levels compared to similar values measured in current subsonic jets (Ref. 4-1). These figures show that the 733-290 sound levels will be substantially equal to or less than those in current subsonic jets. Although the 733-290 sound levels satisfy the subsonic jet equivalence requirement of the standard, they do exceed the mid-frequency requirements of the NCA standard for cruise and takeoff. Figs. 4-3 and 4-4 show that sound levels in current subsonic jets do not meet the NCA standard. During the Phase II-A study, a detailed analysis was made of potential internal noise sources and of the noise reduction characteristics of the structure and the associated sound insulation. The work is used as a basis for the 733-290 prediction and is reported herein. Additional data on internal noise levels are shown in Par. 4.4.

## 4.1 INTERNAL NOISE DESIGN

The sound level estimates are based on the typical insulation configuration cross section shown in Fig. 4-5. The design shown is a development of insulation configurations which have proved successful in Boeing subsonic transports. The design, as shown, achieves the largest possible noise reductions consistent with the available space and with the efficient use of weight. The design includes the installation of highly efficient type AA (or equivalent) Fiberglas which must conform to the Boeing BMS 8-48 acoustic specification. The interior trim panels are isolated from structure, taking full advantage of the "double wall" construction. Insulation is installed approximately 0.7 inches inboard of the frames, eliminating possible flanking noise paths. The air space between the insulation and the trim eliminates possible direct coupling between these elements. In the aft section of the airplane, a 0.5 pound-per-square-foot sheet of lead is embedded within the insulation batt to alleviate the additional noise during takeoff. Noise radiation from the floor panels is reduced by installing rugs and pads which satisfy the Boeing acoustic specification BMS 8-36. The noise reduction characteristics of the fuselage structure will generally be superior to those of current subsonic jets, particularly in the low frequencies, because of the stiffer fuselage construction.

Studies such as those described in Refs. 4-2, 4-3 and 4-4 which are directed toward improving the noise reduction characteristics of the total fuselage structure by methods consistent with other airplane requirements, will continue during Phase II-B.

## 4.2 NOISE SOURCE ANALYSIS

There are three types of noise that affect cabin sound levels; equipment and system noise, engine noise, and boundary layer noise. The characteristics of each are discussed in the following sections.

### 4.2.1 Aerodynamic Boundary Layer Noise

The methods used to estimate boundary layer noise levels for the Phase II-A airplane are the same as those used to estimate levels for the Phase I proposal. Because the accuracy of the method was questioned

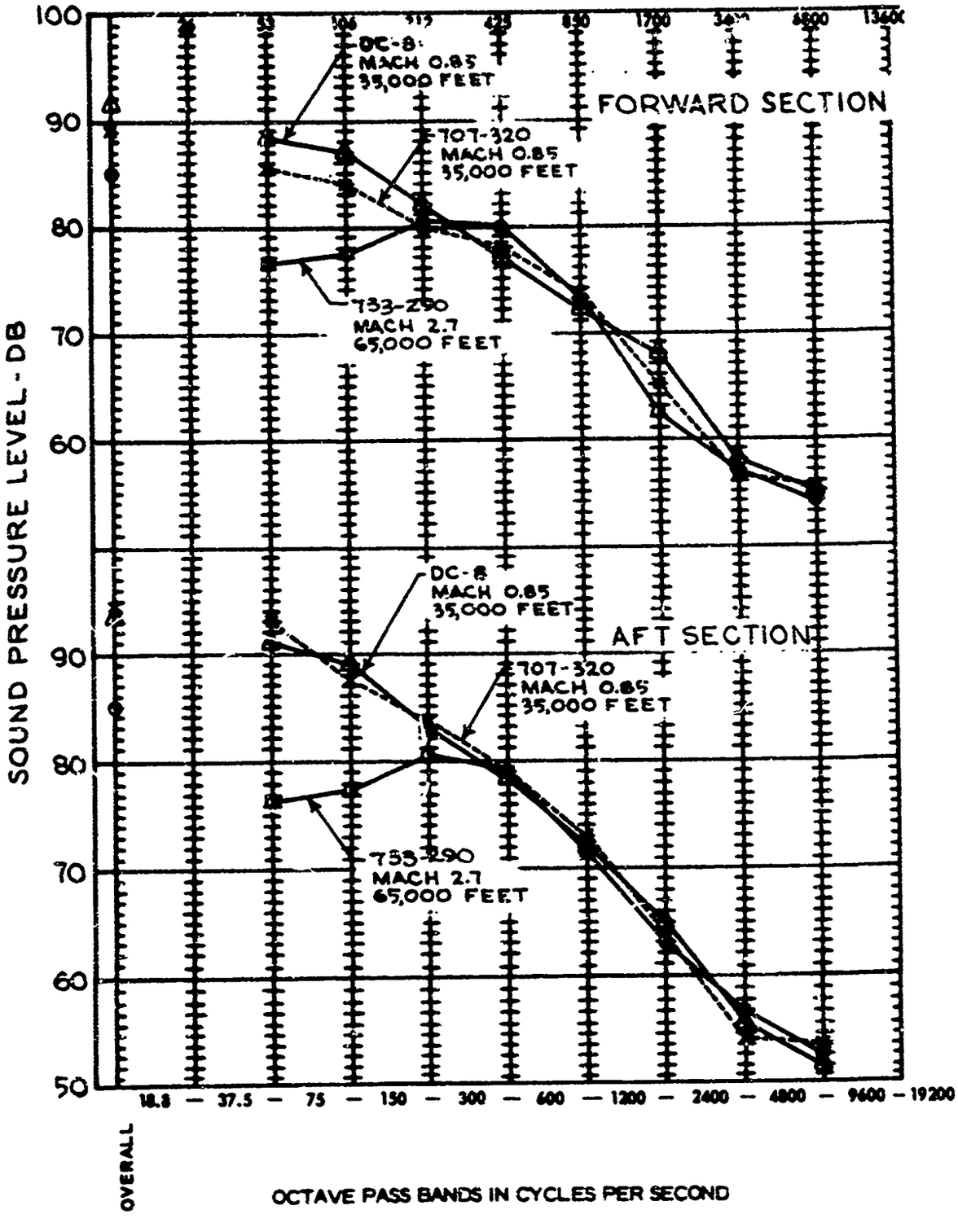


*FIG. 4-1 CRUISE SOUND LEVEL COMPARISON 733-290, 707-320 AND DC-8*

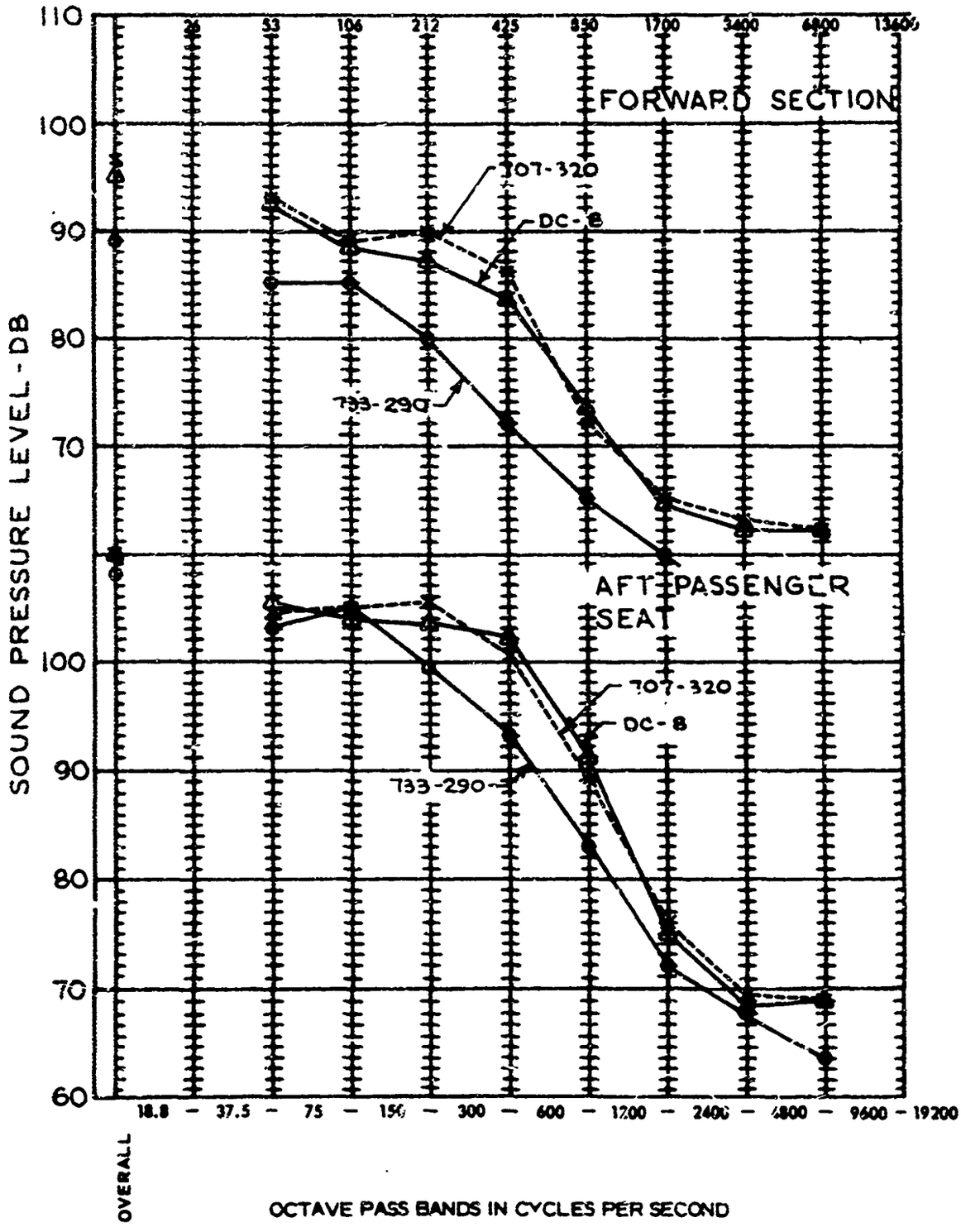


*FIG. 4-2 COMPARISON OF TAKEOFF SOUND LEVELS*

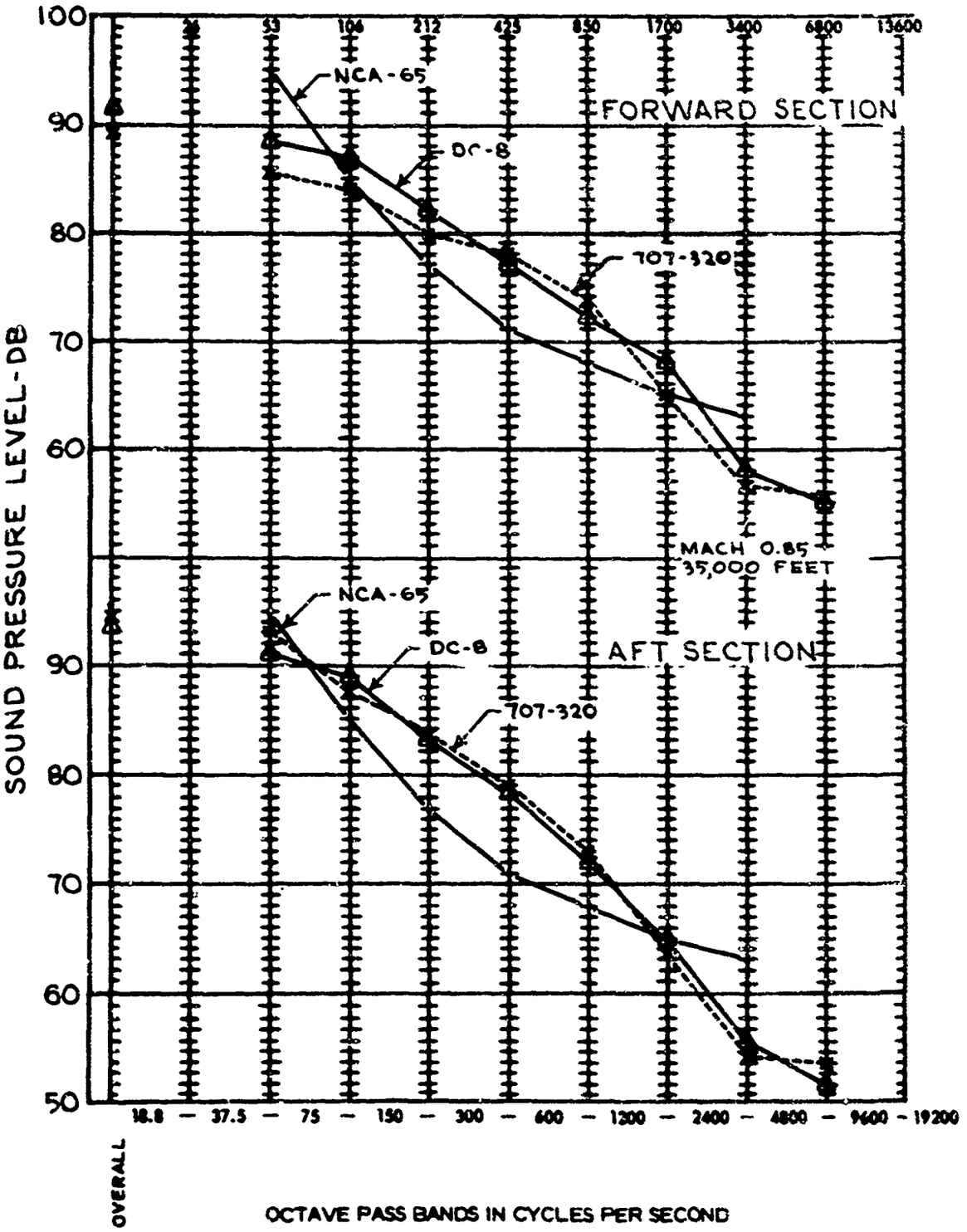


*FIG. 4-3 CRUISE SOUND LEVEL COMPARISON, 707 AND DC-8 WITH NCA-65*

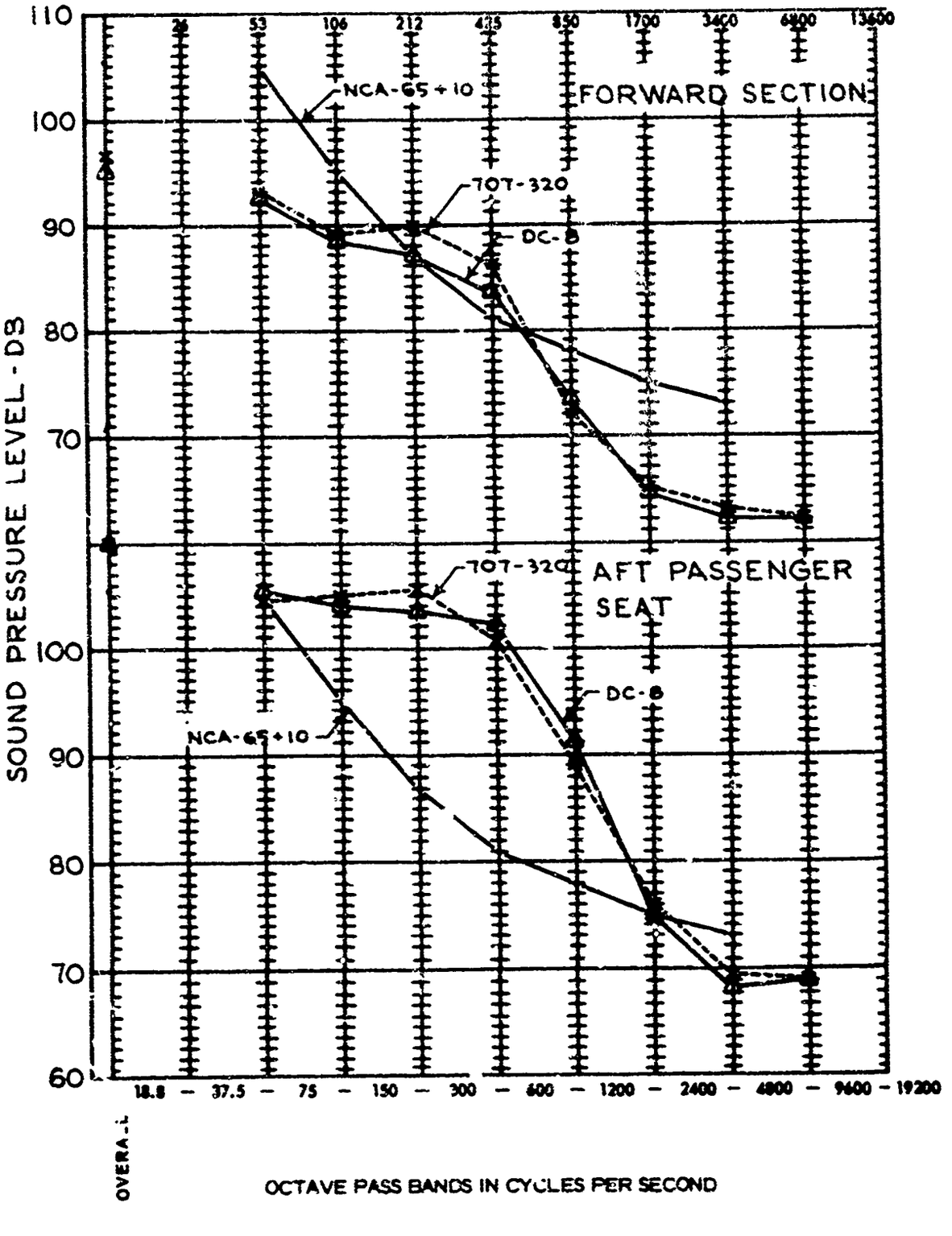


*FIG. 4-4 COMPARISON OF TAKEOFF SOUND LEVELS IN LONG RANGE SUBSONIC JETS WITH NCA-65+10*

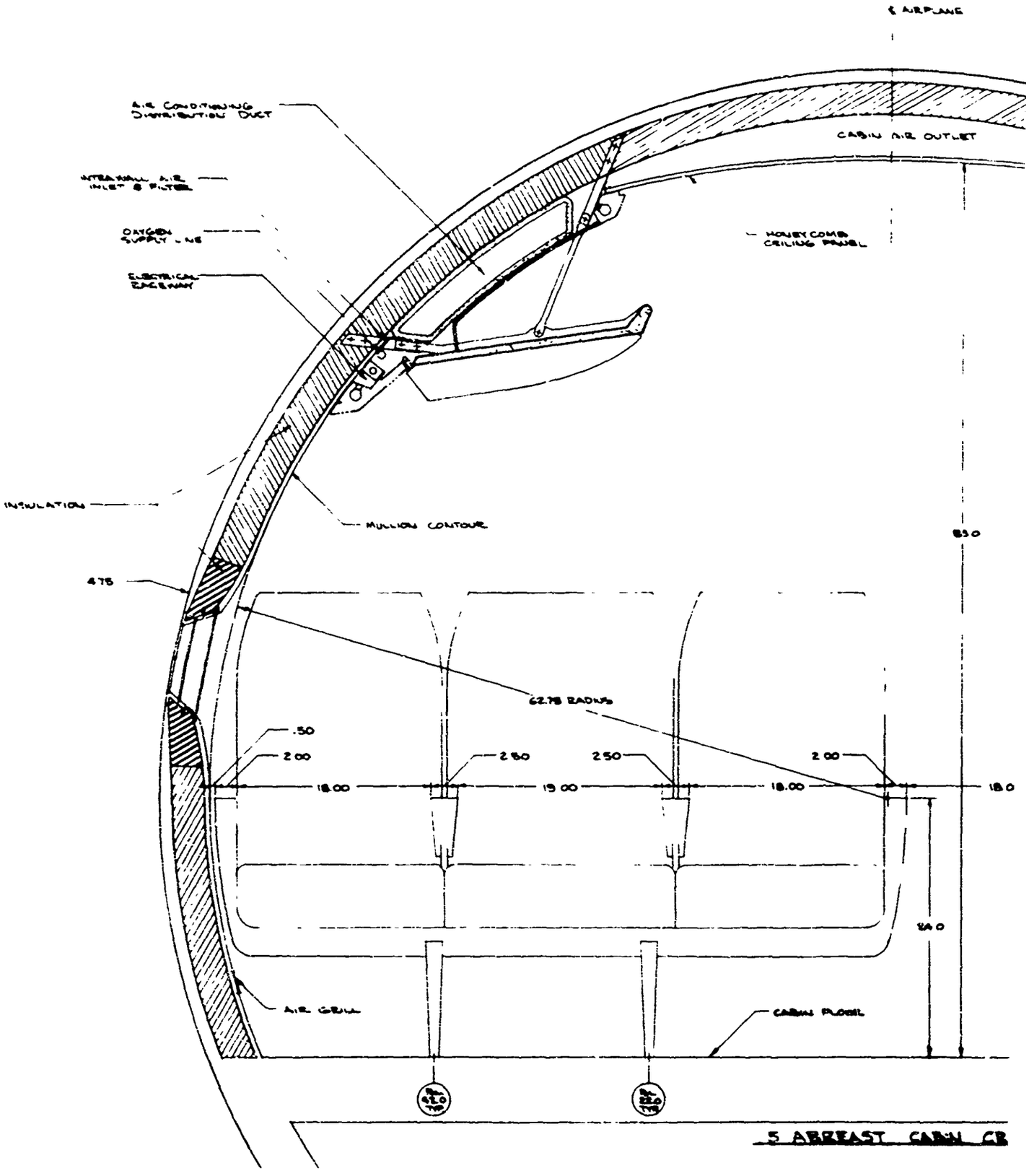


1-5 PASSENGER CABIN CROSS SECTION

A

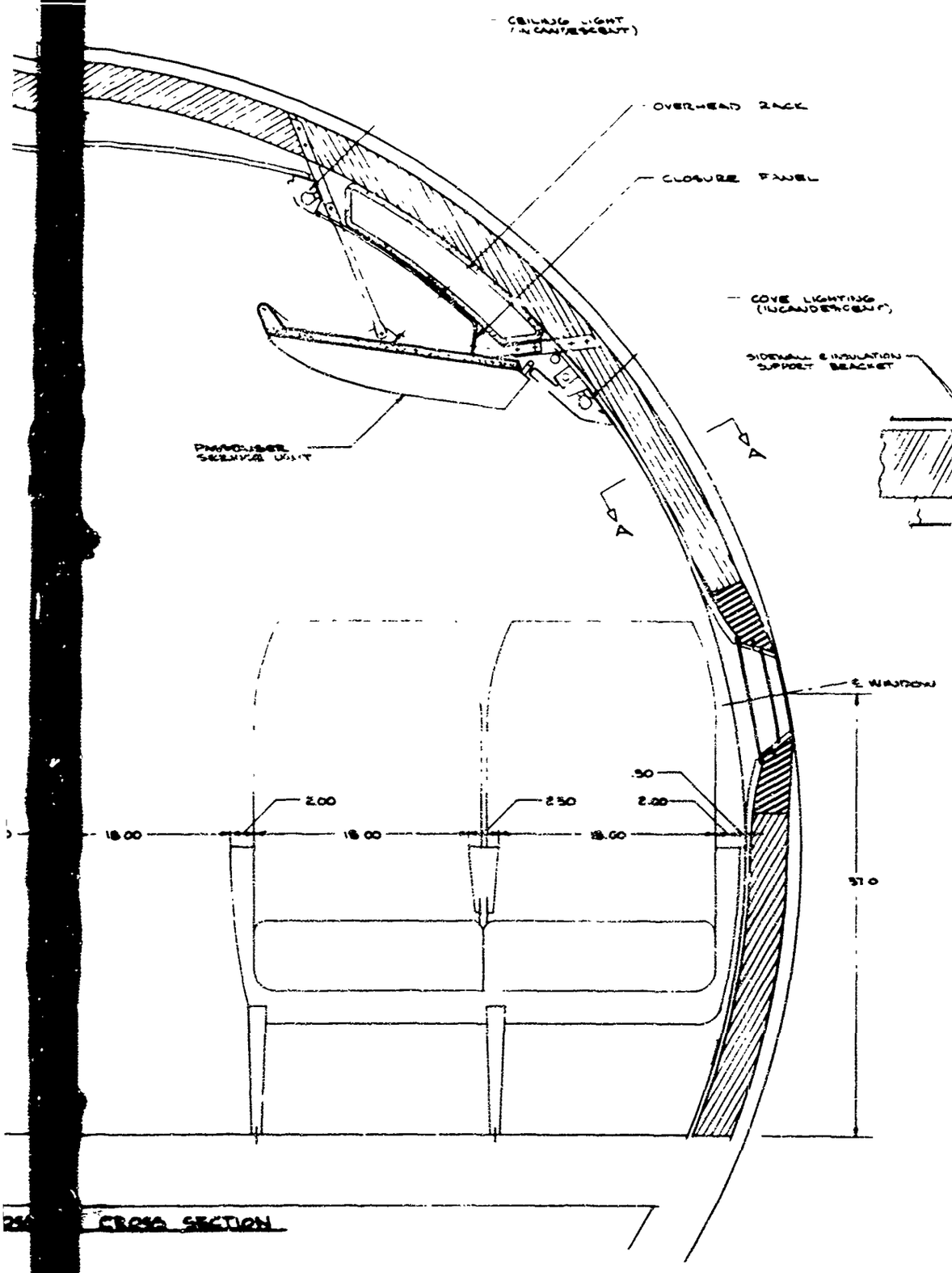


CROSS SECTION

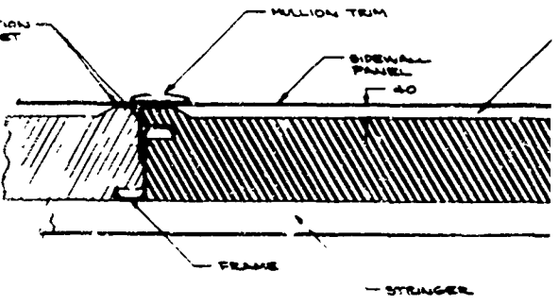


SECTION A-

B

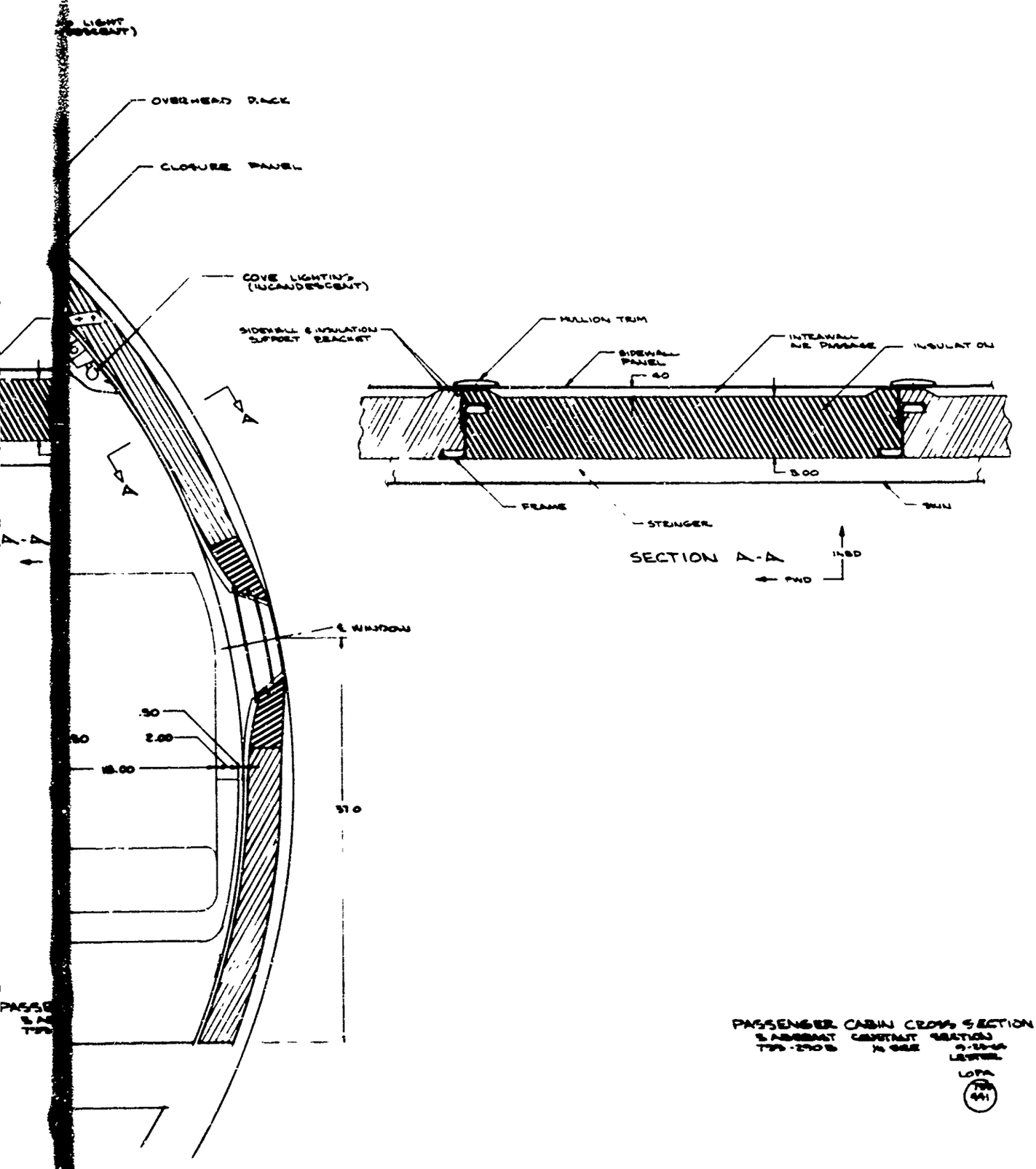


PASSENGER CABIN CROSS SECTION
B ABRAHAM CONSTANT VISCOSITY
TYPE 2707B IN USE
LOPA
TYPE 441

in the Phase I evaluation, the accuracy has been re-evaluated. It is concluded that the original method is the most reliable presently available for estimating the boundary layer pressure fluctuations on the surface of a supersonic transport. The method uses data obtained in a supersonic wind tunnel by Kistler and Chen (Ref. 4-5). The boundary layer pressure data given in this source were measured under conditions which more nearly simulate those encountered on the fuselage of a supersonic transport than any other data presently available.

The basic data curves taken from Ref. 4-5 are reproduced in Fig. 4-6. The power spectral density of the boundary layer pressures [Em(f)] can be derived from these curves as a function of the boundary layer thickness $\delta$ and the free stream velocity $U_\infty$. Charts for estimating boundary layer thickness from the velocity, the pressure altitude, the Reynolds number, and the fuselage station are given in Ref. 4-6 along with charts which give the conversion from power spectral density to octave band sound pressure level.

There is poor agreement between supersonic wind tunnel boundary layer noise data and data measured on flight vehicles. However, most of the vehicle measurements have been obtained under conditions where non-uniform flow conditions were likely, or during conditions where the dynamic pressures were much higher than those obtained in the laboratory experiments, or those which will be encountered on the surface of a supersonic transport. Recent measurements reported in Ref. 4-7 demonstrate that the incidence of strong shock waves on a boundary layer can increase the level by as much as 15 to 20 db. It was also demonstrated that conditions such as surface roughness and separated flow can increase the boundary layer pressure levels by significant amounts. However, in the case of the undisturbed boundary layer, the Ref. 4-7 data substantially agree with the values calculated from the Kistler and Chen data (Ref. 4-5) if account is taken of the different dynamic pressures and boundary layer thicknesses involved.

When using the Kistler and Chen data to predict supersonic boundary layer pressures, it is assumed that the boundary layer adjacent to the passenger cabin is not significantly disturbed by the presence of shock waves or surface discontinuities and that separated flow conditions do not exist. The fulfillment of this assumption is also a necessary condition for satisfactory aerodynamic performance of the airplane. The same assumption is also made in the discussion of supersonic transport noise given in Ref. 4-6.

Although present considerations do not indicate that significant shock waves or other phenomena will disturb the boundary layer adjacent to the passenger cabin, a theoretical and laboratory (supersonic wind tunnel) program is being initiated (Ref. 4-4) to study the possible adverse effects from these phenomena and possible methods of eliminating them. Recent experiments in the Boeing subsonic boundary layer test facility (Ref. 4-3) concerned with the radiation of accoustic energy from skin panels excited by boundary layer fields indicate that it may be

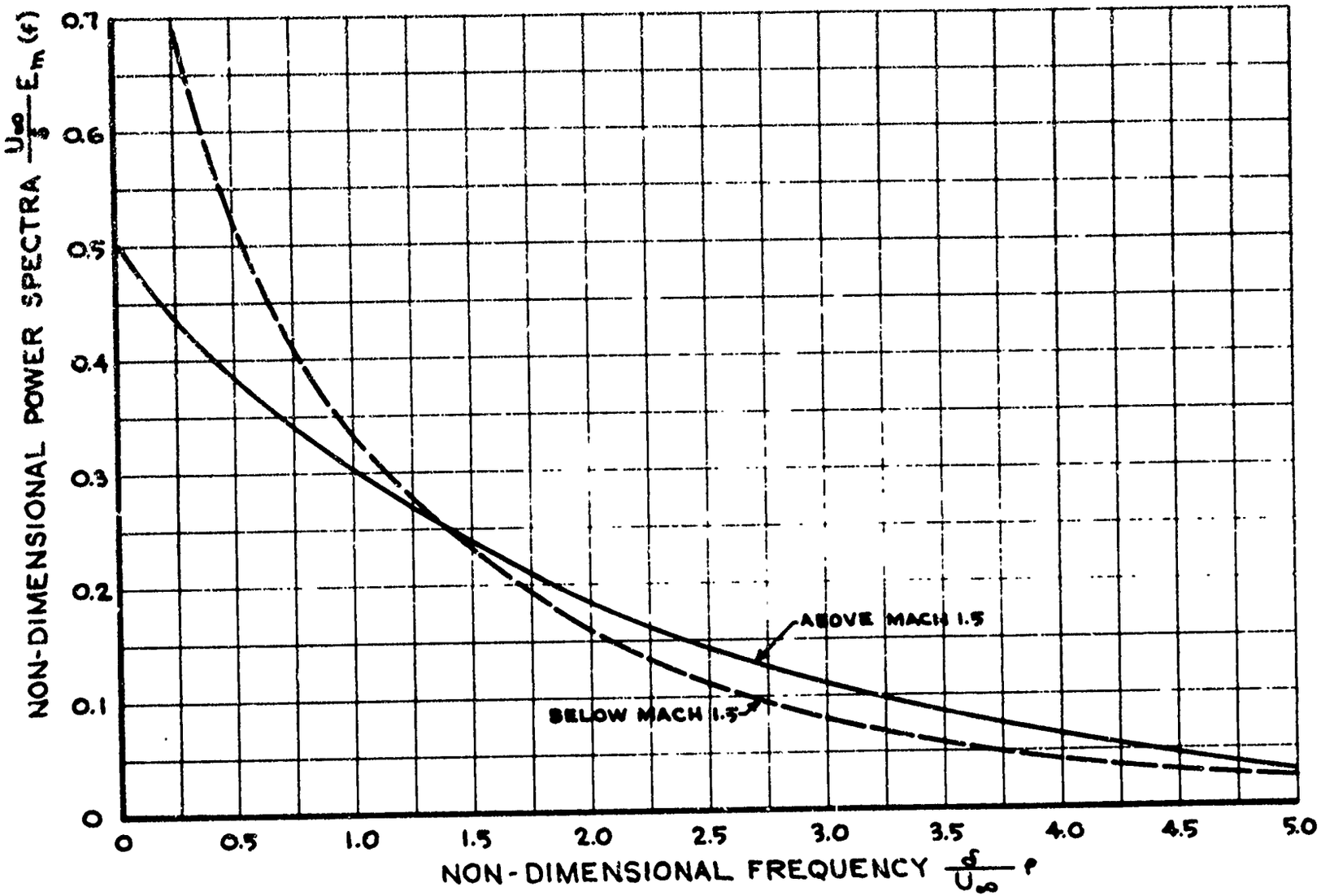


FIG. 4-6 DIMENSIONLINE FLUCTUATING PRESSURE SPECTRUM FOR SUPERSONIC BOUNDARY LAYER

possible to obtain noise reductions well in excess of theoretical prediction by the use of damping material or by modifying the skin panel sizes. These studies will be continued with the objective of developing the best possible structural and insulation configuration to reduce noise and to eliminate any possible adverse effects which might occur because of irregularities in the boundary layer.

The Kistler and Chen data (Ref. 4-5) shows that there is a significant reduction in the magnitudes of the low frequency boundary layer pressures at airspeeds above Mach 1.5 in addition to the normal shift of the maximum pressure frequency towards the higher frequencies as a function of velocity. This effect has also been measured in other laboratory and flight vehicle tests including Refs. 4-7 and 4-9. This factor is significant because it means that the low frequency boundary layer noise levels will be significantly less at the supersonic flight conditions than would be predicted from an extrapolation of subsonic boundary layer data. A large portion of the energy associated with the supersonic boundary layer is concentrated in the very-high-frequency range where it can easily be attenuated by efficient high-frequency noise reduction techniques.

Estimated octave band boundary layer sound pressure levels are shown in Fig. 4-7 at typical fore and aft fuselage stations for flight conditions of Mach 2.7, 65,000 feet and Mach 1, 32,000 feet.

4.2.2 Equipment and System Noise

A certain amount of noise from sources such as the air-conditioning and hydraulic systems is inevitable. Every effort will be expended during design development phases to reduce the noise produced by these sources. Anticipated values for the accumulative effects from equipment and system noise are shown in Fig. 4-8. These data were obtained from a 707 airplane during a low subsonic flight. In some frequency ranges, the noise from these sources contributes to the ambient sound levels (Fig. 4-8).

4.2.3 Engine Noise

The engines on the 733-290 airplane are located significantly farther aft with respect to the passenger cabin than they were on the Phase I airplane. The last passenger seat is located approximately 50 inches forward of the engine tailpipes. The highest internal engine noise levels are found in the aft cargo compartment and in the aft entry way; the aft passenger seat will be shielded from this noise by the cargo bulkhead and by the toilet compartments and galleys. Because of the aft location of the engines, engine noise will not be audible in the passenger compartment during any supersonic flight condition. The most notable effects due to engine noise occur during the initial takeoff. Estimated sound pressure levels on the external side of the fuselage during takeoff are shown in Fig. 4-9. The data estimates are based on full scale J-75 engine noise tests supplemented by model studies (Ref. 4-10 and 4-11).

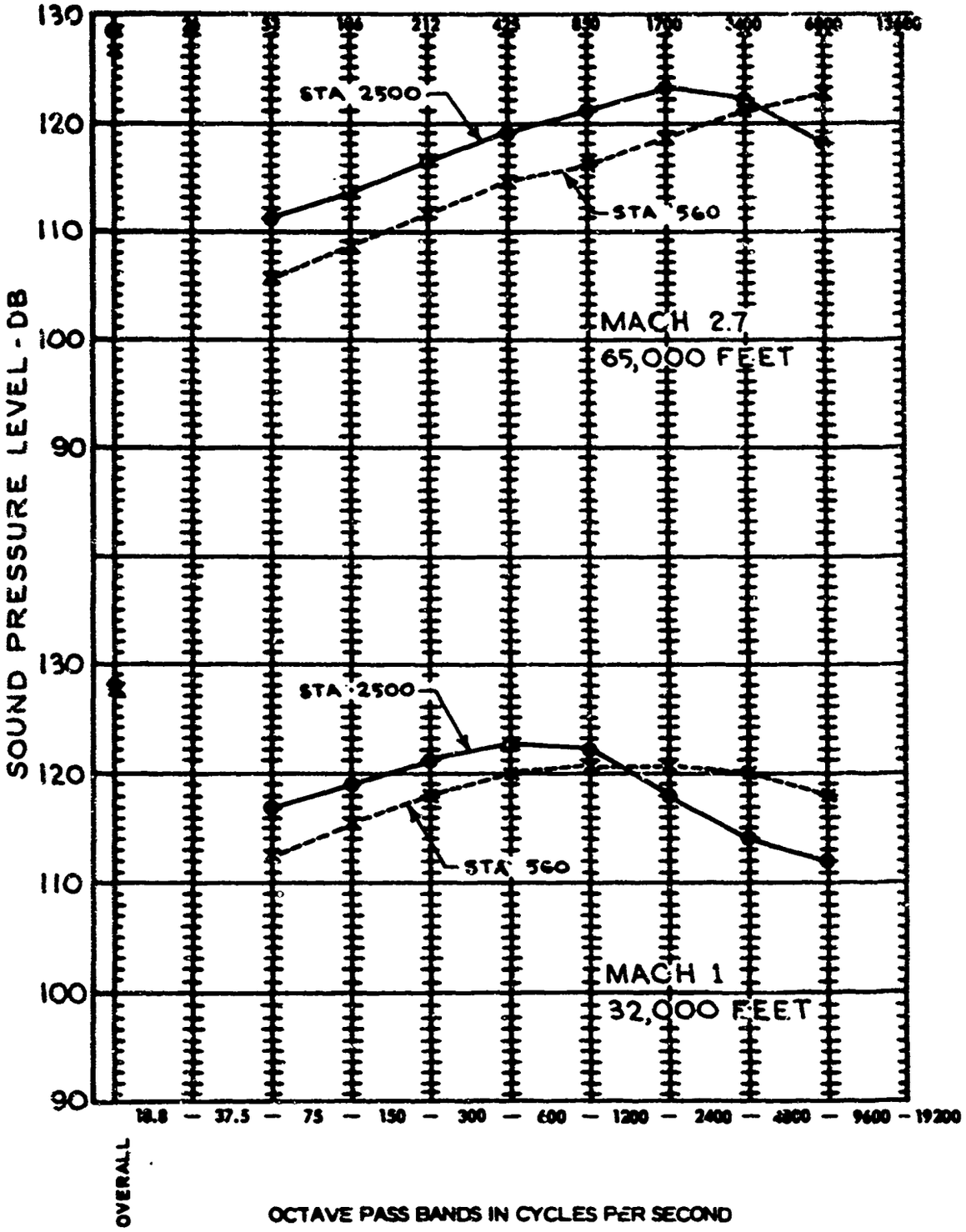


*FIG. 4-7 AERODYNAMIC BOUNDARY LAYER SOUND PRESSURE LEVELS FOR CRUISE AND CLIMB CONDITIONS*

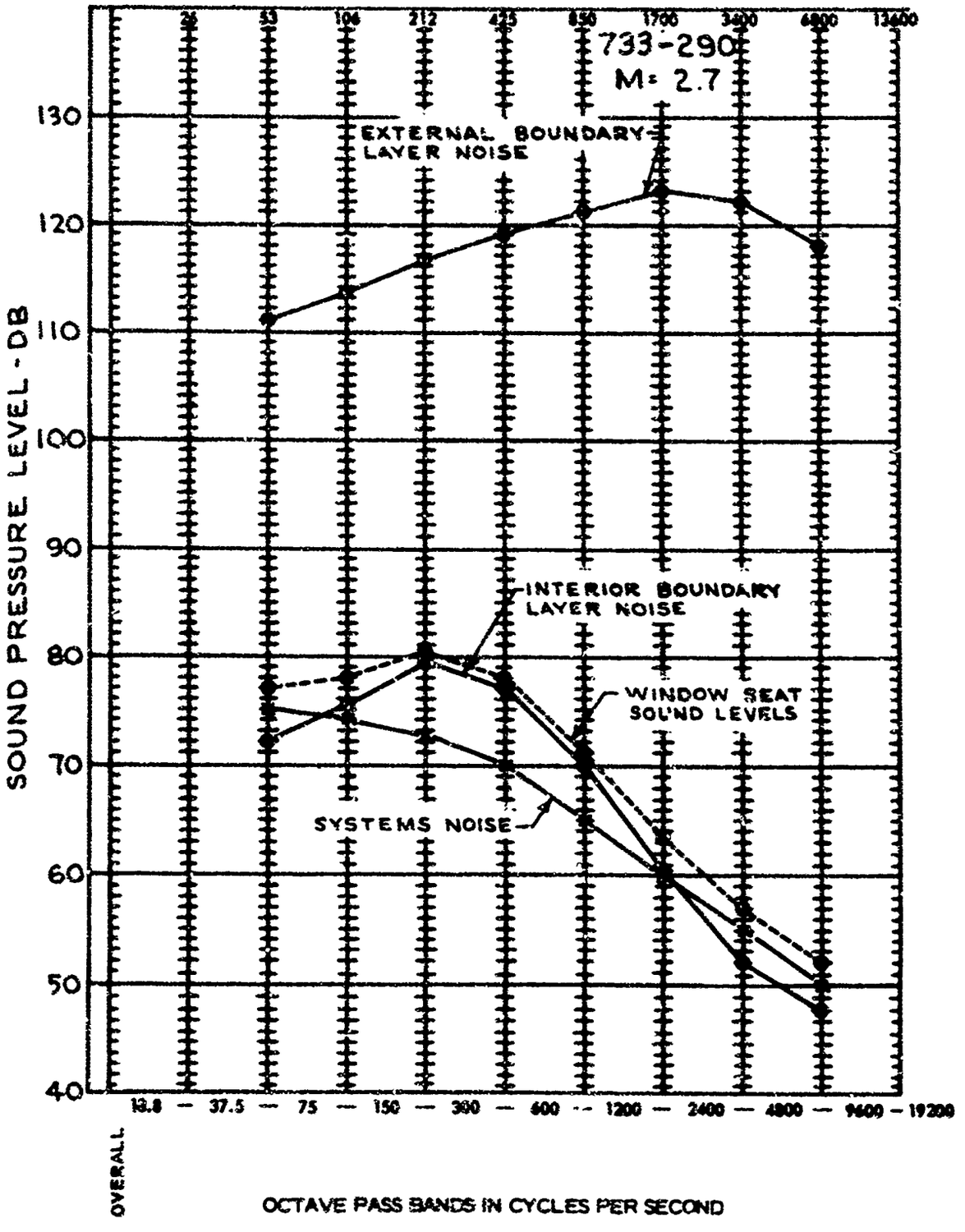


*FIG. 4-8 RELATIVE INTERNAL AND EXTERNAL SOUND PRESSURE LEVELS AT CRUISE ~~IN THE BOEING 727~~*

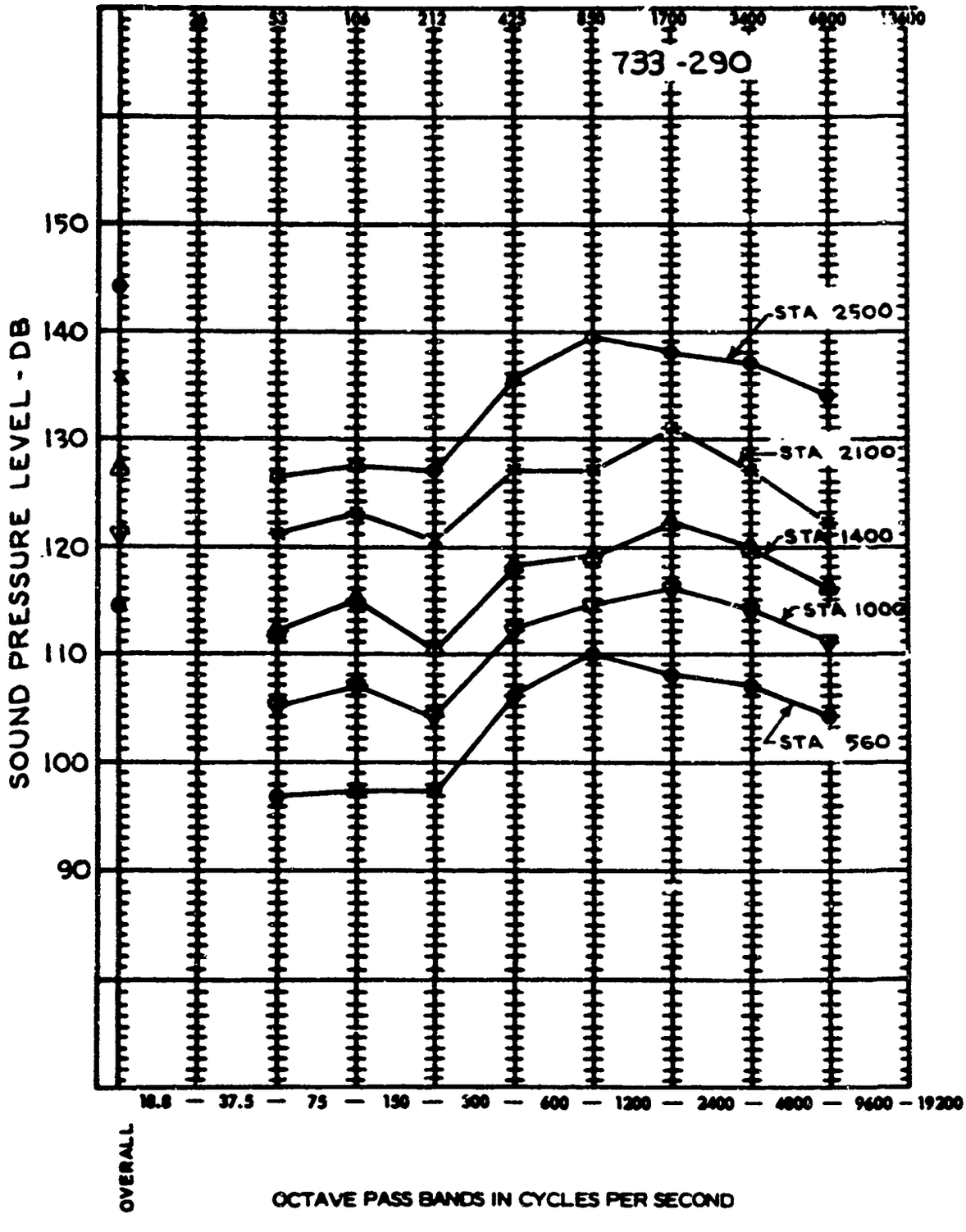


*FIG. 4-9 SOUND LEVELS ON FUSELAGE UNDER STATIC TAKEOFF THRUST CONDITIONS*

## 4.3 ANALYSIS OF STRUCTURAL AND INSULATION NOISE REDUCTION CHARACTERISTICS

The method used to estimate fuselage noise reduction characteristics has been improved. The method used in the Phase I proposal involved the extrapolation of test data obtained with a fuselage mockup test section. A review of the important parameters has shown that the construction of the mockup section is not now representative of the 733-290 configuration and data obtained with the mockup is therefore not valid as a base line for the Phase II-A calculation.

The improved method of estimating noise reduction characteristics is based on Ref. 4-12. The method involves the calculation of the transmission loss characteristics of the basic fuselage structure and includes modifications to these characteristics due to the addition of insulation materials and interior trim panels. The total noise reduction characteristics are then obtained by correcting the transmission loss curve to account for reverberation and standing-wave effects within the airplane fuselage.

According to this method, the noise reduction characteristics of the basic fuselage structure in the low and mid frequencies are a function of the surface density of the fuselage skin panels, the fundamental resonant frequency of the skin panels, and the damping characteristics of the panels. At frequencies above the resonant frequency, the noise reduction is governed primarily by the acoustic mass law and at frequencies below the resonant frequency, the noise reduction characteristics are in the stiffness-controlled region.

A change in the resonant frequency can significantly modify the noise reduction characteristics of the fuselage. This factor is important because studies conducted at Boeing (Ref. 4-13) indicate that there is a significant change in the resonant frequency between unpressurized conditions such as takeoff and pressurized conditions such as cruise. The Ref. 4-13 study shows that the noise reduction characteristics of the Boeing 707 are approximately 10, 15, and 14 db greater in the 37-75, 75-150, and 150-300 cps octave bands, respectively, at cruise altitudes than they are at takeoff. A formula developed at Boeing gives the following relationship between the pressurized and the unpressurized resonant frequency of the structure:

$$f_p = \sqrt{f_{up}^2 + \frac{g}{\gamma h}\frac{\Delta Pr}{4}\left(\frac{1}{2a^2} + \frac{1}{b^2}\right)} \qquad \text{Eq. 4-1}$$

$f_p$ = fundamental resonant frequency at pressurized conditions

$f_{up}$ = fundamental resonant frequency at unpressurized conditions

$g$ = acceleration due to gravity

$\gamma$ = density of skin panel material

$h$ = panel thickness

a = panel dimension in horizontal direction

b = panel dimension in vertical direction

r = fuselage radius

$\Delta P$ = pressure differential

As an example, application of this formula to the sidewall structure at Station 2500 on the 733-290 gives a resonant frequency of 790 cps for the pressurized condition whereas the unpressurized resonant frequency is approximately 230 cps.

Reports in the literature (Ref. 4-8) indicate that attempts to predict cabin noise from aerodynamic boundary layer estimates and noise reduction estimates have not generally been successful in the low frequency region. Actual levels have been 10 to 20 db less than the predicted values. Failure to take account of pressurization effects may be responsible for these differences.

Noise reduction charts showing the total estimated noise reduction characteristics of the Model 733-290 configuration at typical fore and aft fuselage stations are shown for both pressurized and unpressurized conditions in Fig. 4-10. Fig. 4-11 illustrates the individual noise reductions attributed to the structure, and to the insulation and interior trim panels.

The total high-frequency noise reduction attainable in the cockpit is less than can be achieved in the passenger compartment (Fig. 4-10) because of special noise reduction design problems. Among these are the loss of sound absorption due to the absence of high-density passenger type seating and the decrease in sidewall transmission-loss due to equipment and control installations.

Typical parameters used in calculating the characteristics shown in Fig. 4-10 are given below:

***TABLE 4-B TRANSMISSION LOSS PARAMETERS***

| | STATION 800 | STATION 2500 |
|---|---|---|
| Unpressurized Resonant Frequency | 130 cps | 230 cps |
| Pressurized Resonant Frequency | 835 cps | 790 cps |
| Skin Thickness | 0.033 inches | 0.055 inches |
| Skin Surface Density | 0.76 $lb/ft^2$ | 1.262 $lb/ft^2$ |
| Avg. Skin Stringer Surface Density | 1.14 $lb/ft^2$ | 1.89 $lb/ft^2$ |
| Insulation Surface Density | 0.25 $lb/ft^2$ | 0.25 $lb/ft^2$ |
| Trim Surface Density | 0.36 $lb/ft^2$ | 0.36 $lb/ft^2$ |
| Septum Surface Density | 0.092 $lb/ft^2$ | 0.592 $lb/ft^2$ |

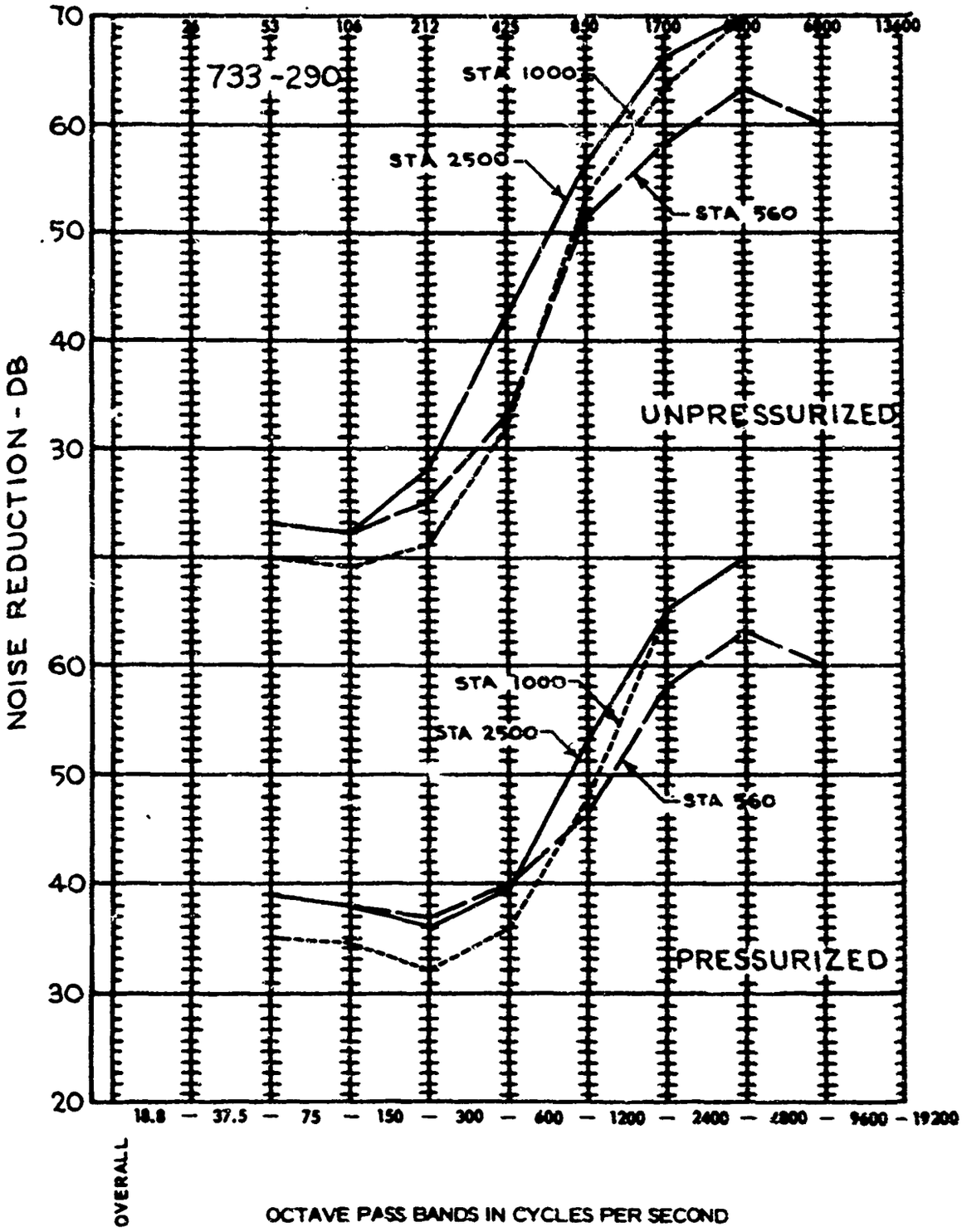


*FIG. 4-10 NOISE REDUCTION CHARACTERISTICS OF THE FUSELAGE AND SOUND INSULATION CONFIGURATION*

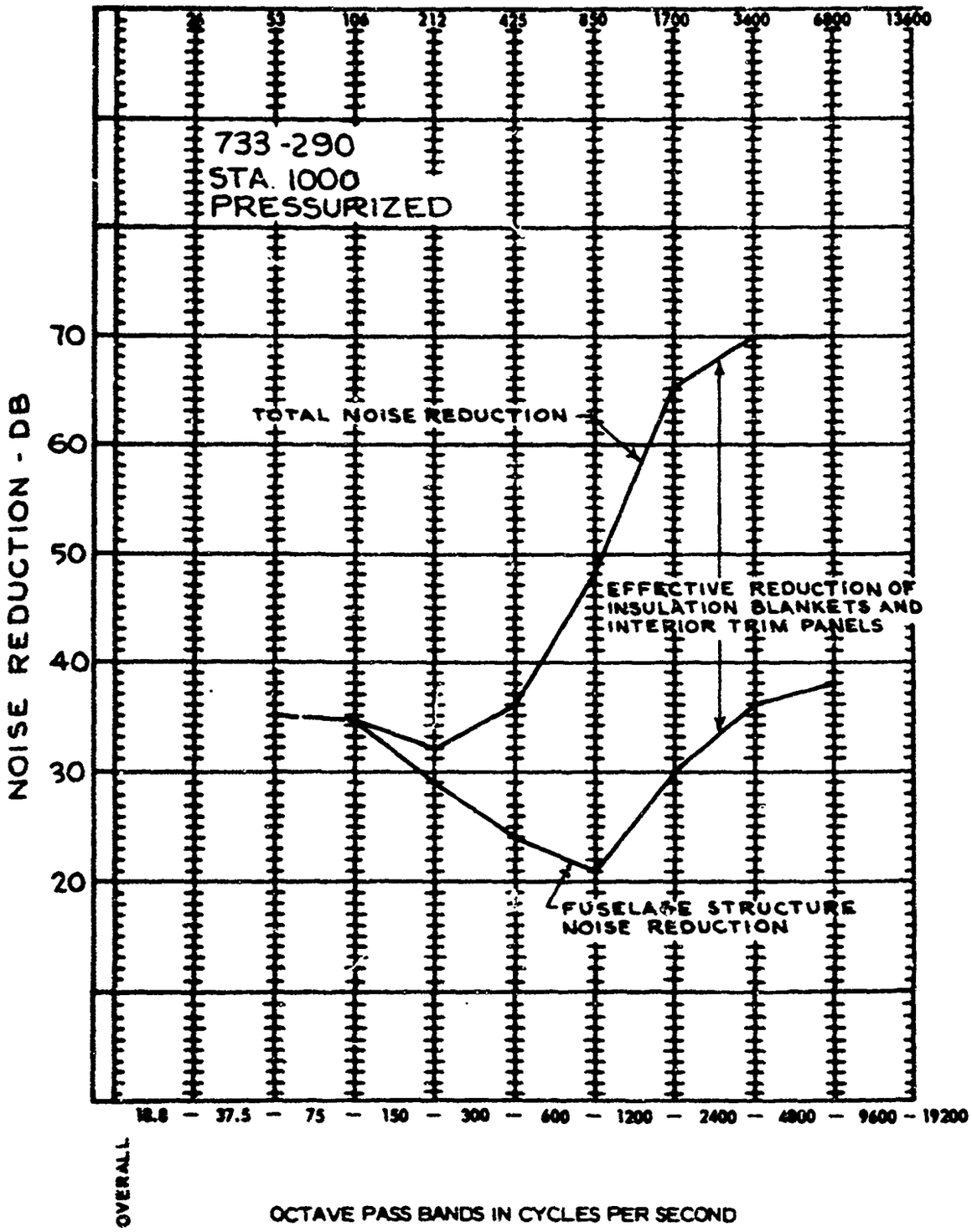


*FIG. 4-11 TYPICAL NOISE REDUCTION CHARACTERISTICS OF THE FUSELAGE AND SOUND INSULATION CONFIGURATION*

The values used for the noise reduction characteristics of the insulation and the isolated trim panels are taken from published and unpublished data obtained in the Boeing acoustic laboratory transmission-loss facilities (Ref. 4-14) and from in-flight data obtained in 707 airplanes.

The high-frequency noise reduction values shown in Fig. 4-10 are relatively high values, but they are not the theoretical maximum values because of the inevitable presence of flanking path noise in any real situation and because of the build up of reverberant noise in the cabin. Experience in 707 airplanes indicates that the relatively high noise reductions shown in Fig. 4-10 are achieved if care is exerted in all design phases to eliminate all possible flanking paths.

## 4.4 ESTIMATED CABIN SOUND LEVELS

Cabin sound levels are obtained by subtracting the noise reduction values given in Fig. 4-10 from the corresponding external noise levels given in Figs. 4-7 and 4-9 and by adding the effects of equipment noise. A typical result was shown in Fig. 4-8.

Cruise (Mach 2.7, 65,000 feet) and transonic acceleration (Mach 1, 32,000 feet) cabin sound levels are given in Fig. 4-12. The body stations indicated in Fig. 4-12 are related to the cabin arrangement in Fig. 4-13. The levels shown are for window seat locations. Sound levels at aisle seat locations are 2 to 3 db lower in the low-frequency octave bands and approximately the same in the high-frequency octave bands (600-1200 cps and above).

Phase II-A takeoff sound level estimates are illustrated in Fig. 4-14. At the noisiest location, the takeoff sound levels in the 733-290 are significantly less than the corresponding levels in a 707, Fig. 4-4. Because the takeoff noise levels are relatively high, 150 pounds of lead sheet has been installed in the aft section of the airplane. The lead sheet is embedded in the Fiberglass insulation between stations 2360 and 2500. At the takeoff condition, the lead sheet reduces sound levels in the 150-300, and 300-600 cps octave bands by approximately 3 and 6 db. The relatively high aft cabin sound level exists for a short period of time, diminishing by at least 10 db shortly after leaving the ground because of the beneficial effects due to the elimination of ground reflection and to the increased airspeed of the airplane.

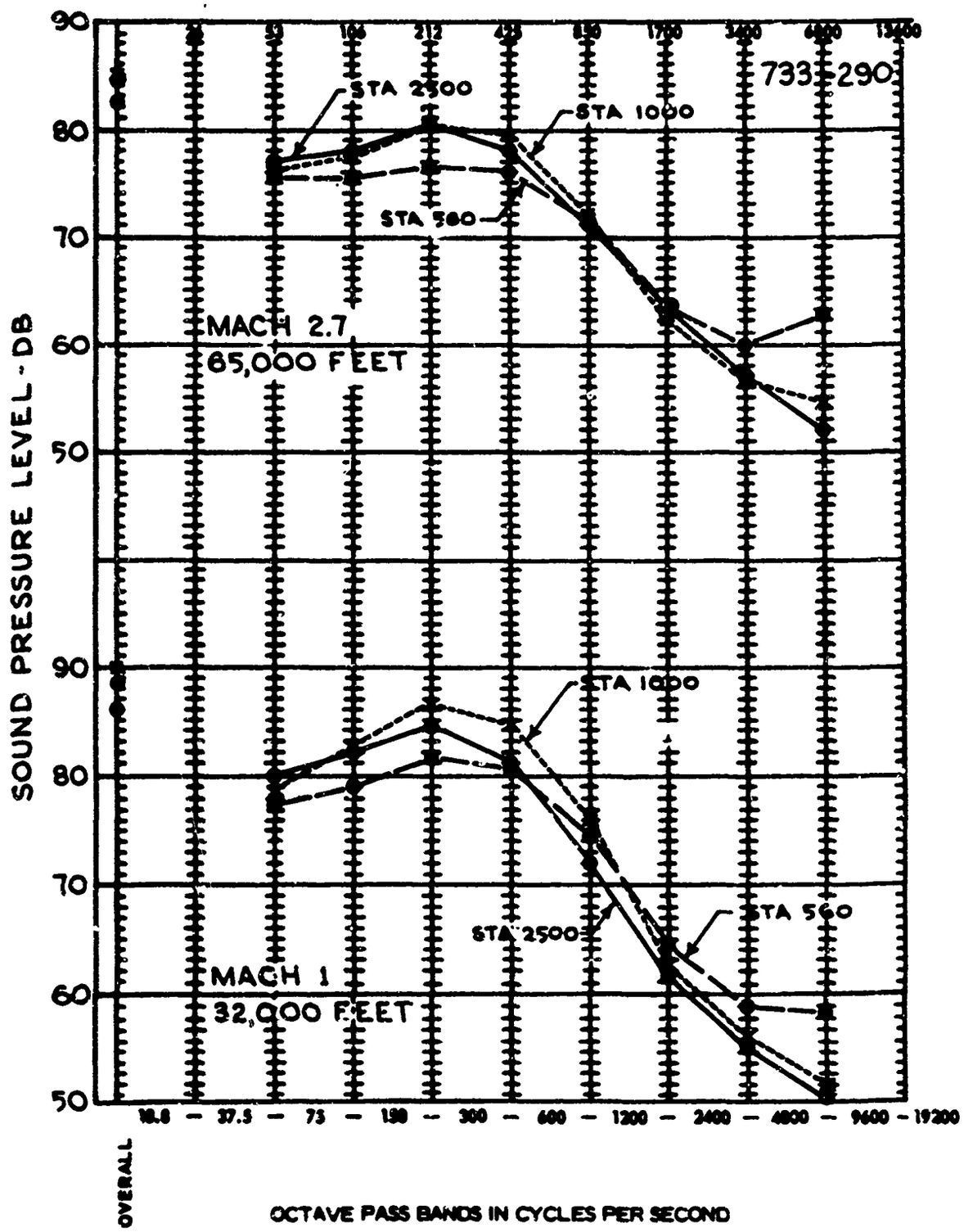


*FIG. 4-12 BOEING SST INTERIOR SOUND LEVELS AT WINDOW SEAT LOCATIONS – CRUISE AND CLIMB*

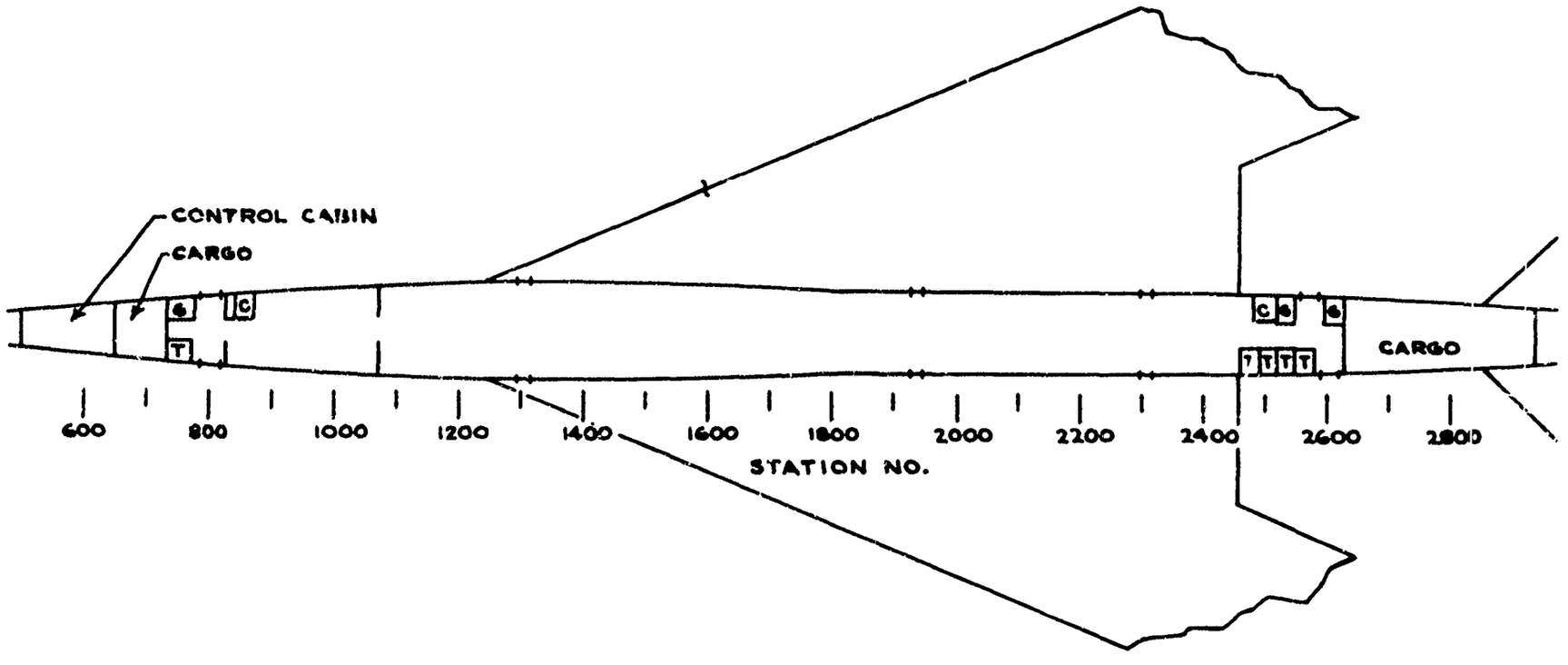


D6-6880-7



FIG. 4-13 BODY STATIONS, 733-290

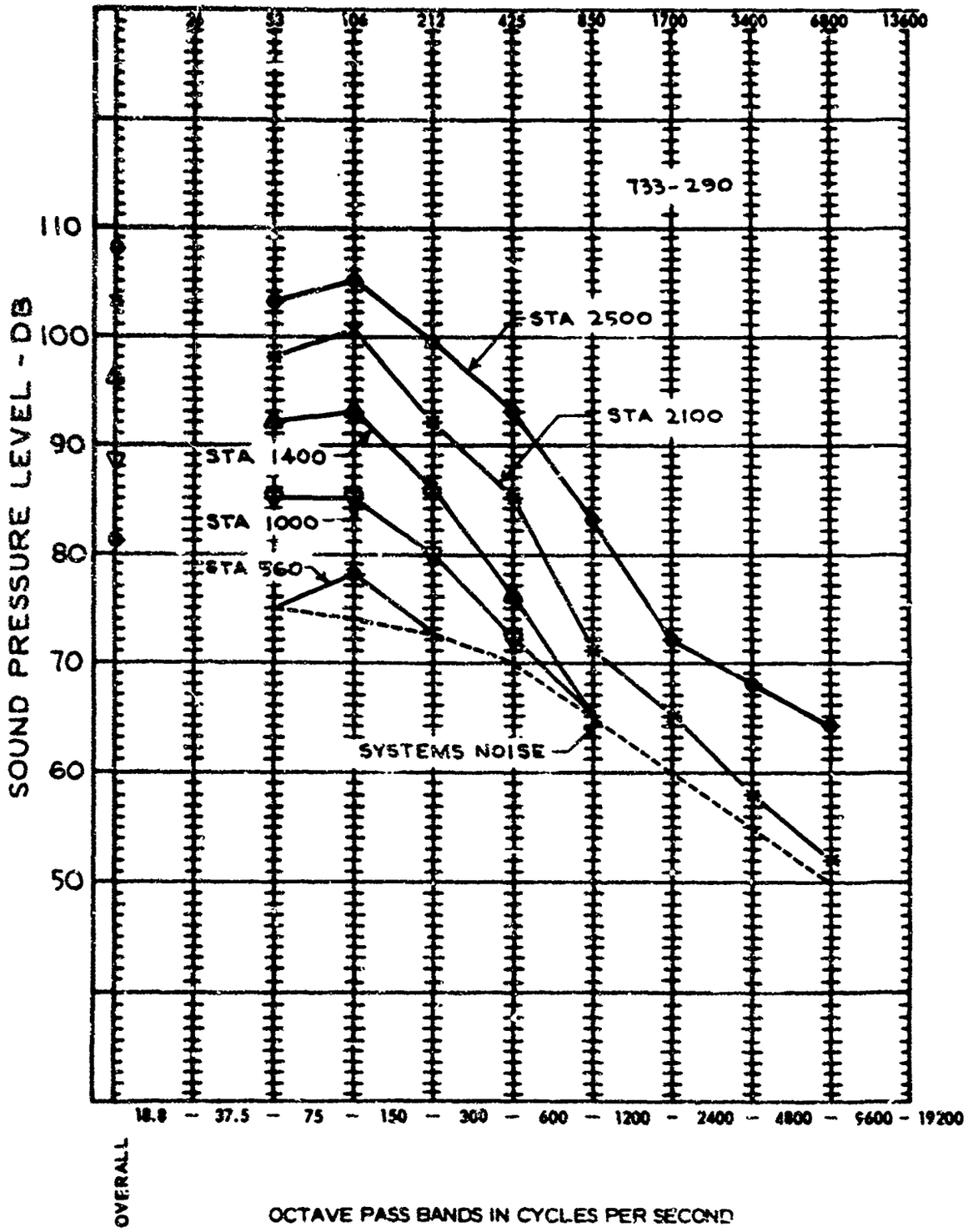


*FIG. 4-14 BOEING SST INTERIOR SOUND LEVELS AT WINDOW SEAT LOCATIONS – TAKEOFF*

## 4.5 REFERENCES

Copies of the following referenced data may be obtained by making a request to either:

**The Boeing Company**
**Suite 1200 Commonwealth Building**
**1625 K Street N. W.**
**Washington 6, D. C.**

or

The Boeing Company
Airplane Division
P. O. Box 707
Renton, Washington

Attn: M. L. Pennell, Organization, 6-2000
Mail Stop 73-60


4-1 Sound Levels in Long Range Subsonic Jets, Waite, W. F., Boeing Technical Note D6-2562 TN. October 1964

4-2 Optimization of the Mass Distribution and the Air Spaces in Multiple-Element Soundproofing Structures, Mangiarotty, R. A., October 1962

4-3 Test Results from Boundary Layer Facility (Noise Radiated by Panels), Maestrello, L., Boeing Document D6-9944, Vol. 1, January 1964

4-4 A Summary of the Test Programs Planned for the Supersonic Boundary Layer Facility, Maestrello, L., Boeing Technical Note D6-2326 TN, October 1964

4-5 The Fluctuating Pressure Field in a Supersonic Turbulent Boundary Layer, Kistler, A. L. and Chen, W. S., Journal of Fluid Mechanics, Vol. 16, Part 4, 1963

4-6 Procedure for Calculating Aerodynamic Noise on the Fuselage of a Supersonic Aircraft, Large, J. B. and Mangiarotty, R. A., Boeing Document D6-9736, September 1963

4-7 Wind Tunnel Investigation of Turbulent Boundary Layer Noise as Related to Design Criteria for High Performance Vehicles, Murphy, J. S., Bies, D. A., Speaker, W. W., and Franken, P. A., NASS Technical Note TN D-2247, April 1964

4-8 Problems of Cabin Noise Estimation for Supersonic Transports, Hay, J. A., Journal of Vibration and Sound, April 1964

4-9 Recent Free-Flight Boundary-Surface Aerodynamic Noise Measurements, Garrick, I. E., Hilton, D. A., and Hubbard, H. H., North Atlantic Treaty Organization Advisory Group for Aeronautical Research and Development, Report 467, April 1963

4-10 Near and Far-Field Noise Survey of a J-75 Engine with Standard Tailpipe, Sawhill, R. H. and Wintermeyer, C. F., Boeing Test Report T6-3176, October 1964

4-11 1/8th Scale Model Near-Field Acoustic Tests of SST Engine Nozzle Configurations, Sawhill, R. H. and Zable, D. R., Boeing Test Report T6-3177, October 1964

4-12 Methods of Flight Vehicle Noise Prediction, Franken, P. A. and Kerwin, E. M., WADC Technical Report 58-343, November 1958

4-13 Noise Reduction Characteristics of the 707 Fuselage Construction, Waite, W. F., Boeing Technical Note D6-2553 TN, October 1964

4-14 Acoustic Properties of Various Sound-proofing Materials, Taniguchi, H. H., Boeing Document D-15853, July 1955

## 5.0 SONIC FATIGUE PARAMETER

Phase II-A configuration test and analysis have resulted in:

- An engine location that provides optimum performance without imposing noise levels on the structure higher than those experienced in contemporary jet aircraft;
- A reduction of approximately 3 db achieved by engine sound attenuation;
- A net reduction in the area exposed to noise levels above 150 db. Acoustic levels are below this critical level on all wing structure and most of the primary body structure;
- An improved definition of the sonic environment through extensive model testing and analysis of airplane operations and ground maintenance engine check-out;
- Structural design parameters verified by sonic tests of structural panels representative of the proposed design;

Structural reinforcement has been provided in those places where static design does not satisfy sonic requirements.

## 5.1 DESIGN FOR SONIC FATIGUE

The sonic noise design environment of the 733-290, Fig. 5-1, is comparable to that imposed on contemporary commercial jet aircraft and is accounted for in the structural design in a similar manner. Exposure times and engine power settings were defined for normal takeoff, engine ground runup, maintenance checkout, inflight operation, and maximum augmented thrust takeoff. Acoustic power levels (presented in Par. 5.2 for the various engine settings) were combined with the exposure times, as shown in Table 5-A to obtain equivalent exposure time for the design sound levels.

Structural panels representative of the proposed design were tested to verify sonic fatigue resistance and to establish reliable design parameters. These results are presented in Section 5.3 with design curves established on the basis of analysis and tests. A summary design curve, Fig. 5-2, is presented in simplified form for use in determining structural reinforcement requirements and weight increments. Requirements for sonic resistant structure are superimposed on static design requirements in Fig. 5-3. Structure that required reinforcement for sonic fatigue is indicated by cross hatching. The weight increment is included in the weight calculation, Section 10.0, Volume VI-A, Airframe Design, and is approximately 100 pounds.

## 5.2 SONIC ENVIRONMENT

The predicted overall sound pressure levels on the exterior surface of the Boeing SST fuselage and tail section are presented in Figs. 5-4 through 5-7. The maximum SPL predicted for the fuselage and tail section is 163 db at the static maximum-augmented thrust.

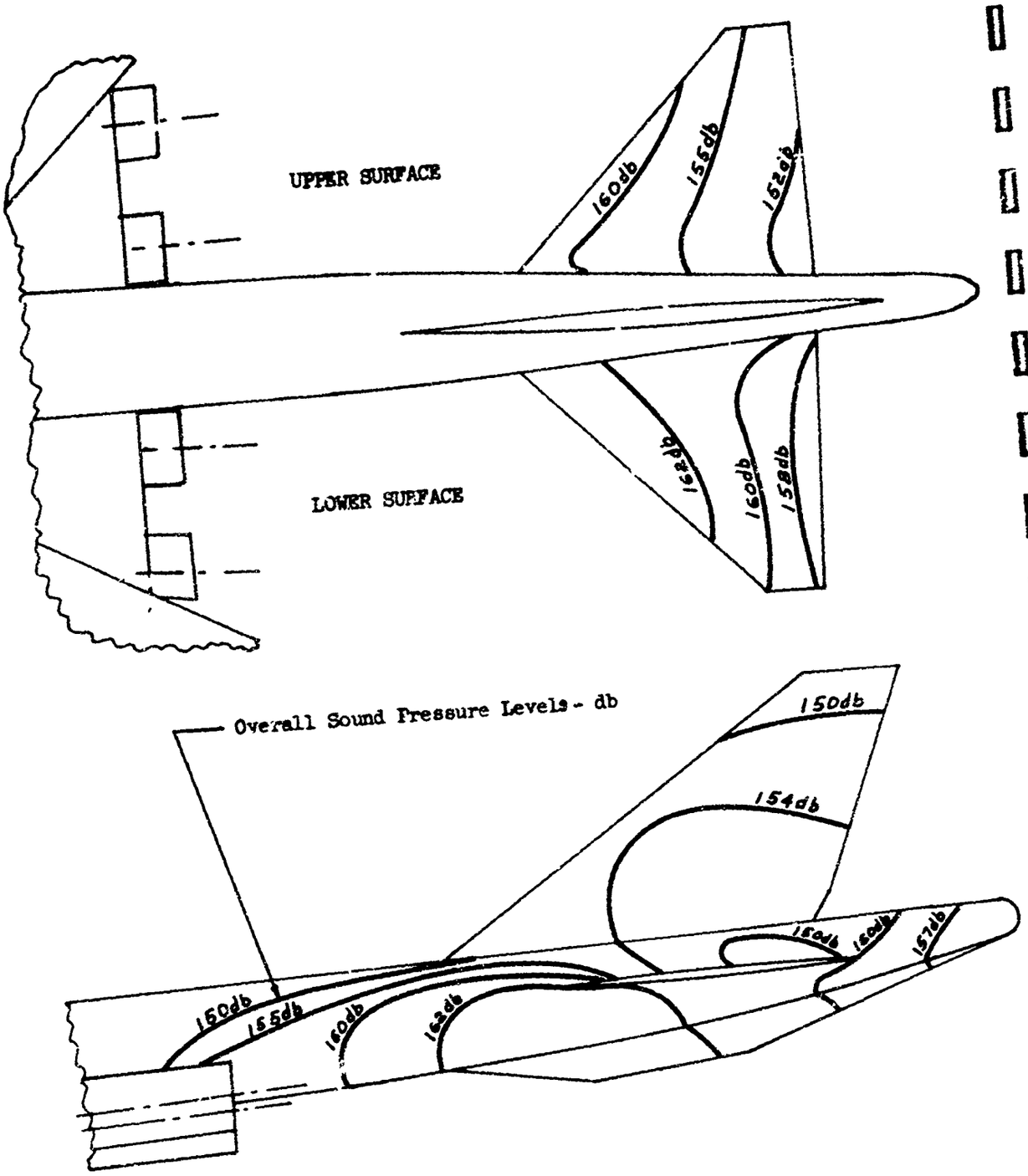


FIG. 5-1 DESIGN ACOUSTIC ENVIRONMENT

**TABLE 5-A SONIC ENVIRONMENT ON SIDE OF FUSELAGE**

| Condition | | Time Increments For 24,000 Flights Or 50,000 Hours (Hours) | Engine Power % Max. Dry | Sound Pressure Level (db) | Adjusted Time Equivalent to Operation at 100% Max Dry Power (Hours) |
|---|---|---|---|---|---|
| Take-off | Engine Checkout | $\frac{(5 \text{ sec})(24{,}000)}{3600} = 33$ | 90 | 161 | 7 |
| | Normal 90% of Flights | $\frac{(21{,}600)(15 \text{ sec})}{3600} = 90$ | 100 | 162 | 90 |
| | Max Augmented 10% of Flights | $\frac{(2{,}400)(15 \text{ sec})}{3600} = 10$ | Max Augmented | 163 | 33 |
| In-flight | Climb | $\frac{(24{,}000)(5 \text{ min})}{60} = 2000$ | 100 | 155 | 0.2 |
| | Transonic | $\frac{(24{,}000)(5 \text{ min})}{60} = 2000$ | 130 | 157 | 2.0 |
| | Cruise | 50,000 | 100 | 128 | 0 |
| Maintenance | 10 Minutes per 100 Hours Flight | $\frac{(50{,}000)(10 \text{ min})}{(100)(60)} = 83$ | 90 | 161 | 18 |
| | | | | | TOTAL 151.2 |

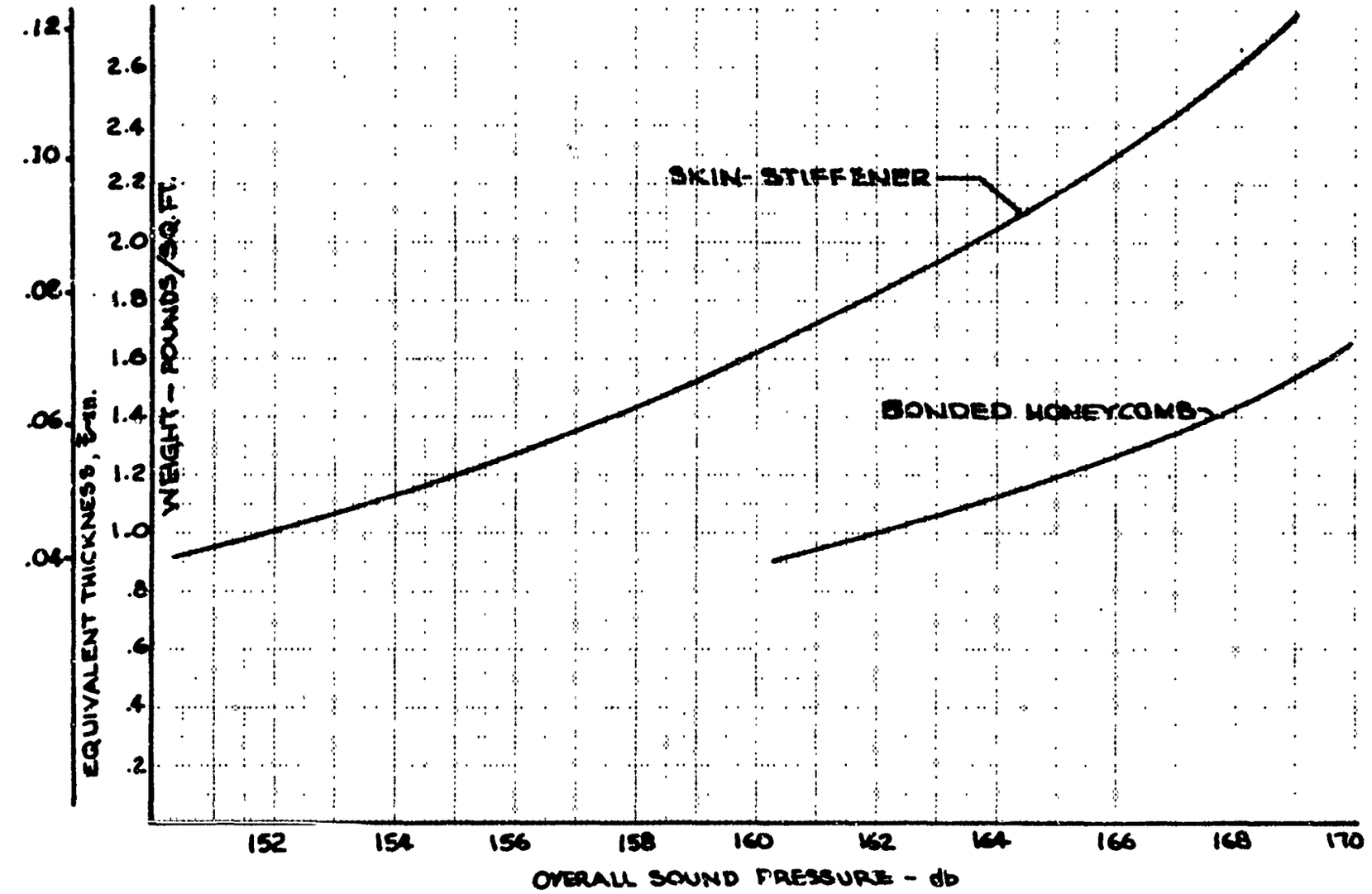


FIG. 5-2 SONIC FATIGUE DESIGN CRITERIA

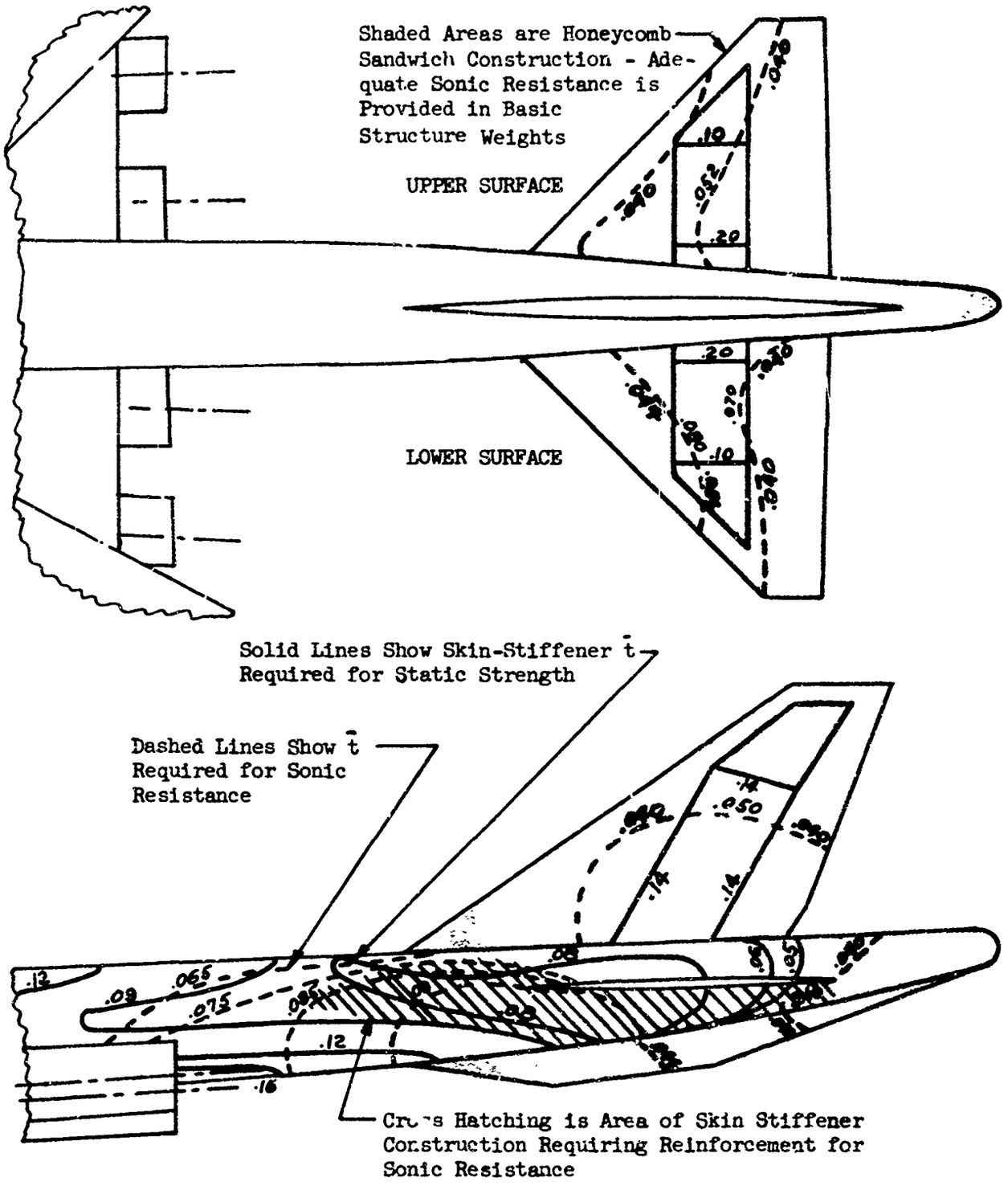


*FIG. 5-3 SONIC FATIGUE-STATIC STRENGTH COMPARISON*

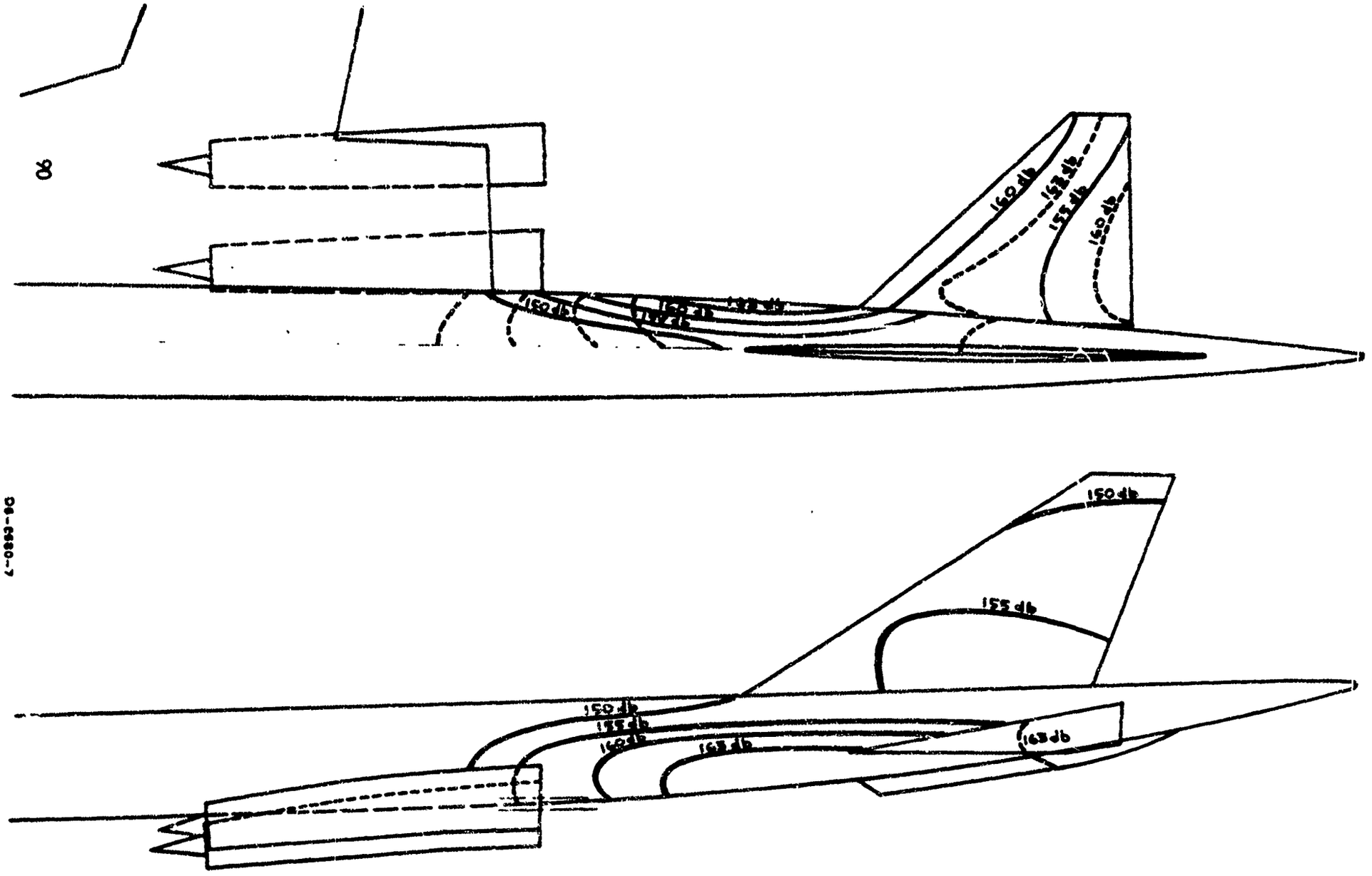


FIG. 5-4 SPL CONTOUR – 109% MAX DRY THRUST

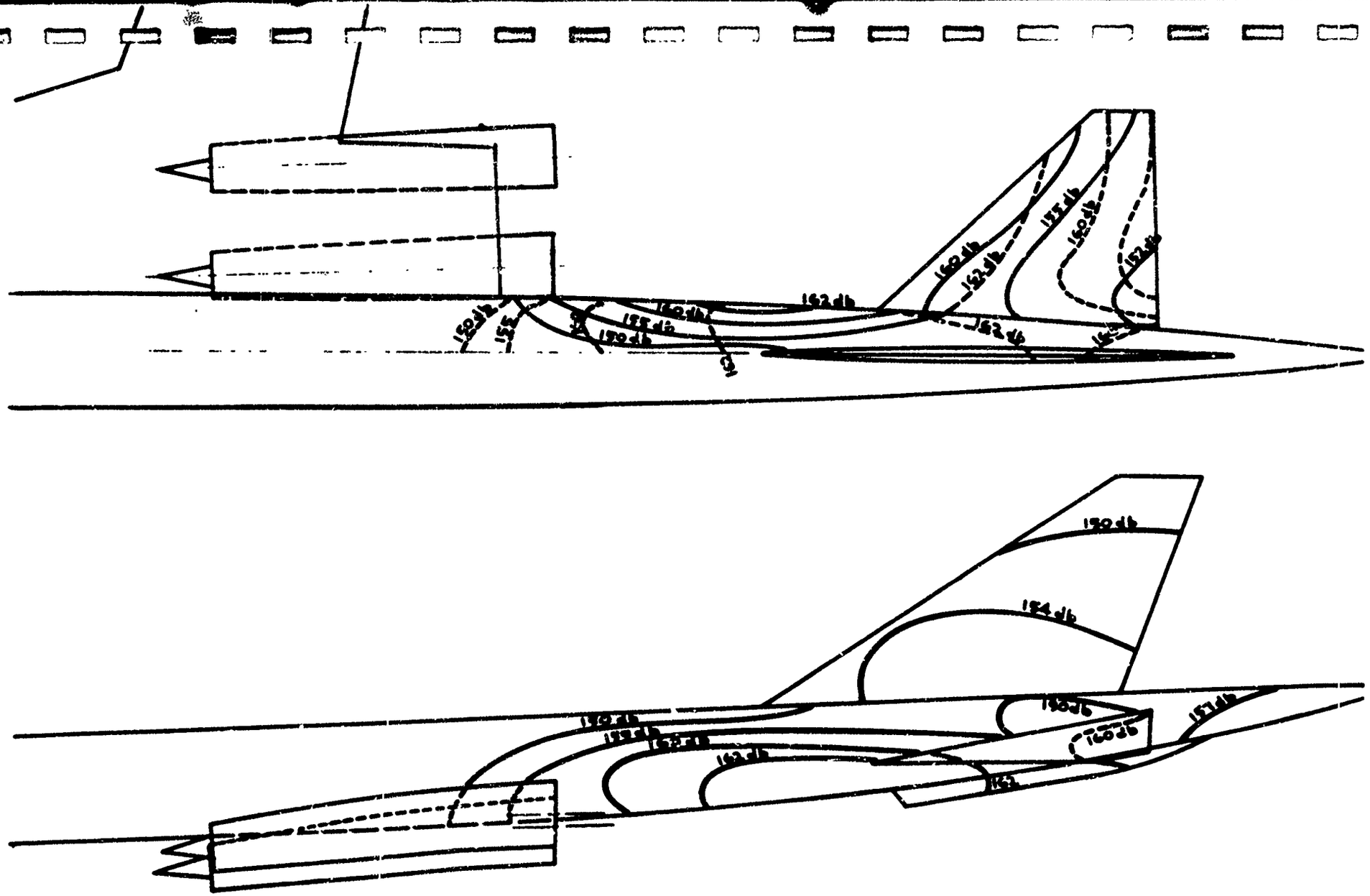


D6-9800-7



FIG. 5-5 SPL CONTOUR – 100% MAX DRY THRUST

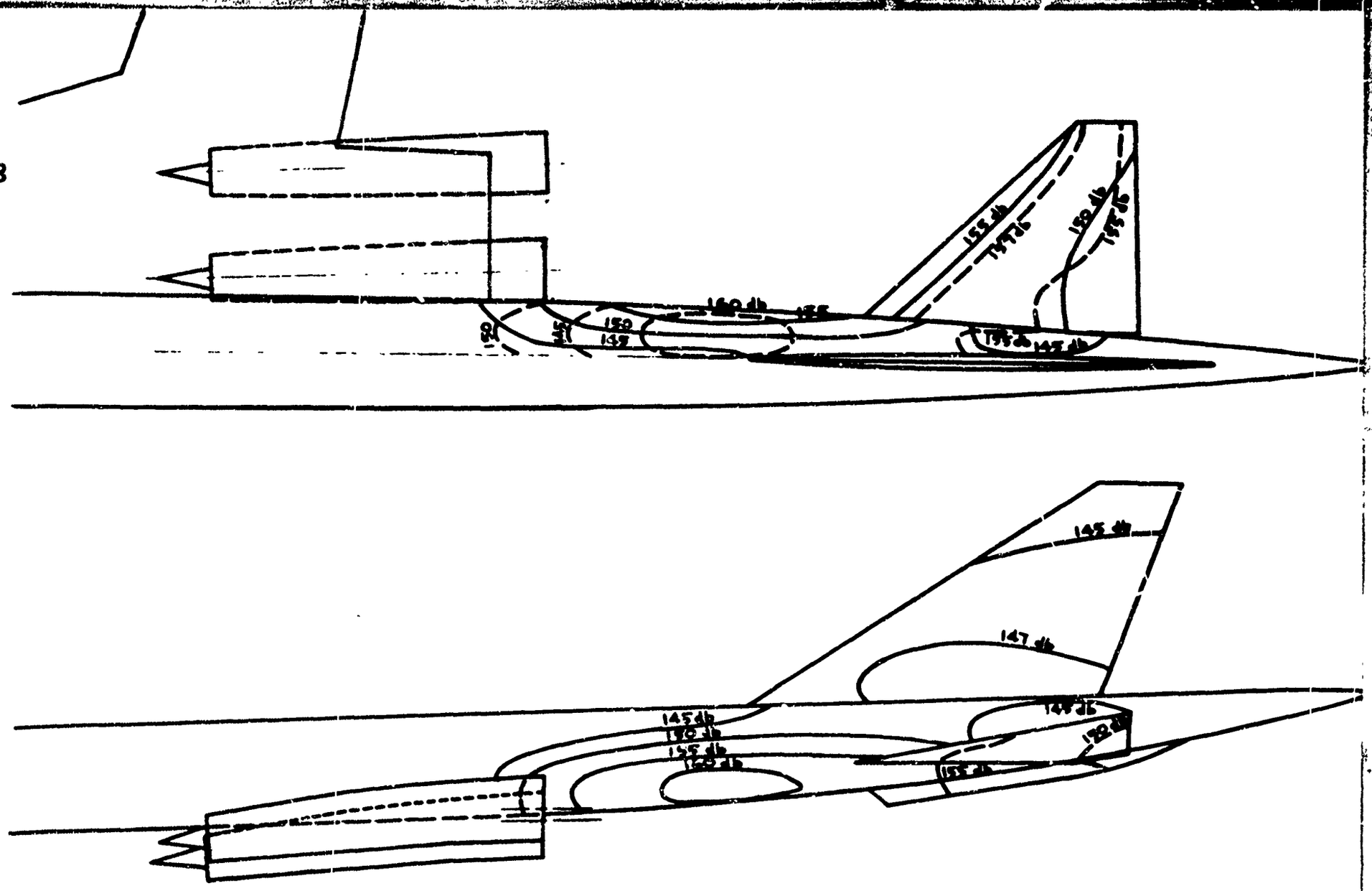




FIG. 5-6 SPL CONTOUR – 90% MAX DRY THRUST

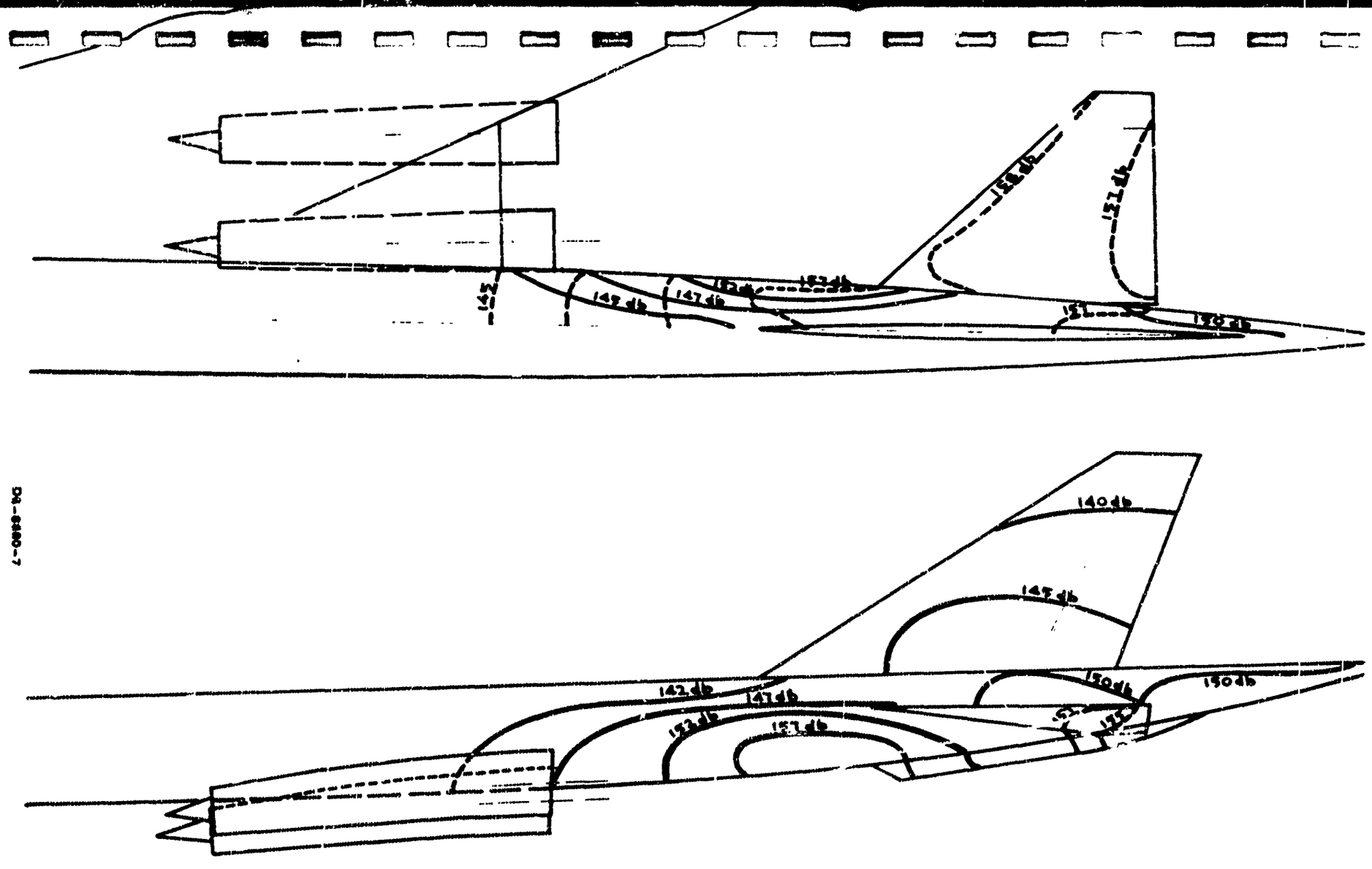


D6-8880-7



FIG. 5-7 SPL CONTOUR TRANSONIC – MAX AUGMENTED THRUST

The sound pressure levels have been determined by extensive acoustic tests run on 1/8th scale models of the GE4/J5G engine exhaust nozzle and the aft fuselage and tail section. The acoustic test facility allowed for duplication of all essential jet noise generating parameters. Augmented as well as nonaugmented GE4/J5G engine jet flow conditions were simulated for these near field noise studies. The test setup used to determine the sonic environment is shown in Fig. 5-8. Tests were conducted with a standard round nozzle as well as the "star shaped" primary throat and nozzle configuration proposed for the GE4/J5G engine. The measured SPL attenuation due to the nozzle design was 3 to 4 db.

Confirmation of the 1/8th scale model data was obtained through acoustic tests conducted in the near field of a J-75 engine with and without afterburner operating. The J-75 engine operating at partial afterburner gave jet velocities and densities very close to those predicted for the GE4/J5G engine at maximum dry thrust. Therefore only minor SPL corrections were required to predict the near field SPL's for the GE4/J5G engine at the maximum dry thrust conditions. The required corrections were based on measured incremental changes in J-75 engine noise levels with change in jet velocity and density. The J-75 engine test and the 1/8th scale model tests are documented in Refs. 5-1 and 5-2.

The engine-generated sound pressure levels on the 733-290 during the transonic flight conditions were also predicted from the SPL's measured in the model jet facility. Corrections to the static SPL data were made to account for sound power output change with change in ambient density, ambient speed of sound, jet relative velocity, jet density and nozzle exit area, and for change in noise directivity pattern due to airplane speed (Ref. 5-3). A 2 db increase in SPL was made because the "star shaped" primary throat is opened to a fully round throat for maximum augmented thrust at transonic flight speed. A 3 db reduction in SPL was made to account for removal of the ground plane as determined by flight test of 707 and KC-135 aircraft.

## 5.3 SONIC RESISTANCE OF STRUCTURE

Extensive design experience has been acquired during the past several years with sonic fatigue resistant aircraft structure and the solutions of the unique problems involved. Preliminary design charts for titanium structure and methods for improving the sonic resistance have been established during Phase II-A. The experimental basis for these developments was obtained in the Boeing sonic facility described in Phase I (Section 13, Volume A-IV, Structural Report).

### 5.3.1 Test Results

Phase II-A sonic panels are described and test results are presented in Fig. 5-9 and Table 5-B. The table shows the capability of conventional structure as well as structure designed for improved sonic resistance. All panels were Ti 8-1-1 spotwelded structure except when noted. In addition to the endurance testing accomplished, Panels Nos. 8 and 20 were heavily instrumented and responses measured under the sonic horn environment and behind a J-75 engine running in afterburner. The

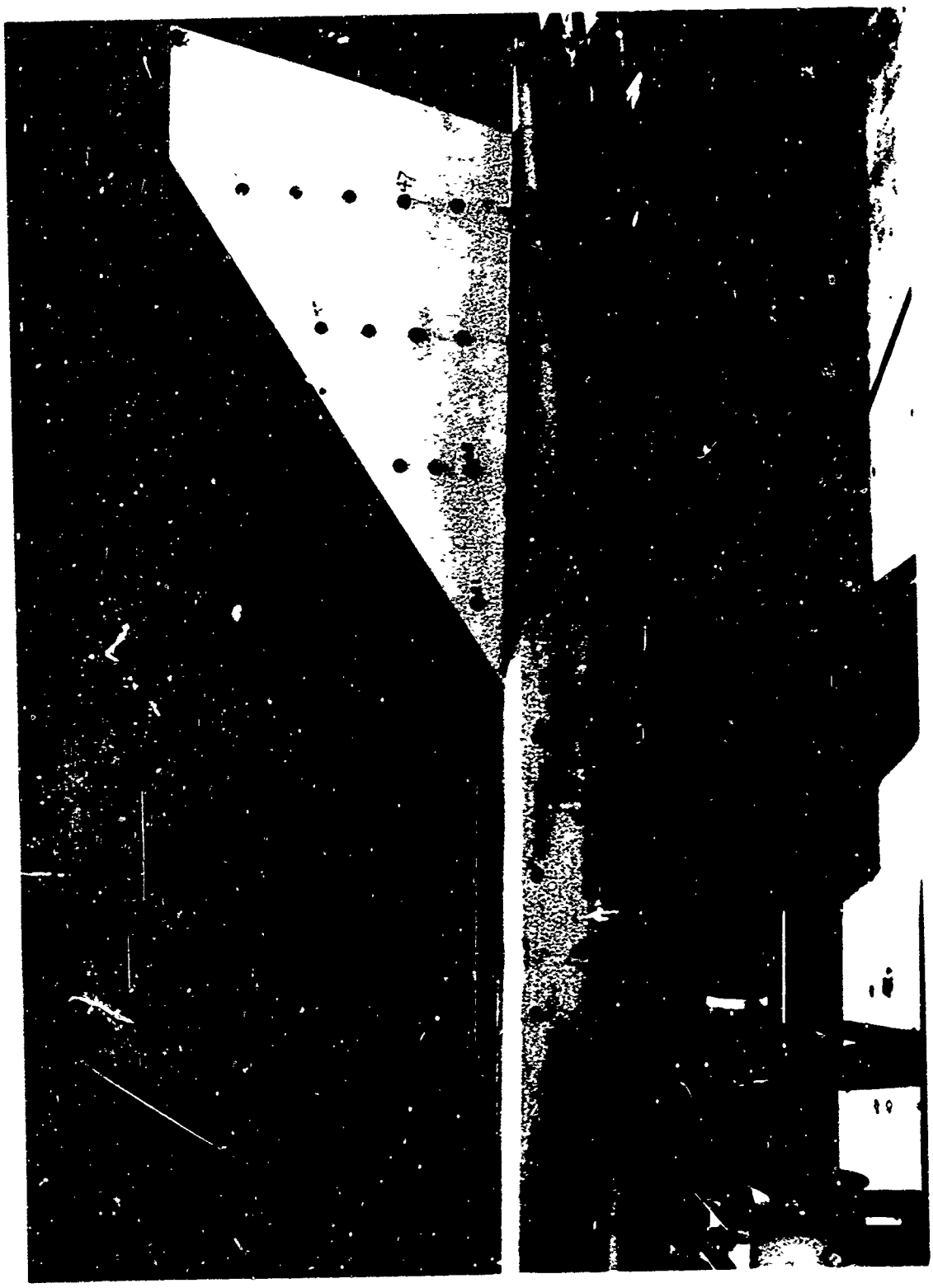

FIG. 5-8 MODEL TEST

TABLE 5-B SONIC PANEL TEST DATA

| NO. | PANEL DESCRIPTION | | | | | | | TEST DATA | | | | ADJ. SPL for 100 hrs life db |
|---|---|---|---|---|---|---|---|---|---|---|---|---|
| | SIZE in. | Skin Gage in. | Stiff Gage in. | Stiff. Pitch in. | Surface Weight t in. | Surface Weight $\frac{lb}{ft^2}$ | | Test Frequency cps | SPL db | Test Time Min. | Failure Location | |
| 1 | 24 x 18 | .030 | .020 | 3.90 | .053 | 1.19 | Hat Stiffeners supported at 20" | 380 | 155<br>160<br>165 | 44<br>44<br>2 | Sml.cracks in skin spotwelds | 154 |
| 2 | 23 x 19 | .030 | .030 | 4.40 | .049 | 1.12 | Zee Stiffeners supported at 19" | 230 | 155 | 87 | Cracks in skin spotwelds | 150 |
| 3 | 23 x 19 | .030 | .030 | 4.40 | .049 | 1.12 | Panel Identical to No. 2 | Wide Band Random | 153 | 600 | Cracks in skin spotwelds | 151 |
| 4 | 23 x 19 | .030 | .030 | 2.93 | .058 | 1.32 | Panel same as No. 2 except for stiffener spacing | 290 | 155<br>160 | 60<br>120 | Cracks in skin spotwelds | 156 |
| 5 | 48 x 24 | .060 | .060 | 4.33 | .108 | 2.47 | 2 Bay Panel - Zee stiffeners supported at 20" | 295 | 163<br>165 | 520<br>152 | Cracks in skin spotwelds | 162 |
| 6 | 23 x 19 | .030 | .030 | 4.40 | .049 | 1.12 | Panel Identical to No. 2 except tested with internal pressure of 2 psi | 240 | 155 | 10 | Cracks in skin spotwelds | 144 |
| 7 | 40 x 24 | .030 | .020 | 1.75 | .063 | 1.44 | Corrugated Doubler Panel with 2 bays | 200 | 155<br>160<br>165 | 180<br>180<br>13 | Cracks in skin & doubler | 157 |
| 8 | 24 x 24 | .050 | .045 | 4.32 | .082 | 1.87 | Zee Stiffeners supported at 20" | 237 | 162 | 206 | Cracks in skin spotwelds | 158.5 |

**TABLE 5-B SONIC PANEL TEST DATA (CONT'D)**

| NO. | PANEL DESCRIPTION | | | | | | | TEST DATA | | | | ADJ SPL FOR 100 hrs life db |
|---|---|---|---|---|---|---|---|---|---|---|---|---|
| | SIZE in. | Skin gage in. | Stiff gage in. | Stiff. Pitch | Surface Weight t in. | Surface Weight lbs/ft² | | Test Frequency cps | SPL db | Test Time Min. | Failure Location | |
| 9 | 24 x 24 | .050 | .045 | 4.33 | .082 | 1.87 | Panel Identical to No. 8 | 239 | 162 | 80 | Sml.Cracks in skin spotwelds | 158 |
| 10 | 24 x 24 | .050 | .045 | 4.33 | .082 | 1.87 | Panel Identical to No. 8 Tested at 450°F | 241 | 162 | 29 | Cracks in skin spotwelds | 156 |
| 11 | 24 x 24 | .030/.050 | .045 | 4.33 | .065 | 1.48 | Panel Identical to No. 8 Except skin chem mill between Stiffeners | 241 | 162 | 62 | Cracks in skin spotwelds | 157 |
| 12 | 24 x 15 | .010 | .010 | 1.50 | .029 | .66 | Corrugated doubler supported on all edges | 480 | 155<br>160 | 180<br>180 | Edge of doubler | 156 |
| 13 | 24 x 15 | .010 | .010 | 1.50 | .029 | .66 | Panel similar to No. 12 except improved edge details | 480 | 155<br>163 | 180<br>28 | Edge of doubler | 157 |
| 14 | 24 x 15 | .010 | .010 | 1.50 | .029 | .66 | Panel similar to No. 13 except spot brazed | 480 | 155<br>160<br>165 | 180<br>180 | Edge of doubler | 162 |
| 15 | 24 x 9 | .010 | .010 | 1.50 | .029 | .66 | Panel similar to No. 13 except smaller | 580 | 155<br>160<br>165 | 180<br>180<br>120 | Edge of doubler | 161 |
| 16 | 21 x 18 | -- | -- | -- | -- | .89 | All Polyimide Honeycomb | 236 | 160<br>165<br>160 | 60<br>60<br>2 | Center of panel | 160 |

TABLE 5-B SONIC PANEL TEST DATA (CONT'D)

| NO. | PANEL DESCRIPTION | | | | | | | TEST DATA | | | | ADJ. SPL FOR 100 hr. LIFE (db) |
|---|---|---|---|---|---|---|---|---|---|---|---|---|
| | SIZE in. | Skin gage in. | Stiff gage in. | Stiff. Pitch | Surface Weight t in. | Surface Weight lbs/ft² | | Test Frequency cps | SPL db | Test Time Min. | Failure Location | |
| 17 | 24 x 24 | .050 | .045 | 3.10 | .095 | 2.17 | Zee Stiffeners supported at 20" | 246 | 165 | 118 | Stiffener Support Frame | 161 |
| 18 | 24 x 24 | .031/.060 | .040 | 3.10 | .076 | 1.73 | Improved Sonic Design Zee stiffeners supported at 20" Chem mill skin | 415 | 165 | 231 | Cracks in Stiffened Spotwelds | 162 |
| 19 | 24 x 15 | .025 | .030 | 2.80 | .063 | 1.44 | Bead Stiffened Panel | 335 | 155 | 120 | End of Bead Cracked | 151 |
| 20 | 24 x 24 | .050 | .045 | 4.33 | .082 | 1.87 | Panel Identical to No. 8 tested to failure behind J-75 engine | Random | 150<br>160<br>166 | 60<br>60<br>15 | Cracks in skin Spotwelds | 158 |
| 21 | 21 x 18 | --- | --- | ---- | .061 | 1.40 | All Polyimide Honeycomb with Titanium Face Sheet | 286 | 165<br>168<br>172 | 120<br>120<br>22 | Skin to Core Bond | 166 |
| 22 | 48 x 24 | .040/.090 | .040 | 2.80 | .088 | 2.00 | Zee Stiffeners Supported at 20 in Chem Mill Skin; Stiffeners Notched for Rib Chords | 247 | 165 to 168 | 50 | Spotweld At End of Stiffener | 161 |
| 23 | 21 x 18 | --- | --- | --- | .050 | 1.13 | All Polybenzymidizol Honeycomb | 255 | 160<br>165<br>168 | 60<br>60<br>16 | Skin to Core Bond | 161 |
| 24 | 21 x 18 | --- | --- | --- | .040 | .91 | All Polyimide Honeycomb | 200 | 165<br>168<br>170 | 60<br>60<br>37 | Cracked Skin | 164 |

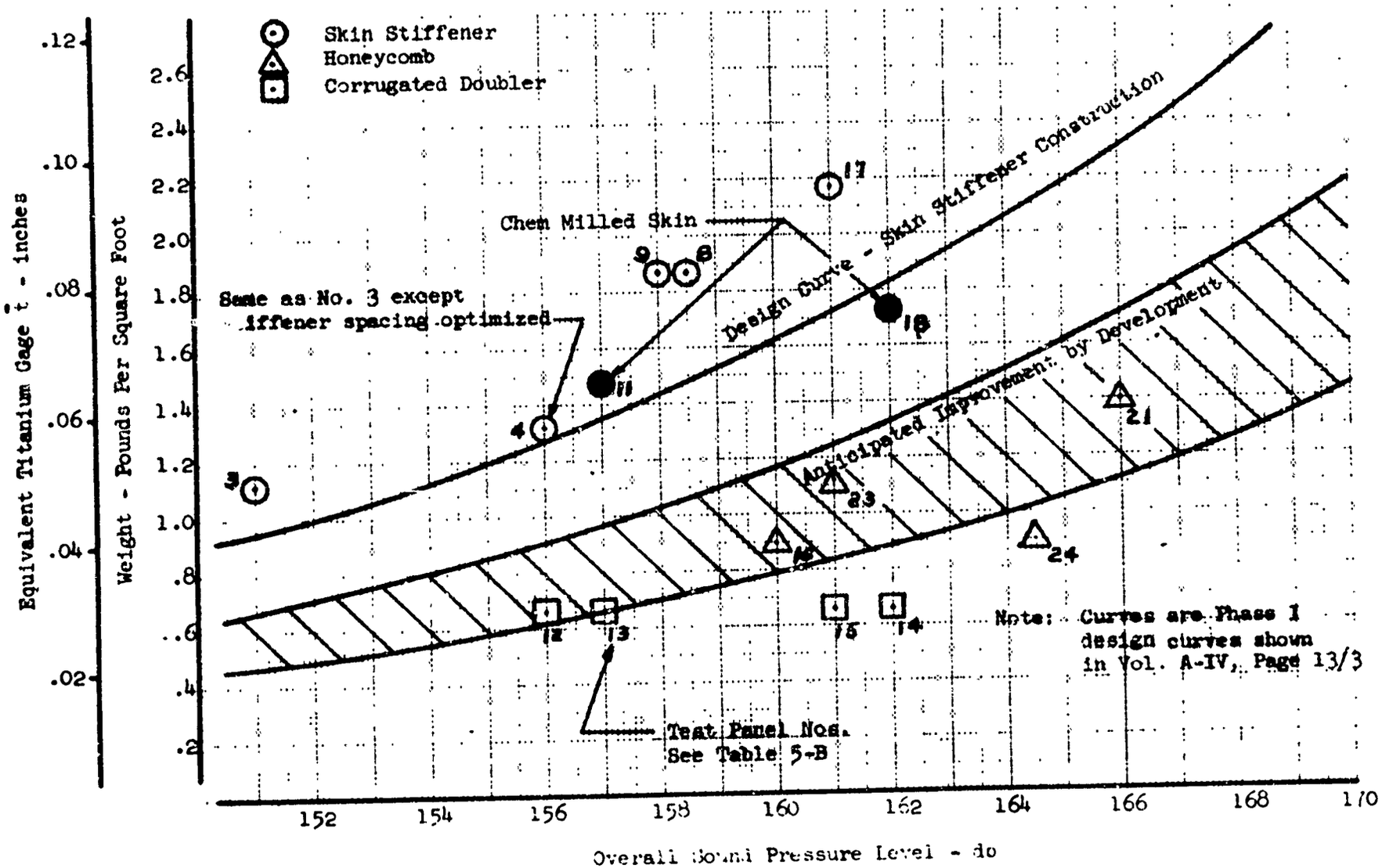


FIG. 5-9 DESIGN CRITERIA VERIFICATION

purpose of these tests was to establish correlation between sonic horn test results and that experienced under actual engine operation. One panel was tested to failure behind the engine following an initial scanning under horn environment to obtain comparative data. The second panel was scanned under the engine environment and then tested to failure in the sonic horn. Results from preliminary strain gage and deflection measurements show that the panel response to engine noise can be duplicated with either random or discrete sine sources in a horn test. While analysis must be accomplished to fully establish correlation methods and factors, these results indicate that horn tests can be used for development of sonic resistant structure.

5.3.2 Analysis and Design Curves

The panel test results have been used to derive the design curves shown in Figs. 5-9 and 5-10. Fig. 5-11 has been used to extrapolate the test results of each test panel to a SPL at which the panel would have lasted 100 hours. This curve is based on available fatigue data in the $10^6$ to $10^9$ cycle range. Since sonic pressure induced stresses are usually near the endurance limit of materials, small changes in stresses result in large changes in life. Strain gages located near the point of failure on the panels showed a linear variation of stress with sound pressure levels and when compared with existing fatigue life data, showed that reasonable correlation is obtained by this method.

Early skin stringer test panels were typical static strength designed structures with minimum optimization for sonic resistance. The results of these panel tests provided a design parameter defining the ratio of stiffener spacing to skin gage. Fig. 5-12 shows a plot of this ratio versus panel sonic resistance. Failures on this type panel were located at the spotwelds in the skin and stiffeners.

Fig. 5-13 provides geometric design relationships between weighted surface thicknesses and panel geometry. Optimum design parameters are shown in Fig. 5-10. This figure is a combination of the geometric relationship shown in Fig. 5-13 and the stiffener spacing requirements shown in Fig. 5-12. As a practical limit, a minimum stiffener spacing of 2.5 inches was chosen.

Several additional methods of construction have been investigated for secondary or minimum weight structure. Results of the tests are plotted against panel weight in Fig. 5-9. Honeycomb sandwich demonstrates a superior sonic resistance and is used on the 733-290.

Panels with beaded stiffeners, No. 19, were shown to be unsatisfactory for use in areas of high sonic environment and are eliminated from the development program.

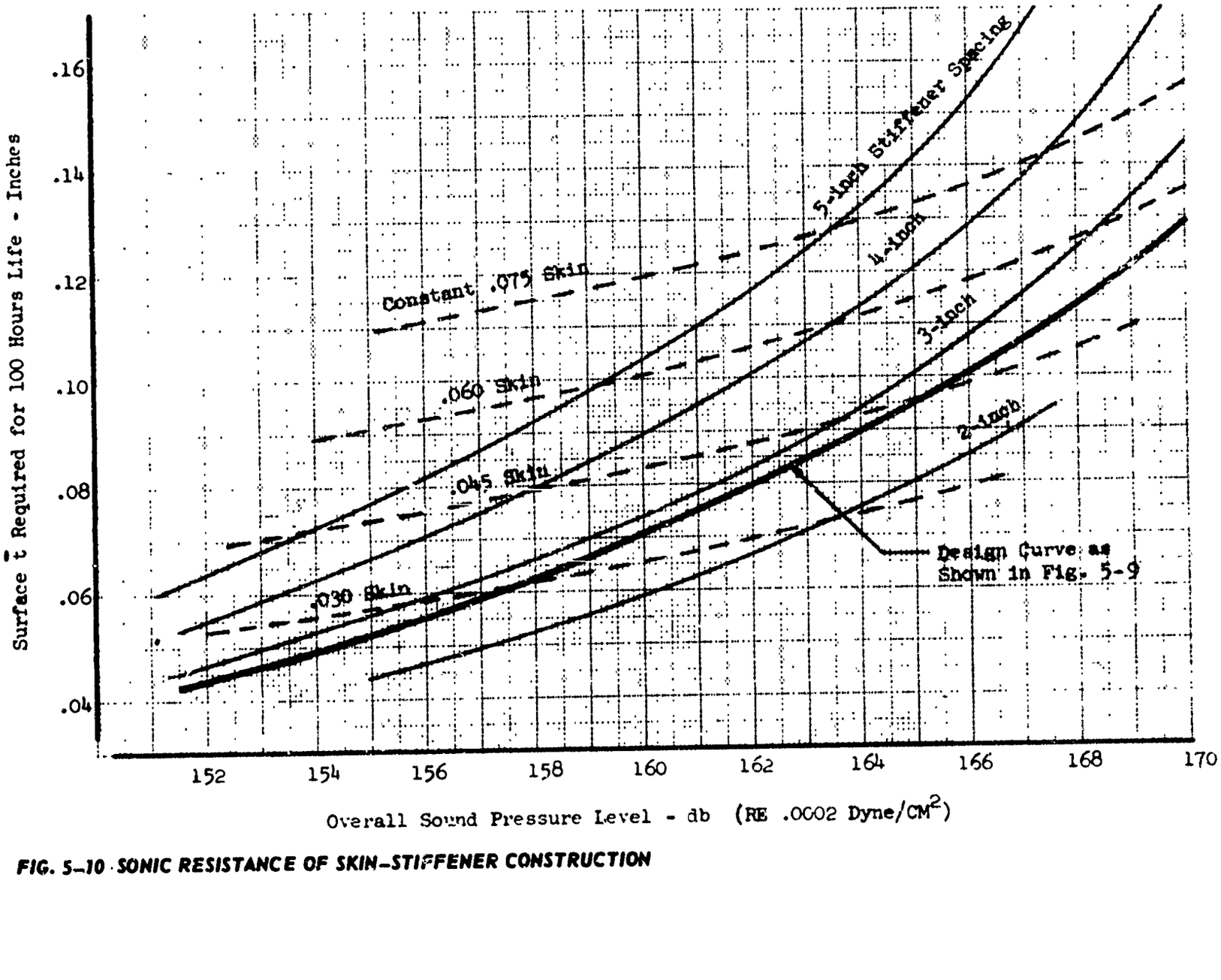


FIG. 5-10 SONIC RESISTANCE OF SKIN-STIFFENER CONSTRUCTION

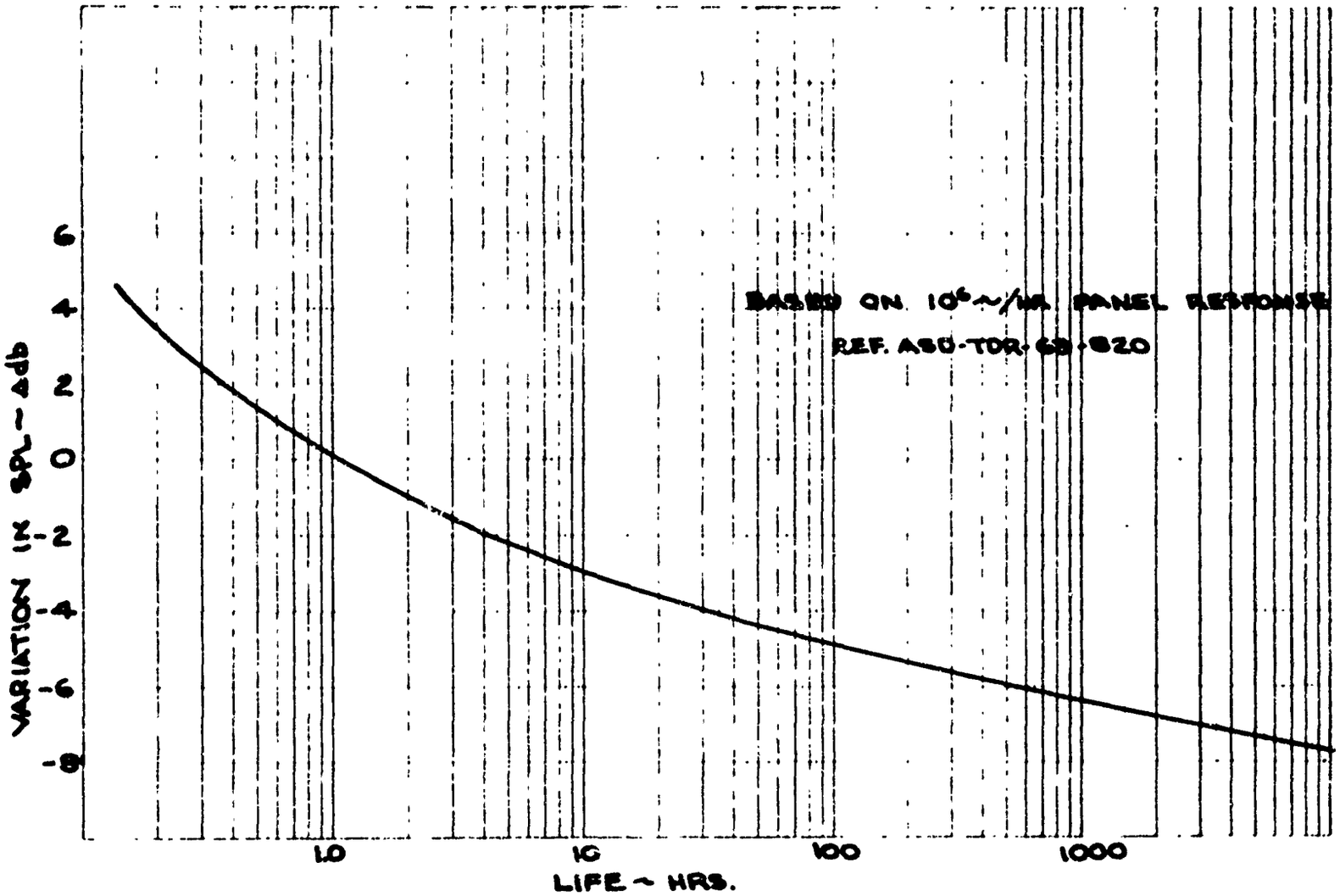


FIG. 5-11 EQUIVALENT SONIC FATIGUE LIFE

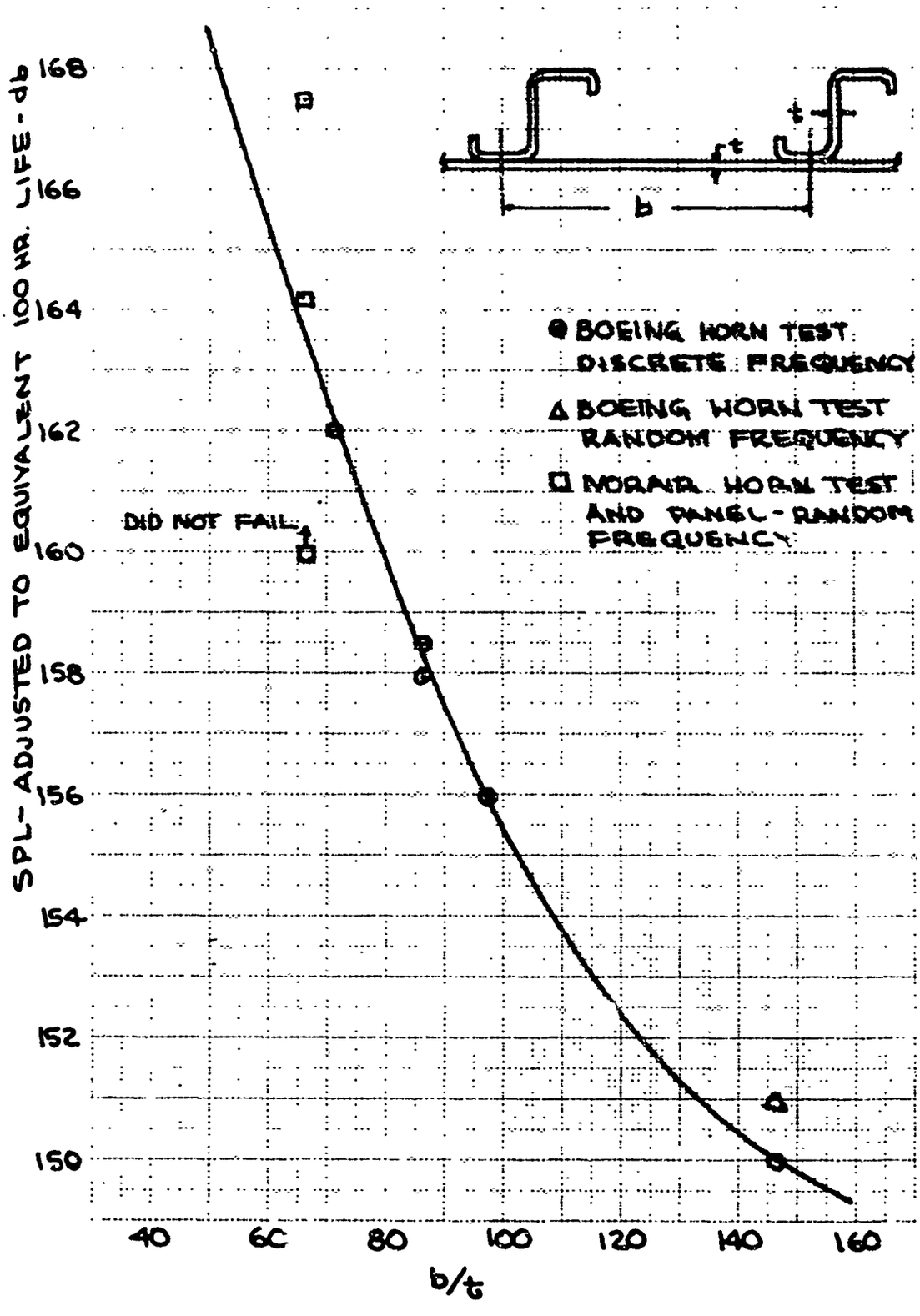


FIG. 5-12 SONIC FATIGUE DESIGN PARAMETERS

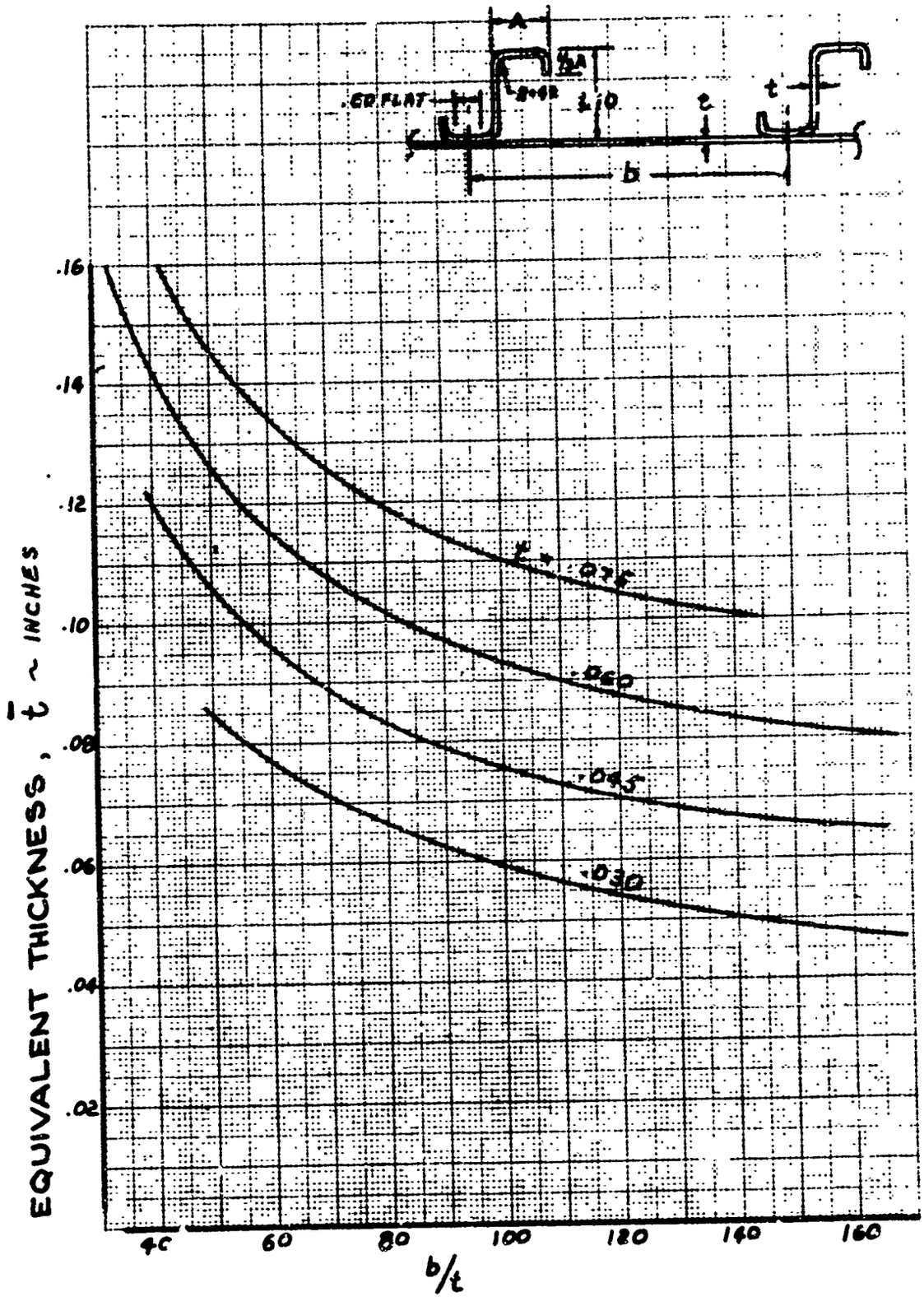


FIG. 5-13 SKIN-STIFFENER PANEL GEOMETRY

5.3.3 Follow-on Program

Testing and analysis will be expanded in Phase II-B to verify detail design concepts such as rib attachments, spotweld spacing, honeycomb core and minimum face thicknesses. Approximately ninety panels are planned for the development program as outlined in Section 13 of the Phase I, A-IV Structures document.

## 5.4 REFERENCES

Copies of the following referenced data may be obtained by making a request to either:

**The Boeing Company**
**Suite 1200 Commonwealth Building**
**1625 K Street N. W.**
**Washington 6, D. C.**

or

The Boeing Company
Airplane Division
P.O. Box 707
Renton, Washington
Attn: M. L. Pennell, Organization 6-2000, Mail Stop 73-60


5-1 Near and Far-Field Noise Survey of a J-75 Engine with Standard Tailpipe, Sawhill, R. H., and C. F. Wintermeyer, Boeing Test Report T6-3176, October 1964

5-2 1/8th Scale Model Near-Field Acoustic Test of SST Engine Nozzle Configuration, Sawhill, R. H., and D. Zable, Boeing Test Report T6-3177

5-3 Noise Reduction, Beranek, L. L. (ed), Chapter 24, McGraw-Hill Book Company, Inc., N. Y., 1960